UNIVERSIDADE DE LISBOA
FACULDADE DE CIÊNCIAS
DEPARTAMENTO DE GEOLOGIA

Environmental evolution of the Ria Formosa barrier islands system during the Pleistocene-Holocene based on very high-resolution reflection seismic profiles

Joana Tavares Perfeito Amaral

Mestrado em Geologia
Especialização em Geodinâmica e Recursos Geológicos

Relatório de estágio orientado por:
Pedro António Gancedo Terrinha
Susana Costas Otero

2024

Acknowledgments

I would like to express my sincere thanks to the people who made this work possible:

First of all, I would like to thank my supervisors, for me they are three: Pedro Terrinha, Susana Costas, and Pedro Brito (IPMA). Without them this thesis would not be possible. I am very grateful to have had the opportunity to work and learn with them. Their help, guidance and knowledge brought this work to life. Thank you for your time and effort. It will not be forgotten.

I acknowledge Instituto Português do Mar e da Atmosfera (IPMA) for access to its facilities, especially access to the Marine Geology and Geophysics Laboratory (SEISLAB), and all the members of the Geology and Marine Geo-Resources division, with a special mention to Luís Batista and João Noiva, who always made themselves available to help me.

I acknowledge Teresa Drago for providing crucial data about the cores that were used for the development of this work, and all the members of the ASTARTE campaign, for collecting and analysing the data that led to the formation of this thesis.

Thank you to all my professors who, in one way or another, have moulded my path.

To all my friends, who stayed with me from the beginning until the end of my academic life. Without them, this journey wouldn't be half as important as it is. Thank you for not failing me.

To Rúben, thank you for always believing in me and for giving me the courage and motivation to keep moving foward, today and, hopefully, always.

To my sister, Maria, despite it all, we will always have each other.

To my mom, Paula, for being my biggest support.

To my dad, Carlos, for believing in my dreams and for never letting me give up.

À minha avó. Por nunca deixares de olhar por mim.

Abstract

This study analyses the seismic stratigraphy of the Algarve coast, in order to understand the evolution of the Ria Formosa Barrier Island System (RFBIS), once is not well established yet. This was based on seismic profiles from previous data collection. The RFBIS consists of five islands and two peninsulas, dynamically shaped by waves, tides, sea-level rise, and storms. These systems are vulnerable to threats like erosion and sea-level rise, making it crucial to understand their geological evolution in response to environmental changes.

The study focuses on interpreting seismic discontinuities and sedimentary units, of the platform adjacent to the system, on its western side, to infer depositional environments, using previously analysed cores. Four seismic discontinuities (D1-D4) were identified, along with five main seismic units (U1-U5). The data indicates that the bottom of the unit U5, the upper most unit, is dating to 8280 ± 30 BP (Conventional Age). Because U5 is the youngest unit it is inferred that its deposition is synchronous to the formation of the barrier islands.

The seismic and core data analysis, including sediment dating, provides insights into the dynamic interaction between sea-level changes, sediment deposition, and erosion. This study helps establish a geological timeline for the system, considering factors such as the complexity of the area in which it is located, and offers a framework for understanding the intricate processes beneath the evolution of the RFBIS over time. However, the system's full development stages remain uncertain due to the area's complexity, but this study is a starting point to better understand the steps for the reconstruction of the system.

Keywords: Barrier islands, Algarve, seismic analysis, sediment cores

Resumo

Este trabalho apresenta uma análise feita através de perfis sísmicos sobre a evolução do sistema de ilhas-barreira da Ria Formosa presente no sul de Portugal, Algarve, com base em dados previamente recolhidos. Este sistema é composto por cinco ilhas – Ilha da Barreta, Ilha da Culatra, Ilha da Armona, Ilha de Tavira e Ilha de Cabanas - e duas penínsulas, que marcam os pontos mais a oeste e mais a leste, respetivamente – Península de Ancão e Península de Cacela.

As ilhas-barreiras são formações costeiras dinâmicas que estão constantemente a ser modificadas pela ação das ondas e das correntes, das marés, da subida do nível do mar e das tempestades. Estas são normalmente interrompidas por barras de maré (*tidal inlets)* que permitem a circulação entre a lagoa e o meio marinho aberto. Os sistemas de ilhas-barreira estão expostos a muitas ameaças, como a erosão, a subsidência e a subida do nível do mar.

A análise da evolução destes sistemas ao longo do tempo geológico é de extrema importância para a compreensão da resposta destas formações a inúmeros desafios, como as mudanças ambientais e climáticas.

Para que possamos compreender o funcionamento e as características do sistema do nosso caso de estudo, é importante relacioná-lo com o conhecimento geral sobre as ilhas-barreira. Com base na informação obtida através da análise bibliográfica que foi realizada, as ilhas-barreira ocorrem principalmente nas planícies costeiras e nos mares marginais e podem variar em morfologia em resposta à interação da amplitude das marés e da energia das ondas. Estes sistemas podem ser encontrados associados a regimes de micro-maré (0-2 m) ou meso-maré (2-4 m). Podemos também referir que estas dependem também do escoamento frequente de rios de importância elevada, ou seja, rios de maior caudal.

Tendo em conta algumas das características, maioritariamente, comuns às ilhas-barreiras que encontramos no globo, ao observarmos as características do sistema em estudo podemos concluir que este tem caraterísticas atípicas associadas à sua localização geomorfológica, devido a se situarem numa costa que não apresenta uma planície costeira desenvolvida, ao seu regime de marés, pois estas ilhas-barreira ocorrem no limite superior da amplitude de maré (3,88 m de amplitude de marés vivas) de ocorrência de ilhas-barreira, e ainda são caracterizadas por uma pequena contribuição fluvial. Todos estes fatores, que diferem este sistema de ilhas-barreira dos restantes, fazem com que a investigação do mesmo seja altamente importante para a compreensão dos processos que levaram a cabo a sua implantação, tal como ele se encontra neste momento. Um dos fatores que é comum ao desenvolvimento deste tipo de formações são as variações eustáticas. Estas mudanças do nível do mar, são causadas por fatores como a tectónica, o volume de água que circula nos oceanos e processos isostáticos e de rotação da Terra. Para realizar esta análise, temos de ter presente que estas desempenham um papel fundamental na formação e evolução das ilhas-barreira ao longo do tempo geológico. Durante um período onde ocorre subida do nível do mar (transgressão marinha), as ilhas-barreira tendem a migrar para o interior, acompanhando a linha de costa e a este processo dá-se o nome de retrogradação. Durante um período onde ocorre descida do nível do mar (regressão marinha), as ilhas-barreira tendem a deslocar-se em direção ao oceano e a este processo dá-se o nome de progradação ou regressão. Estas variações eustáticas deixam marcas distintas no registo sedimentar, que podem ser analisadas através de perfis sísmicos de reflexão, conseguindo assim entender a sua evolução ao longo do tempo geológico.

Neste trabalho, foram utilizados perfis sísmicos previamente recolhidos pela campanha sísmica multicanal ASTARTE, que ocorreu de 19 a 29 de maio de 2014. Esta campanha teve como objetivo principal procurar e mapear depósitos de tsunami e/ou estruturas de erosão causadas por tsunamis no registo sedimentar da plataforma continental ao largo de Quarteira-Tavira no Algarve, sul de Portugal. Para a aquisição dos dados sísmicos de reflexão foi contratado um sistema de alta resolução multicanal sísmico da *Geo Marine Survey Systems* (Holanda) através da *Geosurveys* (Portugal). Nesta campanha foram recolhidos 30 perfis sísmicos, que foram interpretados para este trabalho com o auxílio do

programa *DecisionSpace.* Para a interpretação dos dados disponíveis, em primeiro lugar, foram reconhecidas as principais descontinuidades sísmicas presentes em cada perfil sísmico da campanha ASTARTE. Foram reconhecidas quatro descontinuidades principais, ou seja, aquelas que separam grandes pacotes sedimentares desde a D1 até à D4. Ao reconhecê-las, foi possível identificar as principais unidades sísmicas e analisar as suas fácies sísmicas, para reconhecer a ocorrência de mudanças estratigráficas. Foram analisadas cinco unidades sísmicas principais sendo a mais antiga a unidade U1 e terminando com a unidade mais recente, a unidade U5. Com este reconhecimento podemos inferir diferentes ambientes deposicionais. Após a análise sismoestratigráfica, a calibração estratigráfica das reflexões e unidades sísmicas foi também efetuada com recurso a *cores*. Foram utlizados quatro *cores* para este trabalho, dois deles pertencentes ao projeto POPEI - Popei-1 (1-1CGG) e Popei-2 (2-1CGG) - recolhidos na plataforma continental, no sul de Portugal, a oeste do Cabo de Santa Maria, e ao projeto MOWER – MW14-105 e MW14-107 - recolhidos em setembro de 2014 a bordo do navio de investigação Sarmiento de Gamboa no contexto do projeto nacional espanhol com o mesmo nome. Estes foram separados em secções durante a sua análise no laboratório. De acordo com o relatório da campanha ASTARTE (Drago et al., 2017), durante a análise dos *cores*, a datação dos mesmos foi obtida por *Accelerator Mass Spectrometry* (AMS) a partir de C^{14}. Sabendo as idades dos *cores* é possível determinar idades para o sistema relativas, relacionando esses dados com os dados de sísmica que temos disponíveis. Após a interpretação sísmica, foram também criados mapas de superfícies interpoladas de espessura e profundidade, para haver uma melhor compreensão da dinâmica que ocorre na área de estudo.

Após a análise e interpretação dos dados podemos estabelecer uma cronologia geológica do sistema. Verificou-se que idade mais antiga registada na análise AMS C^{14} dos *cores* foi de 8280±30 BP (Idade Convencional). Uma vez que foi demonstrado que as medições da datação não atingiram nenhuma das descontinuidades interpretadas e que essas idades pertencem à unidade U5, que é a unidade mais recente, podemos dizer que todas as unidades abaixo da unidade U5 são mais antigas do que a idade mencionada. A unidade U4 tem provavelmente uma idade próxima da unidade U5 devido às suas semelhanças sísmicas. A unidade U3 formou-se provavelmente durante uma subida do nível do mar entre 16,5 mil anos e 8280±30 BP, correspondendo a um período de deglaciação. A unidade U2 é mais complexa, possivelmente representando múltiplos picos de baixo nível do mar (LST – *Lowstand System Tracts*) ou flutuações no nível do mar. A unidade U1 é a mais antiga, datando potencialmente do Plio-Pleistocénico. Uma vez que a área de estudo é extremamente complexa, não podemos ainda determinar todas as etapas que estiveram envolvidas na criação da RFBIS tal como ela se apresenta atualmente, mas este trabalho é o ponto inicial para que possamos melhor entender os passos para a reconstrução do sistema.

As análises e interpretações mencionadas em todo este trabalho permitem deduzir a evolução geológica da RFBIS como uma interação dinâmica entre alterações do nível do mar, sedimentação e erosão. As unidades e descontinuidades revelam uma história de transgressões e regressões, superfícies erosivas e ambientes deposicionais complexos. O trabalho fornece informações sobre o tempo geológico destes eventos, ligando-os às flutuações globais do nível do mar e à geologia subjacente, oferecendo um quadro para uma interpretação geológica e paleoambiental mais aprofundada da região.

Palavras-chave: Ilhas-barreira, Algarve, análise sísmica, *cores* sedimentares.

Table of Contents

List of Figures

List of tables

1. Introduction

Barrier islands are dynamic coastal landforms that are found along many coastlines around the world (Stutz, 2011). In the Algarve, there is a chain of barrier islands that are part of the Ria Formosa Natural Park (RFNP). However, the origin of these barrier islands is not yet fully understood.

In recent decades, human activity has intensified, triggering important changes in the patterns of coastal evolution, increasing the complexity of the processes (Kombiadou et al., 2019).

Over the years, oceanographic campaigns have been carried out along the south coast of Portugal as part of scientific research projects, where high-resolution reflection seismic data have been obtained off the Algarve barrier islands system. This work focuses on the ASTARTE (2014) campaign, which is the most recent campaign in the study area with very high-resolution seismic profiles. To this end, seismic profiles from the aforementioned campaign were analysed in combination with information from previous works.

The present work aims to investigate the geological evolution that took place off the Ria Formosa, Algarve, barrier islands, between the peninsula of Ancão and the peninsula of Cacela.

The objectives of this work were based on the identification of the main units that characterize the recent sedimentary record off the islands, namely across the sedimentary shelf. After the identification of the units, as well as the discontinuities, they were interpreted and a tentative of assigning the age to the units was made. The reconstruction of the installation of the islands was made with the data that was available after the interpretation, to see to which extent this can help us to better understand the timeframe of the formation, and the process itself, of those islands.

1.1. Barrier islands

Barrier island systems are scattered all over the globe and have intrigued scientists over the years. These systems are relatively narrow and long sand deposits that are constantly being modified, through wave and current action, tides, sea-level rise, and storms. They are generally separated from the mainland by tidal channels, bays, or lagoons. Barrier islands can migrate and change shape due to some factors. We can refer longshore drift, which is a process whereby wave action moves sand laterally along the shoreline, as one of those factors. We can also refer cross-shore sediment transport, that can be enhanced by changes in sea level, and can also affect the position of these islands significantly. These factors make barrier islands dynamic landforms that can be constantly adapting to changing conditions. Barrier island systems occur throughout the world coastlines regardless of climate, but they must have a fairly shallow shelf on which to develop, and they require a large amount of sediment plus significant wave influence (Davis, 2003).

1.2. General barrier islands characteristics

Barrier Islands occur primarily on coastal plains, are located on the trailing edges of mainland and on marginal seas and can vary in morphology in response to the interaction of tidal range and wave energy (Hayes, 1979). The inundation of coastal plains is the reason for the existence of barrier islands in that the tendency for spit progradation into estuaries or former valleys is the common mode of island formation (cited by Pilkey Jr et al. (1989) from Swift, 1975, 1976).

Stutz et al. (2000) presented a global compilation of barrier islands and ended up with a total of 1500 barrier islands, this being 15,100 km in total length of recognized barrier islands, constituting 6.5% of the world's open ocean shoreline.

These systems can be found associated to micro-tide (0-2 m) or meso-tide (2-4 m) regimes and often are dependent on the outlet of important rivers (cited by Dias, 1988 from Leatherman, 1979).

Even though the morphodynamics of barrier islands are mostly understood, there has been some debate about understanding how they are formed. According to Davis (2003) there have been three primary

scenarios ascribed to the origin of barrier islands: (1) upward shoaling of subtidal sand bars due to wave action, (2) generation of long spits due to littoral drift and then breaching to form inlets, and (3) drowning of coastal ridges.

Barrier island systems are exposed to threats such as erosion, subsidence, and sea-level rise. Among the causes behind coastal erosion, sea-level rise is one of the major global concerns that is likely to affect coastlines throughout the world in the upcoming years (Ceia et al., 2010). According to Mariotti & Hein (2022), it is believed that regional barrier retreat is generally proportional to the rate of relative sea-level rise, however field observations that they made along the coast the USA East Coast indicate that barrier retreat rate has increased less than expected, considering observed sea-level rise rates. To explain that fact the authors used a coastal evolution model that considers disequilibrium dynamics to show that modern barrier retreat rate is not controlled by recent sea-level rise (last decades), but rather by the baseline sea-level rise of the past centuries. From this they took that the cumulative effect of the baseline sea-level rise is to establish a potential retreat, which is then realized by storms and tidal processes in the following centuries, and when the sea-level rise accelerates, the potential for retreat is first realized through removal of geomorphic capital. They conclude that after several centuries, lag dynamics play a fundamental role in the coastal response to sea-level rise, so it takes a while until the response is in equilibrium with the new rate, but, as the sea-level rise rate is accelerating, it is like it will never be in equilibrium or in direct relation with the rate of sea level rise.

From the seaward to the landward location, the barrier island system consists of the nearshore zone (1), beach (2), dunes (3), washover fans (4), and various types of coastal bays with marsh and/or tidal flat margins (Davis, 2003):

1. Nearshore zone: it refers to the area of the shoreline that extends from the low tide mark to where the ocean floor begins to drop off more steeply. It is a wave-dominated environment that is characterized by shore-parallel sand bars and intervening channels (Davis, 2003).
2. Beach: dynamic coastal landform that typically consists of loose sediment. These are formed due to the interaction of various processes, such as wave and tidal action and coastal erosion and deposition.
3. Dunes: aeolian accumulations of sand that are formed, in this case, in coastal environments. Coastal dune morphology over medium term temporal scales (years to decades), results from a balance between the aeolian transport potential, the sediment supply, the intensity of storms that erode the backshore and the scarp of the dune and the changes in vegetation cover (Costas et al., 2020).
4. Washover fans: deposits accumulated at the back of the barrier when storms, as well as the waves that are associated with the storm, and surges overtop low barrier islands or cut through low areas on those barriers, causing overwash flows that erode the barrier and generate these deposits, seen in Figure1. According to Davis (2003), when storms cause the barrier to be temporarily inundated by waves, sediment is carried from the beach and nearshore zone to the landward side of the barrier and are deposited in the form of washover fans. This process is highly relevant to the landward migration of barrier islands.

Barrier islands are typically interrupted by tidal inlets that permit circulation between the coastal bays landward of the barrier and the open marine environment (Davis, 2003). All these general elements are shown in Figure 1.

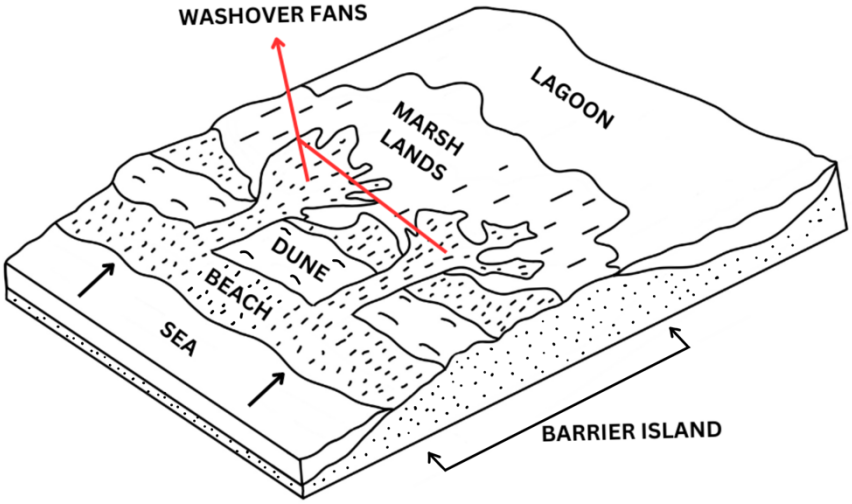

Figure 1: Diagram with the elements from a barrier island system.

2. Settings

2.1. Geographic setting

The Algarve coast can be distinguished between two types of coastlines. On the west, the coast is characterised by cliffs (windward or *Barlavento*) and it stretches from Ponta de Sagres to Quarteira, and on the east we have the sandy (leeward or *Sotavento*) ant it stretches from Quarteira to the mouth of the Guadiana River). The study area falls within the latter.

The eastern coast of the Algarve is a low sandy coast with a high diversity of environments, including cliffed coast, sandy beaches, dune ridges, an estuary, artificial/antrophic sectors and two major environmental units: the barrier islands and the coastal lagoon.

The barrier-lagoon system is composed of five barrier islands – Barreta Island, Culatra Island, Armona Island, Tavira Island and Cabanas Island – and two peninsulas, which mark the westernmost and easternmost points, respectively – the Ancão peninsula and the Cacela peninsula (Figure 2). The islands and peninsulas are separated by six tidal inlets (Figure 3).

The system hosts a variety of ecosystems, as well as a biological diversity of marine and terrestrial life. These factors led to the creation of the Ria Formosa Natural Park in 1987. The Ria Formosa Barrier Islands System (RFBIS) encloses a lagoon and is bordered by the Atlantic Ocean. The system has a roughly triangular or cuspate shape, whose southern apex corresponds to Cape Santa Maria (the southernmost point of mainland Portugal) and stretches for approximately 55km.

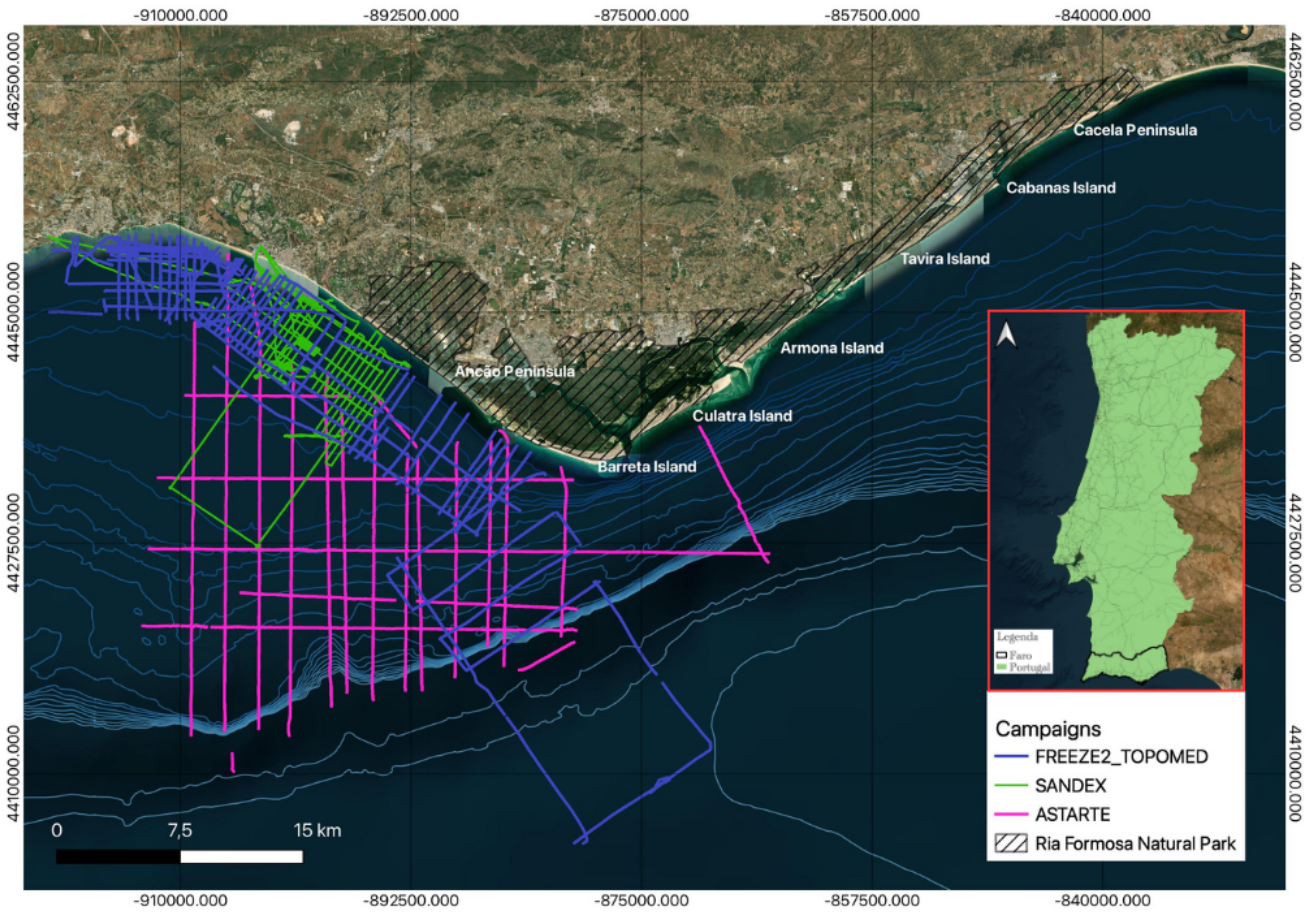

Figure 2: Geographical location of the study area at macro and meso scales with reference to the campaigns and their seismic profiles.

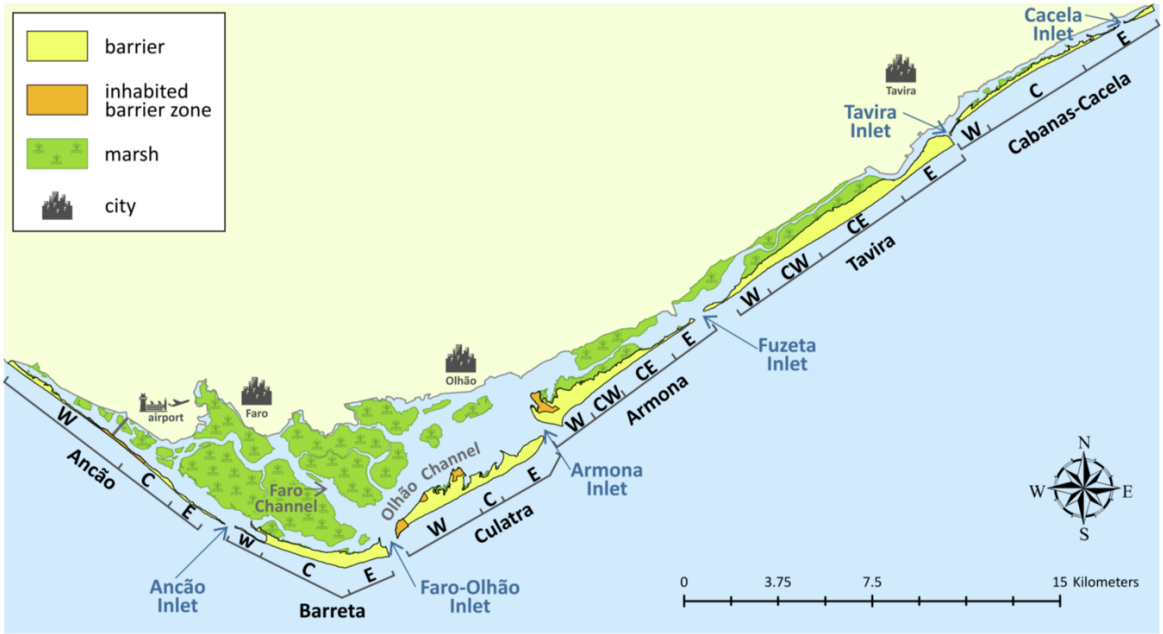

Figure 3: Geographical location of the study, showing the barriers, inlets, main channels, marshes, and main human occupation. W- west; C- centre; E- east. Adapted from Kombiadou et al., (2020).

2.2. Geological setting

2.2.1. The emerged Algarve region

In general, the Algarve is characterised by the existence of Meso-Cenozoic sedimentary formations, which overlie the Palaeozoic basement. The Mesozoic formations are made up of sin-rifting and post-rifting sedimentary rocks, deposited between the middle to lower Triassic and the Cenomanian. The existence of a Volcano-Sedimentary Complex of latest-Triassic age (~200 Ma) and alkaline magmatism from the upper Cretaceous (~72 Ma) are noteworthy. The Cenozoic formations in the emerged area are almost exclusively of Miocene, Pliocene, and Quaternary age, with a small outcrop of Palaeogene age. The Cenozoic sediments were deposited in a post-orogenic context of the Alpine Orogeny. The Miocene is mainly made up of limestone, with the marl component increasing towards the top. The Pliocene and Quaternary are made up of poorly consolidated, heterometric siliciclastic sediments with markedly terrigenous characteristics. The beaches are made of unconsolidated Pleistocene-Pliocene sands (Terrinha et al., 2006).

The coast in the south of Portugal is part of the Algarve Basin of Meso-Cenozoic age. According to Ramos et al. (2015), and as can be seen in Figure 4, Mesozoic sedimentation begins with siliciclastic alluvial deposition in the upper Triassic. The pelitic-evaporitic unit of the overlying Hetangian is made up of lacustrine red pelites, a thin layer of shallow-water dolomites and evaporitic deposits that may consist of halite or gypsum (Ramos et al. 2015). These units are covered by a volcano-sedimentary complex made up of basaltic lavas and pyroclastic rocks interbedded with clay and dolomite beds. This volcanic event is associated with the Central Atlantic Magmatic Province (CAMP; cited from Martins et al. 2008 in Ramos et al. 2016) of the transition from the Triassic to the Hettangian (~2000 Ma), and the end of the first extensional episode of the Algarve Basin (cited from Terrinha et al. 2002 in Ramos et al. 2015).

The Jurassic is essentially made up of limestone and marl. The Lower Cretaceous was deposited during the last phase of extension, after a brief hiatus, and is made up of a mixed succession of carbonates and siliciclastic sandstones and conglomerates (cited from Rey 1983, 2006, 2009 in Ramos et al. 2015). The Upper Cretaceous is represented by reefal limestone of Cenomanian age only.

The mapped Palaeogene is summarised as an outcrop of uncertain age of conglomerates. The Miocene is deposited on an erosional unconformity over the Mesozoic and locally over the Palaeozoic. The Miocene is essentially carbonate, represented by limestones, marls, siltstones and fine sandstones (cited from Pais et al. 2000 in Ramos et al. 2015). These units were karstified and covered by detrital fluvial sediments, episodically marine from the Pliocene to the Pleistocene. The most recent sediments in this basin are lithified beach sands and dunes from the upper Pleistocene and Holocene formed as a result of climatic and sea-level fluctuations (cited from Moura et al. 2007 in Ramos et al. 2015).

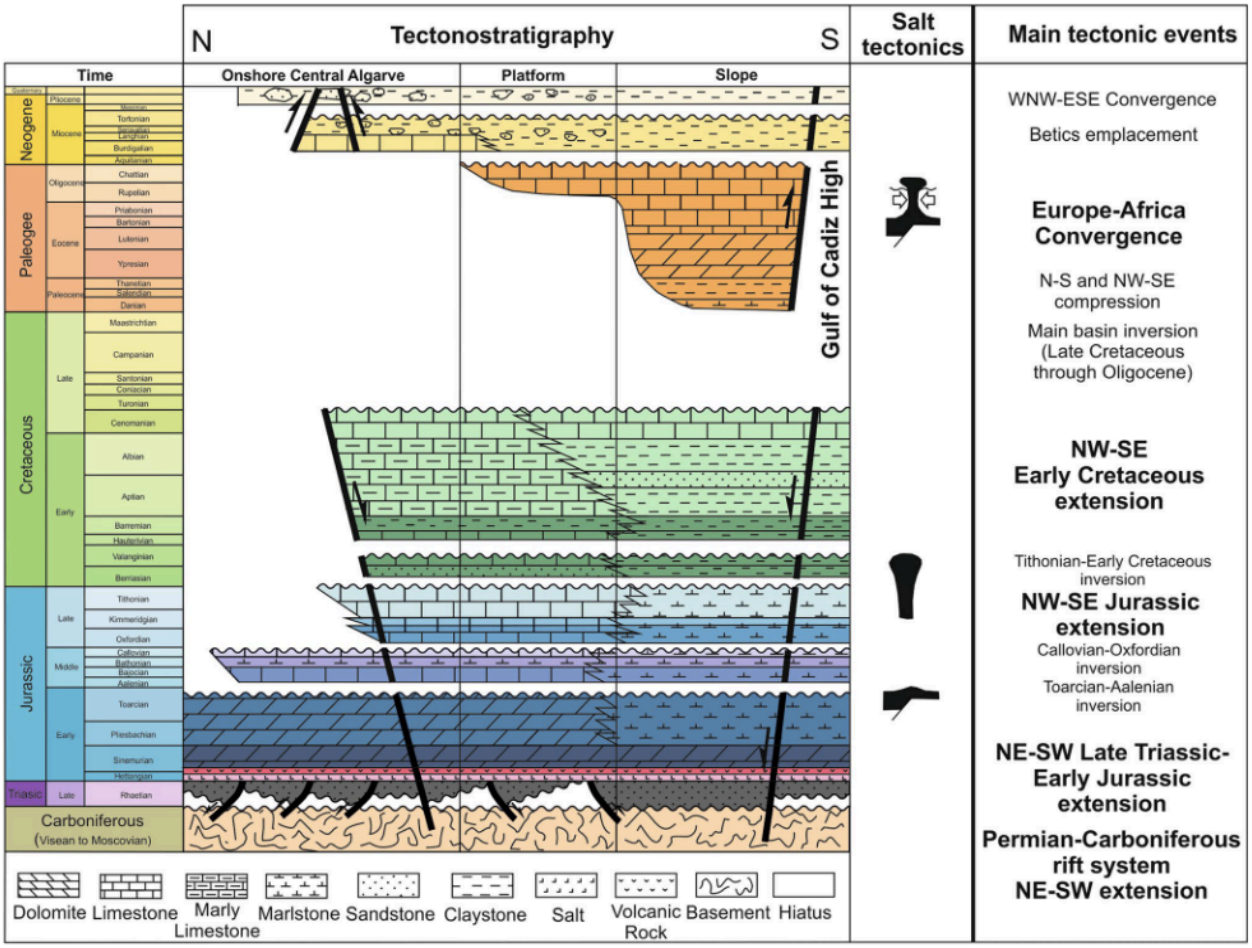

Figure 4: Figure taken from Ramos et al., (2015) and adapted from Terrinha (1998), Matias et al (2011) and Fernandes et al. (2013), showing the simplified stratigraphy of the Algarve Basin with the main stratigraphic units and the main tectonic events.

2.2.2. The immersed Algarve region

The eastern side of the Algarve coastline is low, with wide beaches and the barrier islands, made up of sandy beaches and dunes, which are found protecting the Ria Formosa lagoon.

In the study area, the width of the continental shelf is narrow, ranging from 5 km in the western part in front of Faro, to its maximum width, around 20 km, off the Guadiana River mouth. The shelf presents a gentle slope of 0.40º, increasing westwards to 0.53º (Roque et al., 2010) and a well-defined edge, located at depths of between 110-150 m (Lopes & Cunha, 2010).

During 1975 and 1983, boreholes were made in the submerged region of an area of the Algarve Basin, as part of the search for potential hydrocarbon deposits. These boreholes crossed a variety of lithologies, with a predominance of limestones, dolomites, marls and sandstones, whose ages cover a wide range of time spans, extending from the Triassic to the Pliocene-Quaternary, with an important hiatus and unconformity between the Lower Cretaceous and the Upper Palaeocene, or Eocene or Oligocene or Miocene (Terrinha et al., 2006).

The Pliocene is marked in the south of the Iberian Peninsula by a broad marine transgression with a stabilisation of the sea level in the Middle Pliocene. The beginning of the Quaternary coincides with a marked cooling accompanied by glacial-eustatic variations in the mean relative sea level. As a result, the hydrographic networks were profoundly altered, and the rivers became more fitted in the incised substrate. The Ludo Sands, attributed to the Lower Pleistocene, are evidence of rapid sedimentation from dense suspensions, as happens, for example, in the terminal parts of rivers carrying a high detrital

load (Terrinha et al., 2006). The Ludo Sands are channelled into the Quarteira Sands and are therefore of discontinuous geographical distribution. They are white, coarse to medium grained, kaolinitic sands, generally massive. The Gambelas Sands and Gravels are attributed to the Upper Pleistocene and are composed of three terms, from the oldest to the most recent: a) pedolised siltstones with rhizomorphic structures, b) very coarse red sands with small to medium pebbles and c) large pebbles to quartzite pebbles, graywacke and schist (Terrinha et al., 2006) (Figure 5).

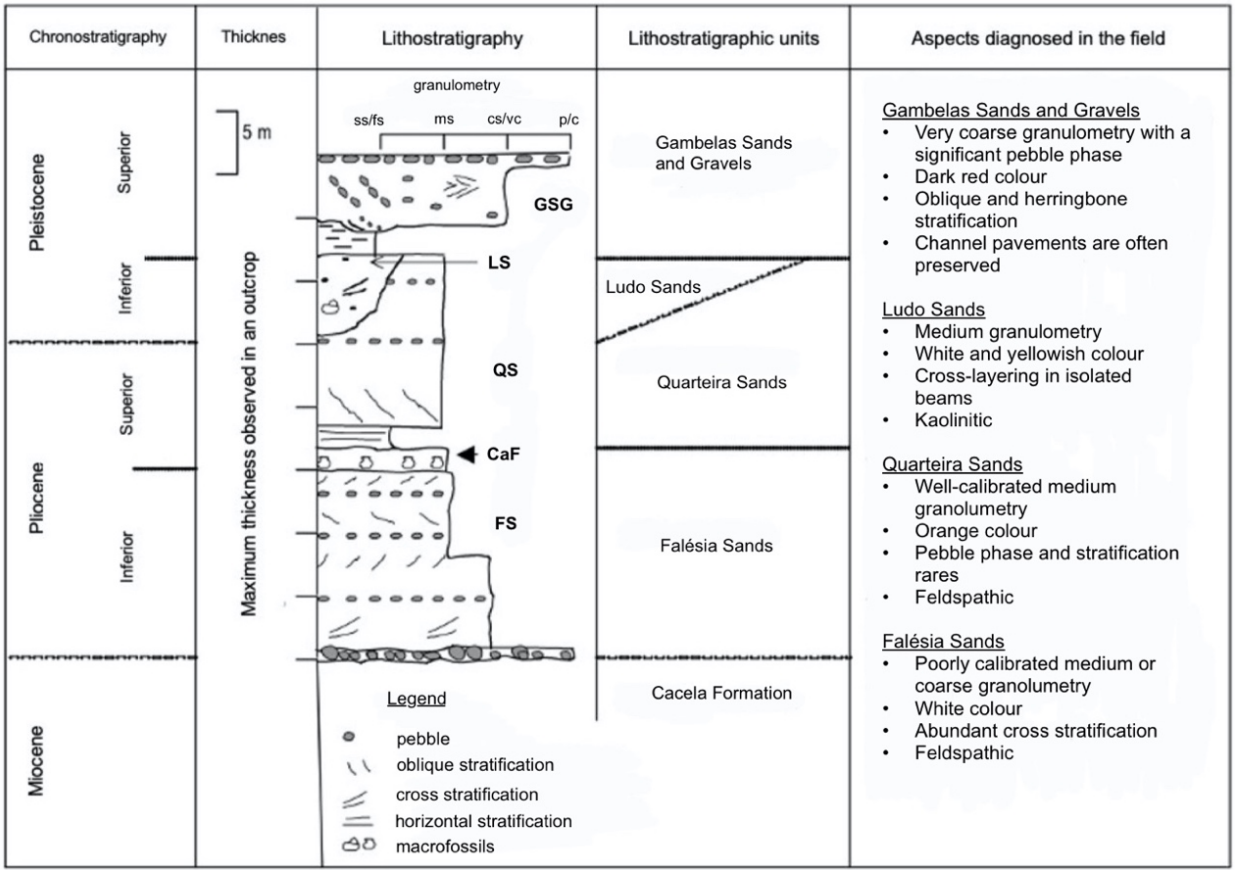

Figure 5: Translated lithostratigraphic column representative of the Plio-Pliocene in the Algarve. In the granulometry indicator bar: ss/fs = sandy silt/fine sand; ms = medium sand; cs/vc= coarse/very coarse sand; p/c= pebble/cod. Gambelas Sands and Gravels – GSG; Ludo Sands – LS; Quarteira Sands – QS; Falésia Sands – FS; Cacela Formation – CaF. Taken from Terrinha et el. (2006).

Sands and muddy sediments are the predominant lithologies exposed in the study area and can be divided according to their percentage in sand (S) and mud (M). According to the Portuguese Hydrographic Institute sedimentological series chart, the Algarve submerged zone is mostly filled with lithoclastic sand of various grain sizes, gravelly sand, lithoclastic silt, lithoclastic sand and lithobioclastic silt, as can be seen in Figure 6 a natural prolongation of the lithological constitution of the Ria Formosa barrier islands.

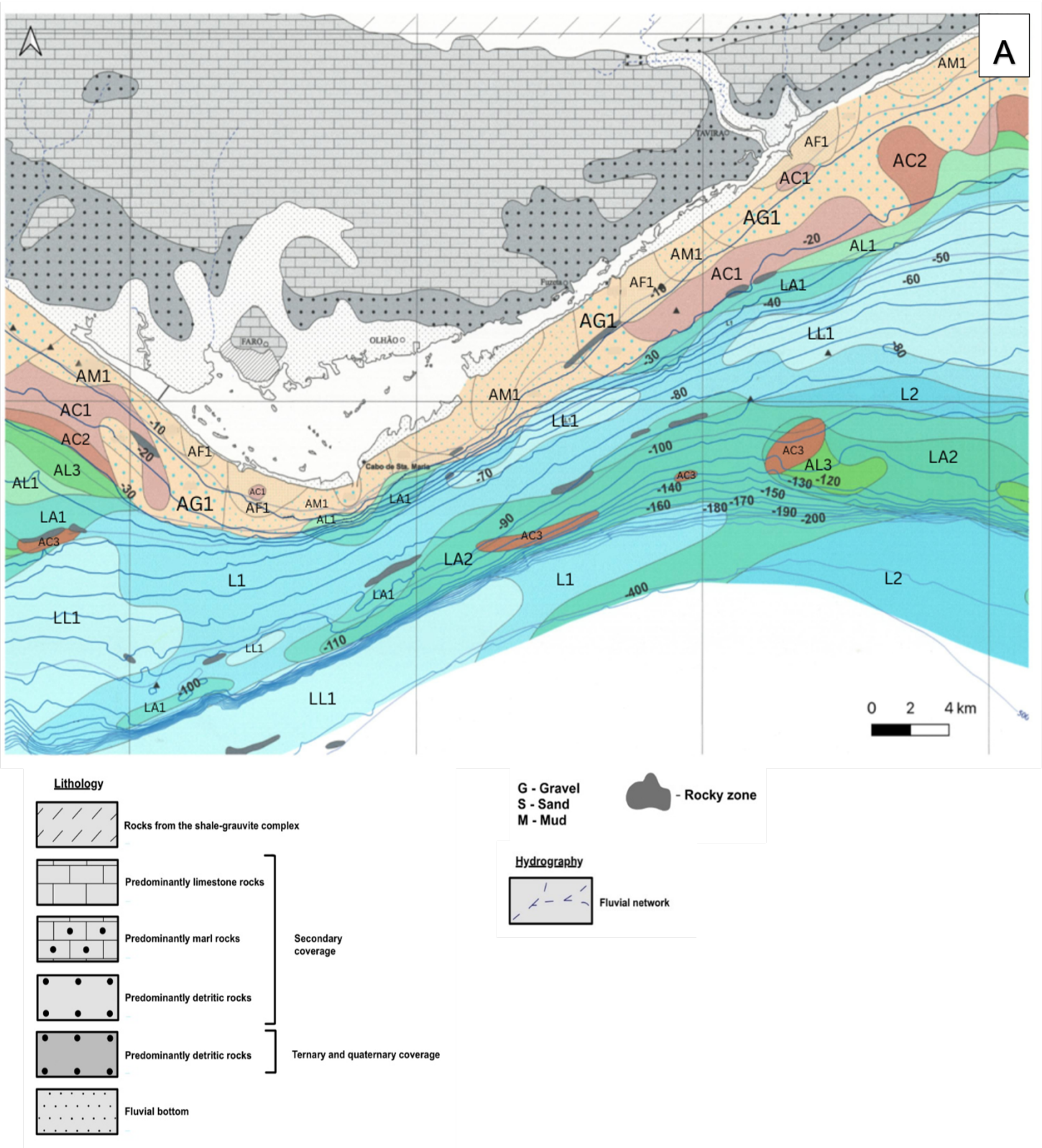

Lithology

- Rocks from the shale-grauvite complex
- Predominantly limestone rocks
- Predominantly marl rocks
- Predominantly detritic rocks — Secondary coverage
- Predominantly detritic rocks — Ternary and quaternary coverage
- Fluvial bottom

G - Gravel
S - Sand
M - Mud

- Rocky zone

Hydrography

- Fluvial network

Figure 6: Chart of the sedimentological series of Portugal produced by the Hydrographic Institute of Portugal in October 2009 (2nd edition), on a scale of 1:150000 (36°55'). A: shows the surface sediments of the continental shelf inserted in the study area, as well as the translated lithology and hydrography legend; B: legend of the sediments present on the continental shelf.

3. The Ria Formosa Barrier Islands System characteristics

As aforementioned, barrier-islands are generally associated with a specific geomorphological setting. The RFBIS have atypical characteristics associated to their geomorphological localization. These barrier-islands sit on a coast that does not exhibit a coastal plain, possibly because this region behaved as a cape during sea-level rise (Pilkey Jr et al., 1989). Also, these barrier-islands occur at the upper tidal range limit (3.88 m spring tidal amplitude) of occurrence of barrier-islands (Hayes, 1979). The lack of a river of significant flow rate located near the study area is also noteworthy. This coast is characterized by minor fluvial input, with the most significant fluvial sediment supply being the Arade River (Lobo et al., 2004), which generates a small prodelta located westward of the study area (cited Lobo et al., 2004 from Moita, 1986).

The triangular shape of the RFBIS produces two areas differentiated in terms of exposure to wave action (Garcia et al., 2010). The western flank, which is exposed to the dominant W-SW waves, is more energetic (Ferreira et al., 2016), while the eastern flank is directly exposed only to the southeast (SE) (*Levante* – Mediterranean wind) waves (Pacheco et al., 2011).

Storms are also a frequent hazard that causes severe impacts, being responsible in the past for the destruction of islands and inlet opening (Garnier et al., 2018). For the study area, they have been defined as events with significant wave heights greater than 3 m, with SW storms being in average more energetic and frequent than SE storms (cited by Ferreira et al., 2016, from Costa et al., 2001; Almeida et al., 2011b). Wave energy is moderate, with an average annual significant wave height of 1.0 m and an average peak period of 8.2 s (Ferreira et al., 2016). The sea wave regime is characterised by waves approaching from a west-southwest direction, resulting in an along-littoral sediment transport, predominantly in a west-east direction (Sousa et al., 2014).

The tides in the area are semi-diurnal, with an average range varying between 1.3 and 2.8 m during neap and spring tides, respectively, and the maximum astronomical tidal level reaching 1.8 m above mean sea level (Garcia et al., 2010). The RFBIS has a vast intertidal area, with a predominance of salt marshes, sandy and muddy intertidal plains, and a complex network of tidal channels.

As previously said, the system is composed of seven features, five islands and two peninsulas. Alongside these, connecting the ocean and the backbarrier area, are six tidal inlets, shown in Figure 7. The west flank only has one inlet, Ancão, although at various times in the past has had up to three tidal inlets (Vila-Concejo et al., 2002). This inlet was artificially relocated in 1997 and in 2015 (Jacob & Cravo, 2019). In the east flank, currently, there are five inlets, although these number varied over time. There are two artificially opened inlets in the system: (a) the Faro-Olhão inlet was open in 1927, and its fixation through the construction of jetties finished in 1952 (Dias, 1988); (b) the Tavira inlet moved naturally to a position east of Cacela around 1923, closing completely in 1930. After, an artificial new inlet was opened in 1927 in Tavira Island, but in 1941 there was a cyclone that reopened a new inlet (*Barra do Cochicho*) immediately to the east of the position of the old artificial channel and began to migrate eastwards. Faced with navigational difficulties, the artificial inlet was reopened in 1961 (Dias, 1988), and was stabilised with jetties in 1985 (cited by Vila-Concejo et al., 2002 in ESAGUY, 1987).

From all the inlets, Armona inlet is considered to be the only naturally stable inlet of RFBIS (Pilkey Jr et al., 1989).

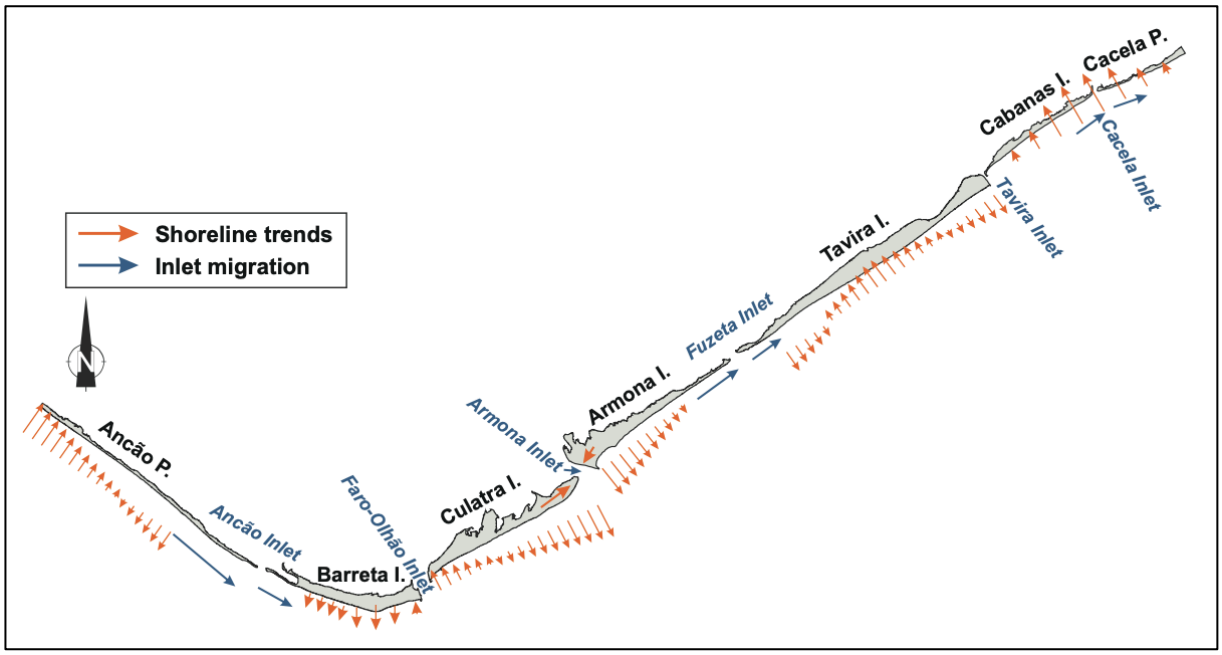

Figure 7: Scheme taken from Kombiadou et al. (2019), where it shows the Ria Formosa barrier island system as well as its inlets, shoreline trends and inlet migration.

3.1. Characteristics and processes involved on the evolution of the system

The evolution of barrier-island systems depends on the interaction of several processes like sediment availability, sediment transport mechanisms (driven by waves and tides, and their interaction), accommodation space controlled by antecedent geomorphology, and sea-level changes (Sousa et al., 2018). According to Pilkey Jr et al. (1989), the evolution of the RFBIS was controlled by six major processes:

According to Pilkey Jr et al. (1989), the evolution of the RFBIS was controlled by six major processes:

1. **Shoreline Retreat** – The factor that most affects the rates of island retreat across the globe is sand supply. In the Algarve, sand supply is large, judging from island volumes and widths, rates of lateral growth and seaward progradation adjacent to inlets. Kombiadou et al. (2019) made an estimation of the recent evolution of the system based on aerial photographs, including human activities with impact to de system (Figure 7).
2. **Longshore sediment transport** – It is a process by which sediments are transported along a coast parallel to the shoreline. In this case study, lateral processes related to the longshore current system may be of greater importance than in most barrier island systems (Pilkey Jr et al., 1989). According to Santos et al., (2014), as cited by Costas et al. (2023), the most recent estimates of longshore sediment supply have mean values on the order of 110,000 m^3/year.
3. **Overwash** – This process brings sediments from the shorefront into the lagoon shoreline from the narrow barriers, contributing to the growth of the backbarrier and eventually, to the landward migration of the barrier through roll over. Usually, this process is associated with storm events and, for this reason, the occurrence of washover deposits in the sedimentary record has been interpreted as evidence of storms (Matias, 2006). The importance of studying overwash processes stem on the need to understand the dynamics of natural barrier systems, obtaining scientific background to inform coastal engineering practices (cited by Garcia et al., 2010 from Schwartz 1975).
4. **Vegetated Dune Formation** – Vegetated dunes are the dominant topographic feature of the RFBIS, and vegetation helps with dune growth. The dunes show significant alongshore morphological variability, as well as changes in the patterns of sediment accumulation within a dune segment (Costas et al., 2020).
5. **Tidal Delta Incorporation** – According to Pilkey Jr et al., 1989, Tavira and Armona islands (location in Figure 7) owe their origin to the incorporation of flood-tidal deltas, inherited or formed after the formation of the islands, after inlet migration or closure. The author also adds that the complex pattern of spring tide channels on the backbarriers resembles the channels and major bedform network of a flood tidal delta, and because of the spring tide amplitudes, flood tidal deltas are often built well above normal high tide levels.
6. **Inlet Migration** – Inlet migration refers to the natural process where tidal inlets shift their position over time. Pilkey Jr et al. (1989), characterizes the RFBIS by having high rates of inlet migration and four patterns or modes of inlet behavior from west to east: (1) progressive easterly migration in a continuous mode followed by a new inlet opening in a former western position and repeating the migration pattern (e.g., Ancão Inlet); (2) stable inlet position that widens and narrows (e.g., Armona inlet); (3) easterly migration in a series of "jumps" as a new inlet opens during a storm a short distance east of the former position (e.g., Fuzeta inlet); (4) inlet breaching after the impact of a storm event in which an island or island segment is totally overwashed and inundated followed by shoaling reemergence and the formation of channels, one of which remains open as an inlet as the island reforms (e.g., Cabanas island).

3.2. Characteristics of the islands and peninsulas

Kombiadou et al., (2019), collected a series of main characteristics – approximate length, width, shoreline trends and overwash vulnerability - from the RFBIS and the evolution trends between 1952 and 2001, based on aerial photographs (Table 1).

Table 1: Compilation of the main RFBIS characteristics and evolution between 1952 and 2001. Table taken from Kombiadou et al., (2019)

Barrier	Approximate length [m]		Width		Shoreline trends[b]		Overwash vulnerability	
	Min	Max	W	E	W	E	W	E
Ancão	8500	12,800	Narrow	Narrow	−	+ (inlet)	Medium	
Barreta	5000	9200	Narrow	Wide	− (inlet)	+ (jetty)	Extreme	Low
Culatra	6200	8800	Narrow	Wide	− (jetty)	+ (spits)	Low	Medium
Armona	3000	6300	Wide	Narrow	+ (inlet)	− (inlet)	Low	Medium
Tavira	11,100	13,700	Narrow	Wide	− (inlet)	+ (jetty)	Low	
Cabanas	0	5100	Narrow	Narrow	− (jetty)	− (inlet)	High	
Cacela	2900	7400	Narrow	Narrow	− (inlet)	÷	High	

b. The symbols used in the Shoreline trends are erosion (-), stability (÷) and accretion (+)

3.2.1. Ancão Peninsula

The Ancão Peninsula is long and narrow (Figure 8). This Peninsula, as well as Barreta Island, is narrow in vicinity of Ancão inlet (Vila-Concejo et al., 2002). This Peninsula has the largest diversity in terms of dune morphologies, it presents the higher dune ridges within the system (Costas et al., 2020) and narrower widths (up to 50 m) along the west part and lower stable and incipient foredunes (4 to 6.5 m above MSL) along the east part (cited by Kombiadou et al., 2019 in Dias et al., 2003; Achab et al., 2014), arranged in a NW-SE direction (Dias, 1988). The western part is characterized by stable frontal dunes and dune cliffs, indicative of an erosive trend (Kombiadou et al. 2019) According to Kombiadou et al. (2019), the west-central coast of the peninsula shows mild erosion. The eastern part is more dynamic, with incipient frontal dunes (Ferreira, 2016, Costas et al. 2023) associated with an accumulative trend. According to Kombiadou et al. (2019), on the east side there are accretive tendencies and dune construction prevails with highly variable rates in the inlet-affected zone (Figure 7). They also refer that the marshes are generally stable, with low average growth rates and that

The inlet that separates this peninsula from the nearest island (Barreta) is the Ancão inlet. The natural migration tendency of this inlet is a cyclic migration eastward (Jacob & Cravo, 2019), as we can see in Figure 8.

Figure 8: A: Satellite photography from Google Earth of Ancão Peninsula from 2013. B: Satellite photography from Google Earth of Ancão Peninsula from 2023. Zoom out image at the top right corner.

3.2.2. Barreta Island

Barreta Island has a curved shape (Figure 9) and its southern tip is known as Cape Santa Maria. Is about 8000 m long and its width varies between 85 and 700 m (Dias, 1988). There are several dune ridges, the complexity of which increases from west to east (Dias, 1988). The island is more or less stable but in the zone affected by the Ancão inlet migration, the coastline is prograding seawards (Kombiadou et al., 2019, Herrero et al. 2020). The construction of the artificial Faro-Olhão inlet, located on the east part of the island, interrupted the longshore sediment transport, causing an intense accumulation of sand near the west jetty or updrift inlet shoreline (Kombiadou et al., 2019, Herrero et al. 2020). In Figure 9 we can see the inlet jetties that separate Barreta from Culatra island whose construction started in 1927 and ended in 1952 (Dias, 1988).

Figure 9: A: Satellite photography from Google Earth of Barreta Island from 2013. B: Satellite photography from Google Earth of Barreta Island from 2023. The sandy cuspate shape that marks the southern-most part of the island is the Santa Maria Cape. Zoom out image at the top right corner.

3.2.3. Culatra Island

Culatra Island is SW-NE orientated and it has a distinct shape (Figure 10). The island is wider on its west side (479 m), with a higher and generally continuous frontal dune, and it becomes narrower toward the east (387), with low interrupted dune ridges that are connected to tidal channels (Garcia et al., 2010). Its western part is a sediment-starved zone due to the updrift construction of the Faro-Olhão inlet jetties (Ferreira et al., 2016) and it shows signs of erosion and shoreline retreat over the ocean shore. In the eastern part, the growth has been very rapid over recent years (Kombiadou et al, 2019).

According to Pacheco et al. (2011), in the period from the opening of Faro-Olhão inlet to the present, the length of Culatra Island has almost doubled, and there appears to be an obvious relationship between the narrowing of Armona inlet, the cross-sectional increase of Faro-Olhão inlet, and the increase in size of Culatra Island. Their data also indicates that the cross-section of the Faro-Olhão inlet has reached stability, suggesting that the inlet is now stable in a morphodynamic sense, which means that the dimensions of Culatra Island have stabilized or are near stabilization.

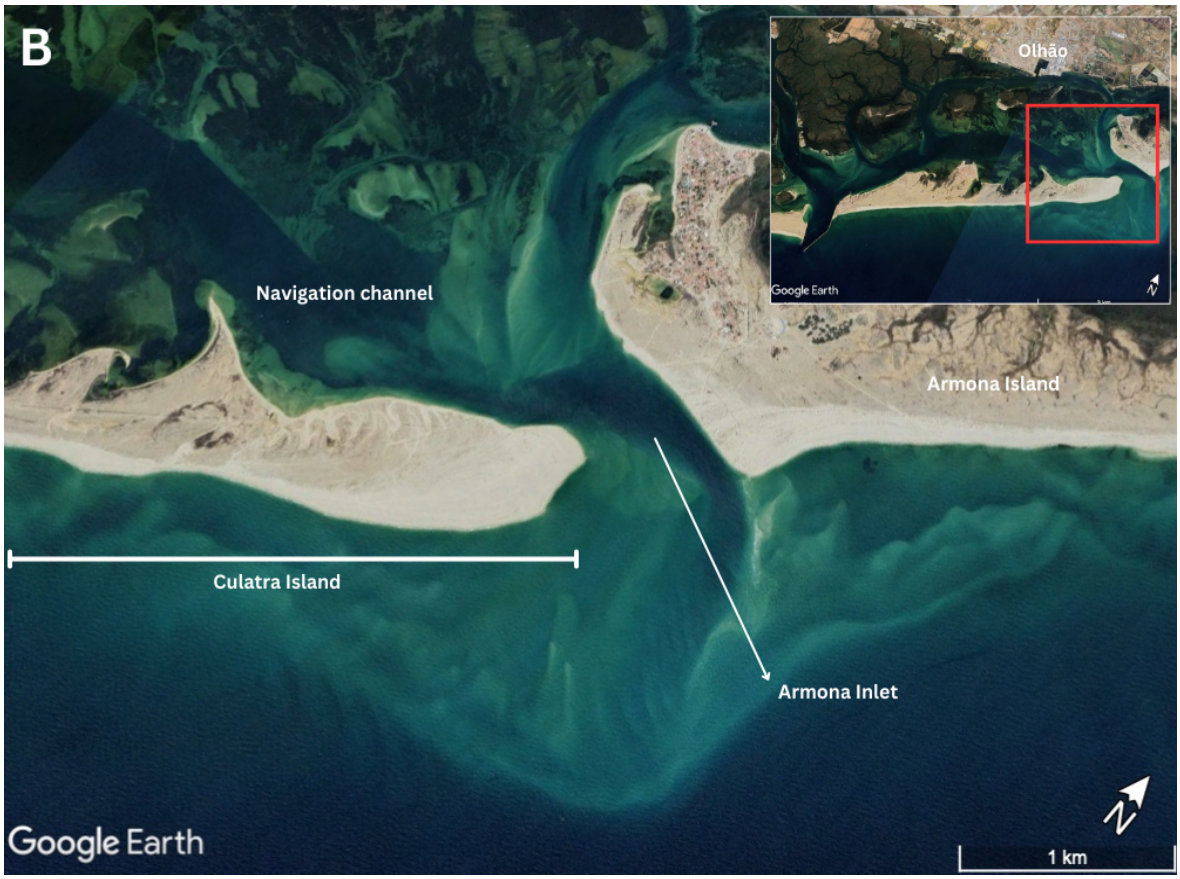

Figure 10: A: Satellite photography from Google Earth of Culatra Island from 2013, the complete island is shown in a smaller image at the top-right corner of the figure, showing with a red square the area of zoom. B: Satellite photography from Google Earth of Culatra Island from 2023. Zoom out image at the top right corner.

3.2.4. Armona Island

Armona Island is orientated SW-NE. The western side of the island (387 m) is wider than the eastern side (73 m) (Figure 11), and it has a generally high and continuous frontal dune while dunes along the eastern part are low or absent (Garcia et al., 2010). Still on the west side, the island is characterized by dune progradation and shows fast barrier and dune width growth, and it has become the widest section in the barrier island system (Kombiadou et al., 2019). Its western growth is due to a littoral drift inversion at the Armona ebb delta (Garcia et al., 2010). Over the last 40 years, the island has grown to the NE (Kombiadou et al., 2019). It is characterized by high, continuous frontal dunes and large backbarrier areas (Ferreira, 2016).

Figure 11: A: Satellite photography from Google Earth of Armona Island from 2013. B: Satellite photography from Google Earth of Armona Island from 2021. Zoom out image at the top right corner.

3.2.5. Tavira Island

Tavira Island is the largest and longest in the system (Figure 12), with a SW-NE orientation and an elongated shape. The island maximum width is 394 m (Garcia et al., 2010) and has a single continuous frontal dune, supported by an extensive backbarrier (Ferreira et al., 2016). The island is retreating along its western-end due to a lack of sediment supply, while the eastern end is accumulating sediment due to the construction of the Tavira artificial inlet in 1961 (Dias, 1988). The island narrows progressively to the SW, with signs of strong erosion at this end, and, at low tide, there are clear outcrops of silty-clay materials at this end, with high vegetation content typical of a salt marsh environment, which is overlaid by the sands that make up the island (Dias, 1988). Due to the perched marshes the lagoon-side is stable. According to Kombiadou et al. (2019) barrier and dune widths follow the coastline trends, with low and variable values near Fuzeta inlet, narrowing trends in the west and central parts of the island and widening in the eastern side.

Figure 12: A: Satellite photography from Google Earth of Tavira Island from 2013. B: Satellite photography from Google Earth of Tavira Island from 2021. Zoom out image at the top right corner.

3.2.6. Cabanas Island

Cabanas Island is the smallest island in the system (Figure 13), with a width of 123 m (Garcia et al., 2010), and corresponds to the NE extension of Tavira Island, from which it is separated by the Tavira artificial inlet (Dias, 1988). It was completely eroded by a major storm in 1961 and has been recovering by natural processes since then, switching to a system at a fully mature state in 1985, and this also applies to Cacela Peninsula (Kombiadou et al., 2020). Cabanas Island is highly interlinked with Cacela Peninsula, especially after the stabilization of Tavira inlet (Kombiadou et al., 2019). These two, were initially, during the phase of inland migration, characterized with loss of width, rapid increase of precariousness and immature barrier, marsh, and dunes during the phase of inland migration (Kombiadou et al., 2020).

Figure 13: A: Satellite photography from Google Earth of Cabanas Island from 2013. B: Satellite photography from Google Earth of Cabanas Island from 2019. Zoom out image at the top right corner.

3.2.7. Cacela Peninsula

The Cacela Peninsula is the eastern end of the system (Figure 14), and its approximately width is 113 m (Garcia et at., 2010). It has certain similarities to the Ancão Peninsula, as it is made up of a single dune ridge. This peninsula is narrow and low and it is covered by vegetated dunes (Ferreira et al., 2016) and is subject to accelerated erosion due to the migration of the Cabanas inlet (Dias, 1988). Similarly, to the Ancão Peninsula, it has cliffs in a state of inactivity, in the backbarrier (Dias, 1988).

Figure 14: A: Satellite photography from Google Earth of Cacela Peninsula from 2014. B: Satellite photography from Google Earth of Cacela Peninsula from 2023. Zoom out image at the top right corner.

3.3. Last Glacial Maximum (LGM)

Throughout the geological time there has been changes in the relative sea-level, due to tectonic, isostatic and Earth rotation processes, as well as variations in ocean volume and mass induced (primarily) by climatic changes (Leorri et al., 2012). During ice ages, the main cause for the sea-level changes is the exchange of water between ice and ocean and the Earth's dynamic response to the changing surface load (Lambeck et al., 2014).

During a period of sea-level rise (marine transgression), barrier islands tend to migrate inland, following the coastline and this process is called retrogradation. During a period when the sea-level drops (marine regression), barrier islands tend to move towards the ocean and this process is called regression. These eustatic variations leave distinct marks in the sedimentary record, which can be analysed using reflection seismic profiles, thus enabling us to understand their evolution over geological time.

There have been measurements of the past sea level made from numerous records observed from around the globe. With that data, curves that relate relative sea level and time can be made. Lambeck et al. (2014) analysed 1,000 observations from around the world indicative of relative sea-level changes for the past 35 ka, underpinned by independent near-field analysis for the individual major ice sheets of the Northern Hemisphere and inferences about the past Antarctic ice sheet. With this, a curve, that relates the observed relative sea level (m), and the time (ka), was made (Figure 15). According to the authors, and as we can observe from Figure 15, from the start there has been a period of relatively slow fall in the sea level from 35 to 31 ky BP followed by a rapid fall during 31-29 ky. Approximately constant or slowly increasing ice volumes occurred from ~29-21 ky BP. Following the maximum low, deglaciation occurred at ~21-20 ky BP with a small sea-level rise of ~10-15 m before 18 ky. A major phase of deglaciation occurred from ~16.5-7 ky BP. From 6.7 ky to recent time there was a progressive decrease in the rate of sea-level rise, i.e., stabilization.

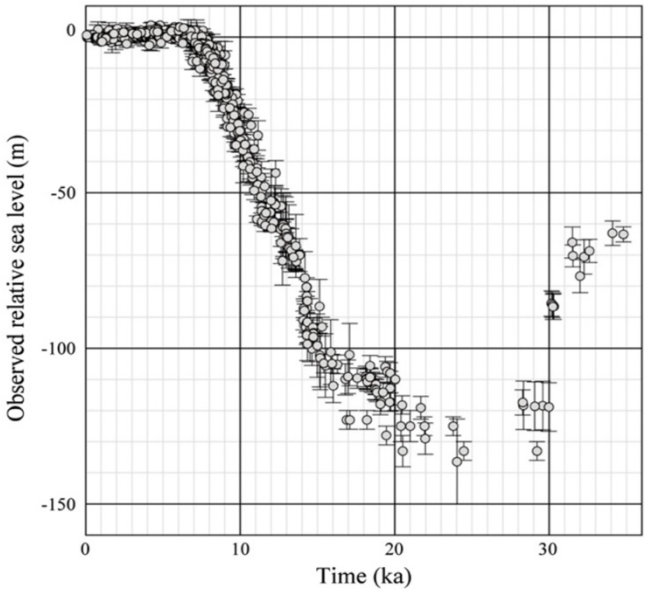

Figure 15: Curve representing relative sea-level. Depth-age relationship of all data with 2σ error estimates. Taken from Lambeck et al., 2014.

Although global sea-level curves are extremely important for understanding various events that have taken place on Earth, local and regional changes become more important as the temporal scale resolution increases (cited by Leorri et al., 2012 from Lambeck and Chappell, 2001). This is due to the combination of eustatic sea-level changes, changes in the gravity field and vertical land movements, producing significant special and temporal variability in sea-level changes (Leorri et al., 2012).

In Portugal, the first proposal for a relative sea-level rise variation (Figure 16), covering the last 18 ky was published by Dias et al., (1985). Over time we have seen that this proposal does not agree with the global and more recent curves, although this curve doesn't go that far back in time and it also suggests a rise around 11.5 ky that is not seen in other curves, so this has been updated. According to this curve, the sea level would have been around -120 m to -140 m during the Last Glacial Maximum (LGM), after which it started rising until it reached approximately -100 m level 16 ky BP, when it stabilized or fell slightly. Since 13 ky BP, there was another very rapid sea-level rise, reaching - 40m between 12 and 11 ky BP, after which it fell rapidly to – 60 m. Around 10 ky BP there was a further very rapid rise in sea level, with rates of rise until around 8 ky BP, when the sea level was around – 30 m. The present sea level was reached ca 3500 y BP according with the same curve.

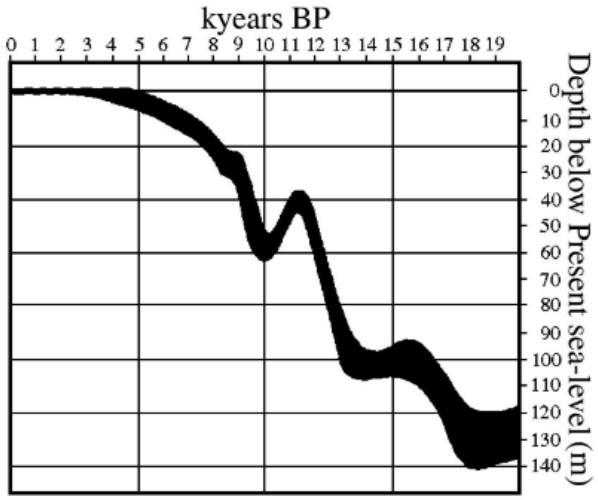

Figure 16: Sea level rise curve for the N part of the Portuguese shelf since the LGM. The curve width expresses the quantitative incertitude with respect to sea level and age. Taken from Dias et al. (2000).

During the Holocene, since 11.7 ky BP, the sea advanced very rapidly on the Portuguese shelf, rising about 40 m in just 2 ky (Dias et al., 1997). The migration of the coastline would have been so rapid (Figure 16) that coastal processes would not have been able to erode the coastal sedimentary forms of the previous phase (Dias et al., 1997). New coastal features like barriers and lagoons developed after 4000 – 5000 y BP at the time when the rates of sea level rise were strongly attenuated (cited by Dias et al., 2000 from Bao et al., 1999). According to Costas et al., (2016), the work made to provide a new sea-level reconstruction for the central Portuguese coast shows that a continuous but slow sea-level rise after 6.5 ky with an accumulated change in elevation of about 2 m.

According to Bettencourt (1994), as cited by Dias et al. (2000), data from the Ria Formosa Lagoon indicate that the sea level reached its present position between 5 to 2.5 ky BP.

Comparing the global that was used in this work and the curve from Dias et al. (2000), we can see that in Figure 15, the variations of the curve were less abrupt in the global curve, i.e., there are not major fluctuations of the sea-level curve.

3.4. Previous studies and propositions for the RFBIS barrier islands formation

Some authors made proposals to explain the formation of the RFBIS throughout the years, although, there is still no conclusion about the formation of the RFBIS. The one thing that is common to all is that the origin of the system occurred after the rise of sea level, so it is related to sea-level fluctuations.

According to the definition of Oertel (1985) about what is necessary for systems to be considered as barrier island systems, the RFBIS contains true barrier islands because they have the six required sedimentary environments (mentioned above) and the processes of their evolution are almost the same as for other systems.

Pilkey Jr et al. (1989) proposed that the existence of this unusual chain of barrier islands is related to the presence of a shallow shelf bounded by a relatively steep scarp or protuberance on the inner continental shelf. The author suggests that as sea level rose beyond the base of the shelf scarp, the shoreline began to pivot on the escarpment. That is, shoreline retreat on the scarp was less than shoreline retreat in the areas to the east and west. When the sea-level rose over the edge of the continental shelf, shoreline retreat was suddenly quite rapid, causing the former spits to begin evolving as barrier islands. At some point in this scenario, a spit from the mainland to the west joined the barrier island chain resulting in the interrelated sediment system of the present barrier-island chain. Putting it another way, the RFBIS probably originated as spits connected to a cape. These spits were detached when the shoreline retreat accelerated in response to the sea level rise over the lip of a platform. The former spits became true barrier islands existing in a dynamic equilibrium between wave and tidal energy, sand supply and sea level. Their existence is a geologically ephemeral one as mainland attachment is a certainty in a future rising sea level. The evolution proposed by Pilkey Jr et al. (1989) is showed in Figure 17.

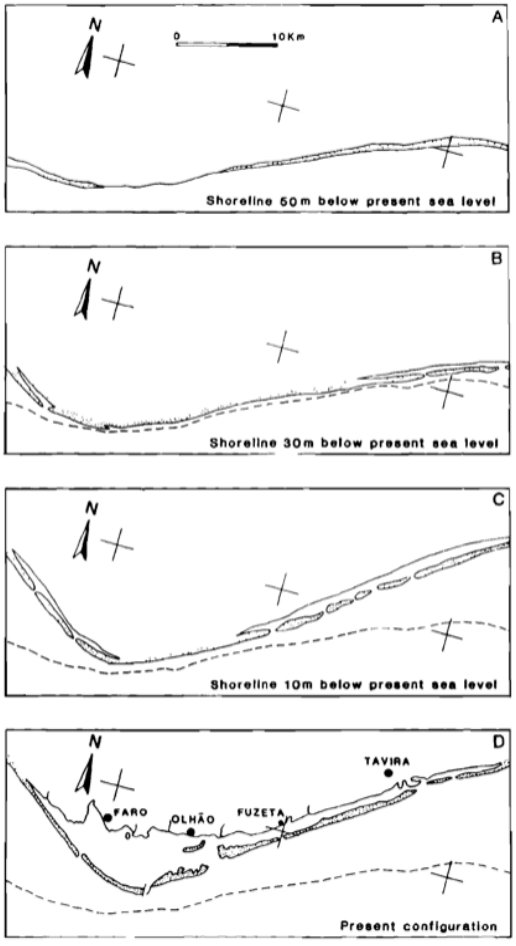

Figure 17: Model retrieved from Pilkey Jr et al., 1989 in which it shows the evolution of the barrier islands.

Sousa et al. (2018) acquired subsurface stratigraphy data from boreholes in the backbarrier area of the RFBIS. These were combined with a multi-proxy analysis and a three-dimensional surface model of the previous Holocene topography, in order to create the first comprehensive sequence of processes leading to the Holocene sediment infilling of the lagoon. The conceptual model for the origin and Holocene evolution of the RFBIS that was made in this study is shown in Figure 18. From their study, we take that the Holocene evolution of the system followed a twofold pattern due to a significant shift in sea-level rise rate, changing from transgressive to aggradation processes. Over the transgressive stage, during the early Holocene ca. 10.000–8000 cal. yr BP, sand migrated landward as sea level quickly flooded an irregular topography, giving place to bayhead deltas where water depth created accommodation space. Over the aggradation phase, following a sea-level rise slowdown around 7500 cal. yr BP, the surface occupied by the flooded valleys diminished rapidly due to increasing sedimentation at the interfluves steeper margins. They conclude that the geomorphology of the system quickly modified, giving place to dynamic equilibrium processes that maintained the present configuration of the RFBIS.

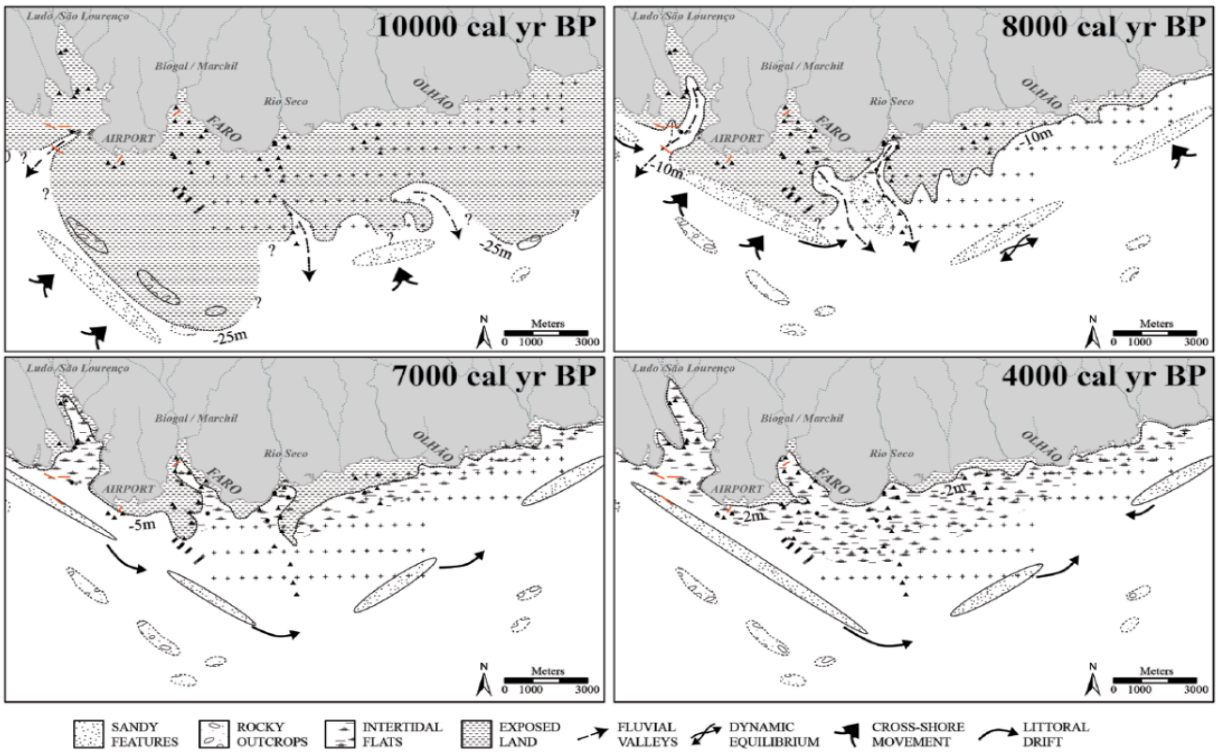

Figure 18: Paleo-reconstruction of the changing geomorphology of the RFBIS during the Holocene, in which four time steps were selected as representative: 10,000 cal. yr BP; 8000 cal. yr BP; 7000 cal. yr BP; and 4000 cal. yr BP. Taken from Sousa et al. (2018).

The two models proposed by Pilkey Jr et al. (1989) and Sousa et al. (2018) provide different conceptualizations for the formation and evolution of the RFBIS, primarily linked to sea-level rise and the geomorphological responses of the region.

Summarising, the Pilkey Jr et al. (1989) model says that the formation of the RFBIS is attributed to shoreline retreat over a continental shelf, with spits evolving into barrier islands as sea level rose beyond the continental shelf edge. The shoreline pivoted around a steep escarpment, causing differential shoreline retreat. The Sousa et al. (2018) model is based on subsurface stratigraphy and a detailed

analysis of Holocene sediment infill, this model describes a two-stage evolution driven by changes in sea-level rise rates.

Comparing the two models, regarding the shoreline dynamics, Pilkey Jr et al. (1989) emphasize the role of the continental shelf escarpment in shaping the differential retreat of the shoreline and the subsequent evolution of barrier islands, while Sousa et al. (2018) focus on the role of subsurface stratigraphy and topographical features, suggesting the systems geomorphological changes were driven by shifts in sea-level rise rates and sediment infilling. The evolutionary stages and the role of the sedimentation of the two models also differs. Pilkey Jr et al. (1989) primarily discuss the evolution after the sea level crossed the shelf edge, resulting in a sudden acceleration of shoreline retreat, and the sedimentation is tied to wave and tidal energy acting on former spits and the dynamic equilibrium of the system. Sousa et al. (2018) offer a more nuanced view with two evolutionary phases—transgression followed by aggradation - both influenced by sea-level fluctuations, and when it comes to the sedimentation, the model presents it as a major factor during the aggradation phase, driving valley infilling and the stabilization of the barrier system.

Despite the insights provided by both models, several unresolved questions remain regarding the formation and evolution of the RFBIS. For example, while both models agree that sea-level rise played a crucial role, the precise timing and rate of sea-level rise influencing the systems evolution remain uncertain. Pilkey Jr et al. (1989) propose the RFBIS originated as spits that detached due to shoreline retreat, but how exactly these spits detached and evolved into barrier islands still requires further clarification.

4. Previous campaigns data and interpretations

4.1. Campaigns

Over the years, oceanographic campaigns have been carried out along the south coast of Portugal as part of scientific research projects. High-resolution reflection seismic data have been obtained off the RFBIS, through three different campaigns: (a) ERSTA-SANDEX - carried out between 19th and 28th November 2008; (b) FREEZE2_TOPOMED – carried out between 4th and 15th April 2011; (c) ASTARTE - the only seismic lines analysed were those from this campaign.

4.1.1. ASTARTE

4.1.1.1. High-resolution multichannel seismic data collection

The ASTARTE high-resolution multichannel seismic campaign was funded by the ASTARTE project (Assessment, Strategy and Risk Reduction for Tsunamis in Europe, ENV.2013.6.4-3: Endangered coastlines in Europe: tsunamis and climate-related risks). It took place from 19 to 29 May 2014.

The main objective was to search for and map tsunami deposits and/or erosion structures caused by tsunamis in the sedimentary record of the continental shelf off Quarteira-Tavira in the Algarve, southern Portugal. Additional objectives included investigating the geographic-environmental changes that affected the Quarteira coastal area in the recent geological past, i.e., the Holocene and Upper Pleistocene, and their relationship with neotectonics and seismicity. The coverage of the ASTARTE campaign is shown in Figure 19. The vessel used to carry out the seismic survey was Xunauta. A high-resolution Multichannel Seismic (MCS) system from Geo Marine Survey Systems (Netherlands) was contracted through Geosurveys (Portugal) to acquire the seismic reflection data. At the same time, high-resolution single-channel seismic reflection (SCS) data were also acquired using Geo Marine Survey Systems equipment. A Geo-Spark 1000 1kJ Pulsed Power Supply unit was used together with a Geo- Source 200 Light Weight Marine Multi-Tip Sparker and a 75 m Geo-Sense Light-weight 24 Channel Ultra High Resolution Streamer with group interval of 3.125 m. The processing and interpretation focused on the Late Quaternary depositional units.

At the end of the ASTARTE campaign, a report was made in 2017 (Drago et al., 2017), containing information about the new results of the offshore record of tsunami deposits and MTDs (Mass Transport Deposits) in the NEAM (North-Eastern Atlantic, Mediterranean and Connected Seas) region.

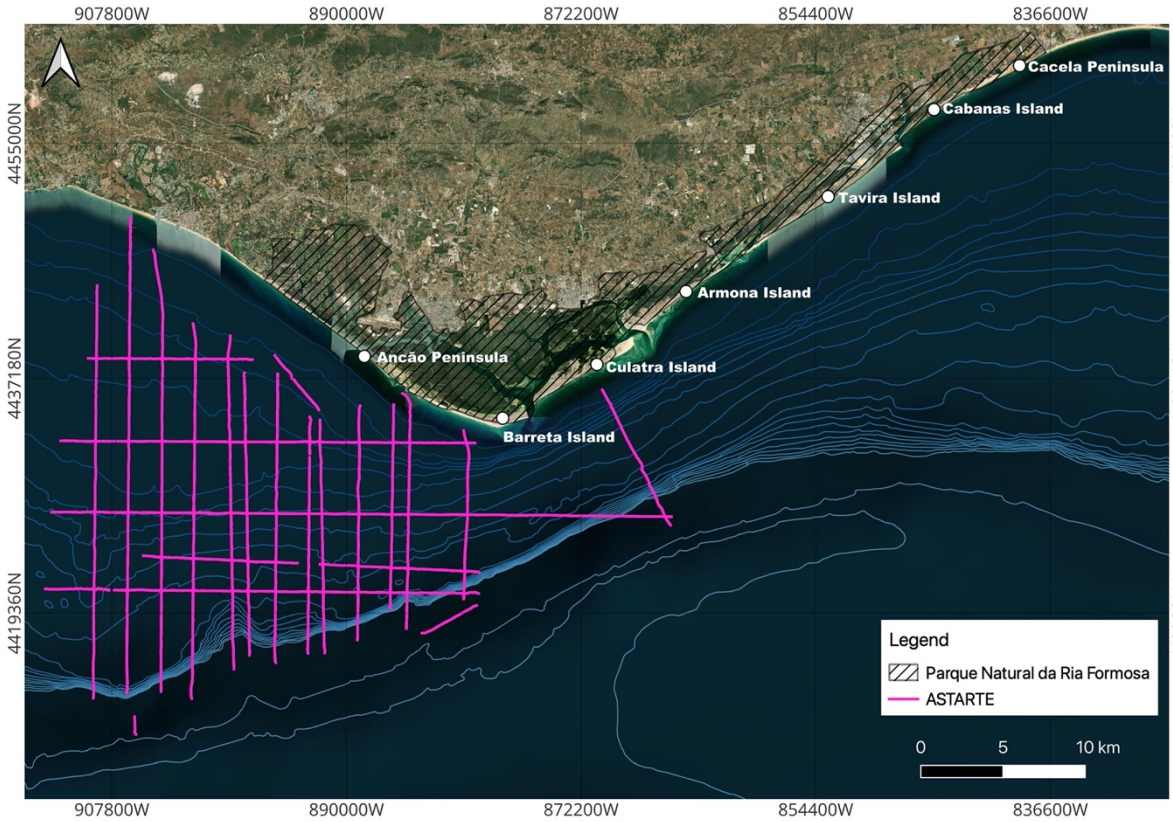

Figure 19: The map shows the work carried out in the study area, of the ASTARTE seismic lines. The bathymetric lines are 10 m apart starting at 10 m depth.

4.1.1.2. Sediment record from cores

During the ASTARTE campaign new cores were supposed to be collected, but it was not possible to collect them, so it was necessary to analyze previously collected gravity cores that overlap the seismic profiles, once the campaign was over. The study focused on pre-existing cores collected during the POPEI and MOWER projects located in the area of interest.

The POPEI gravity cores Popei-1 (1-1CGG) and Popei-2 (2-1CGG) (project reference: FCT-POCTI/MAR/55618/2004) were collected in southern Portuguese continental shelf, westward of Cabo de Santa Maria (Figure 20). They were collected in 2008 and preserved at temperatures of 4ºC.

MOWER gravity cores MW14-105 and MW14-107 were collected in September of 2014 on board of the research vessel Sarmiento de Gamboa in the context of the Spanish national project with the same name (reference: CTM 2012-39599-C03). They were obtained at sites near the POPEI cores (Figure 20). The information of the cores that are located in the area of the ASTARTE seismic lines is presented in Table 2.

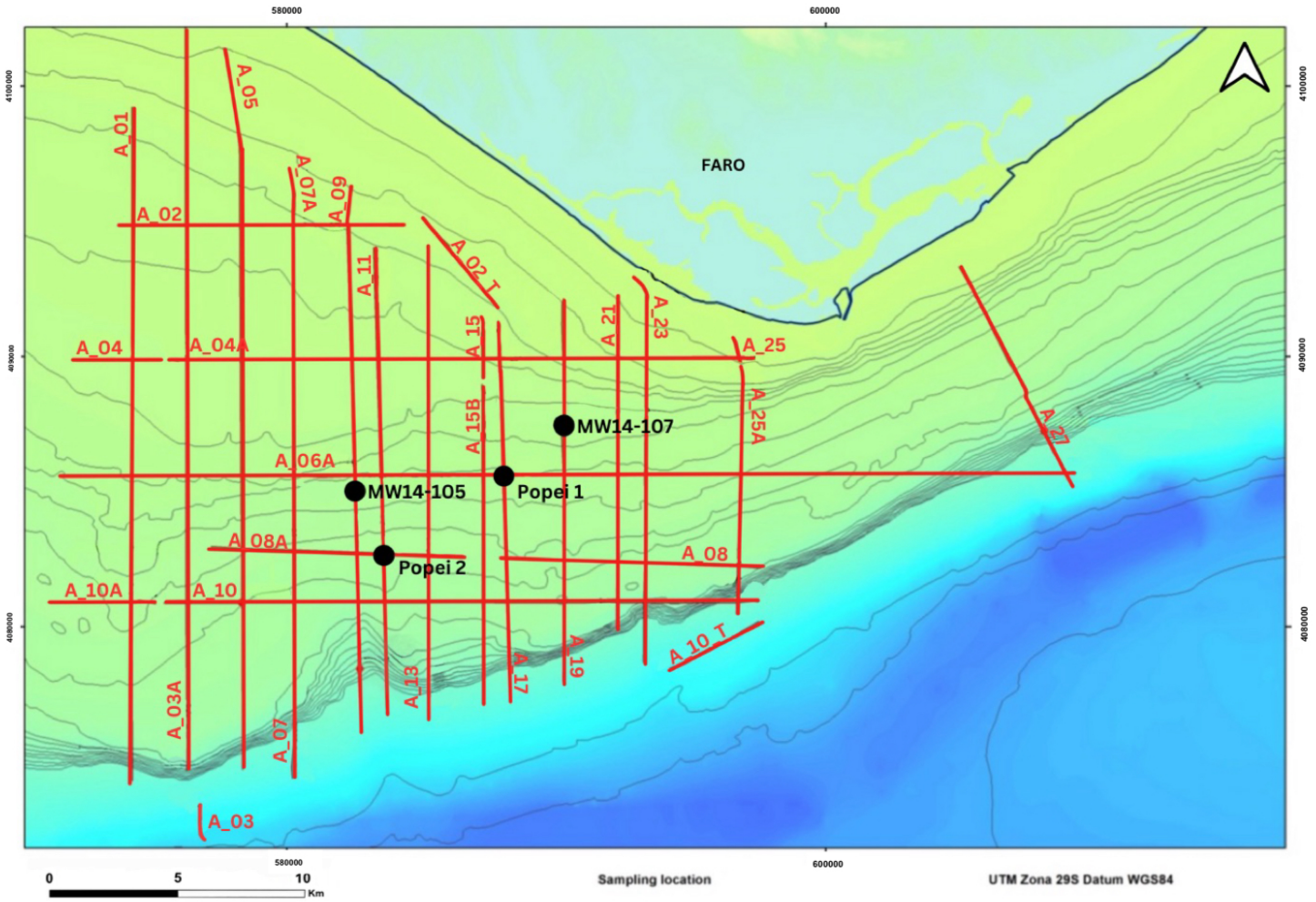

Figure 20 - Location of the POPEI and MOWER cores. The red lines are the ASTARTE seismic lines. Adapted from (Drago et al., 2017).

Table 2 - Location, water depth and length of the cores that intersect ASTARTE seismic lines.

Core name	Coordinates		Water depth (m)	Core length (m)
	Latitude	Longitude		
POPEI 1-1-1CGG	36.9123235 36°54'44.36'' N	-8.0117995 8°00'42.48''W	76.0	1.84
POPEI 2-2-1CGP	36.8859583 36°53'9.45''N	-8.061872 8°03'42.74''W	84.5	1.80
MW14-105	36.9079325 36°54'28.56''N	-8.073539336 8°04'24.74''W	76.1	2.50
MW14-107	36.92940173 36°55'45.85''N	-7.986915312 7°59'12.90''W	56.8	1.25

The cores were separated into sections, as we can see in Figure 21and Figure 22, for their laboratory analysis. Visual inspection of POPEI (Figure 21) and MOWER (Figure 22) cores are mostly fine grained sand, silt and mud, homogenous and with clear signals of bioturbation. Sediment colour varies usually between light olive gray to olive gray. Sediment becomes coarser towards the base with occurrence of fragmented shells. The POPEI and MOWER cores show a typical transgressive succession with sediments suggesting decreasing energetic depositional regimes from bottom to top of the cores.
The base of the MOWER cores contain chaotic massive and unstructured sand rich in large shells, found in MW14-107 varying between 1.5-7 cm, and fragmented shells. X-ray CT scans were conducted on the cores, and they confirm the lamination structure of the cores.

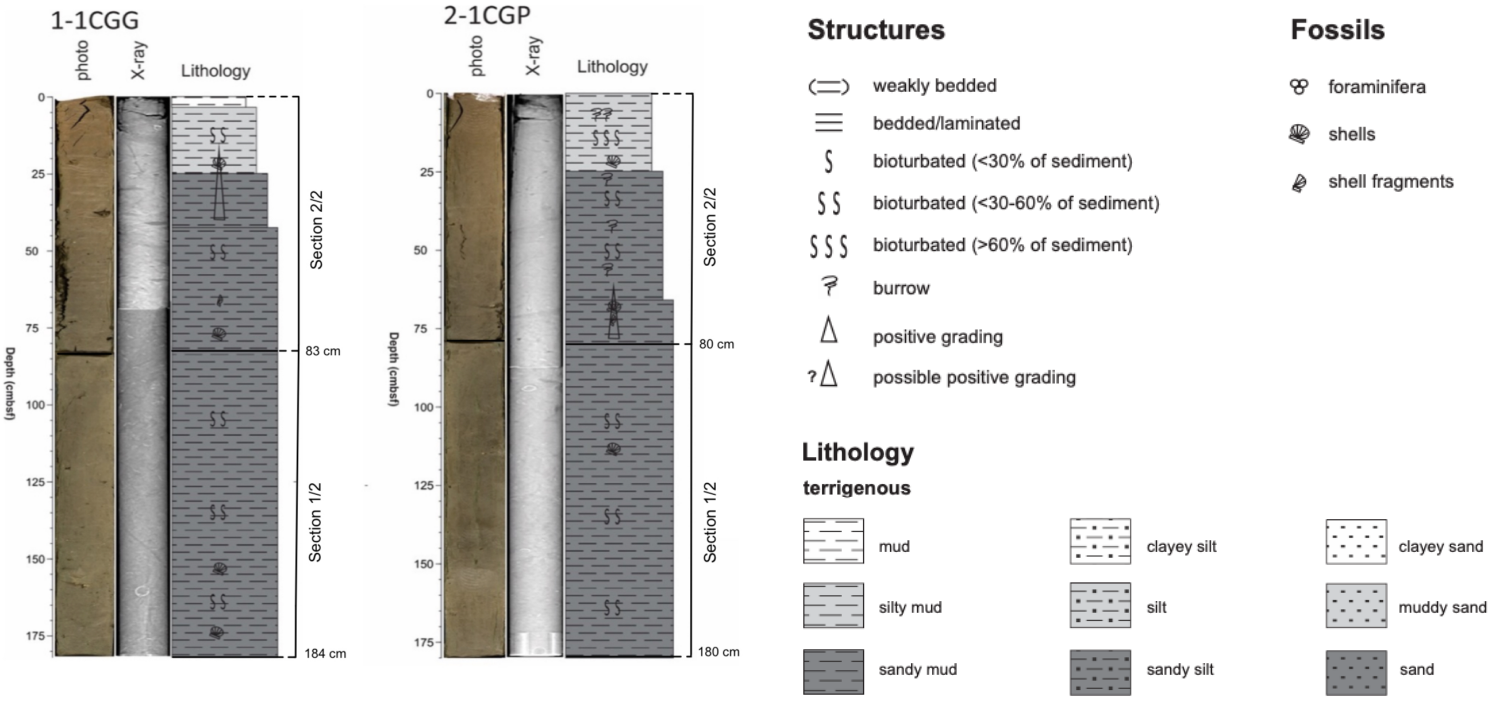

Figure 21 - X-ray, photo, and visual description log of the POPEI cores used and respective stratigraphic and lithological legend. 1-1CGG = POPEI 1; 2-1CGP = POPEI 2.

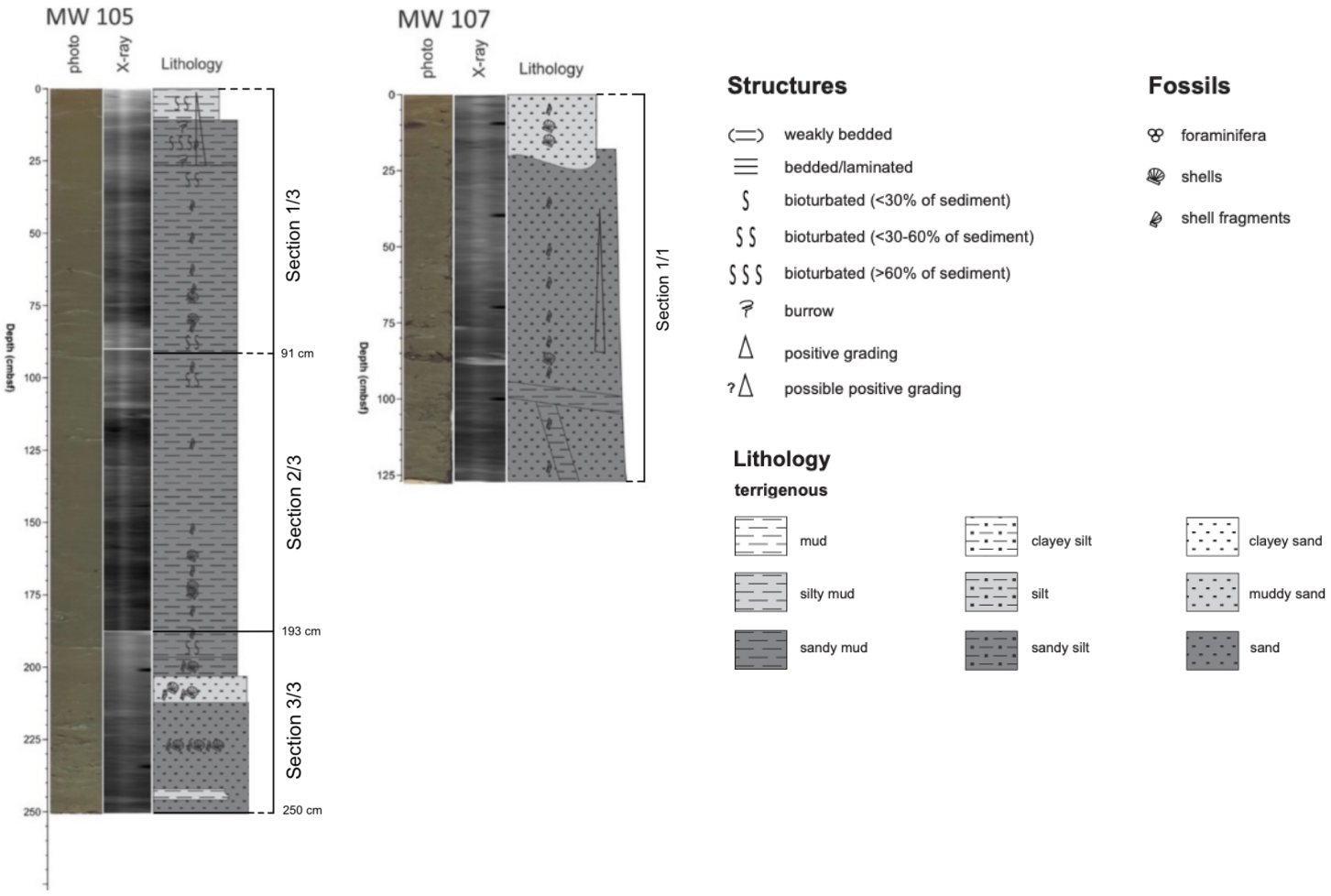

Figure 22 - X-ray, photo, and visual description of the three MOWER cores used and respective stratigraphic and lithological legend.

According to the ASTARTE campaign report (Drago et al., 2017), during the analysis of the cores, the dating of the cores was obtained by Accelerator Mass Spectrometry (AMS) from ^{14}C. Of all the analyses made on the cores, Table 3 shows the results of the dating of the cores that intersect ASTARTE lines.
In Table 3, the "Conventional Age" refers to the estimates of the age of organic materials by measuring the amount of C^{14} present. The "Calibrated Age" refers to the actual age of an object in calendar (Gregorian) years, and this calibration is necessary because C^{14} concentrations in the atmosphere vary over time. There were also some different notations that the authors used to classify the ages in Table 3. The notation BP (Before Present) is used in radiocarbon dating, which defines the 'present' as the year 1950. The notation AD ("Anno Domini") indicates calendar years after Christ. The notation BC (Before Christ) is close to the BP notation, but in this case refers to calendar years before the birth of Christ (the year 0 in the Gregorian calendar). Thus, both systems provide calibrated dates, but Cal BC is expressed directly in terms of years before the birth of Christ, while Cal BP is based on years before 1950.

Table 3: AMS C^{14} dating of the cores that intercepted ASTARTE lines. Information taken from Drago et al. (2017).

Event number	Core	Depth bsf (bottom of sea floor) (cm)	Conventional Age	Calibrated Age
1	**POPEI 1-1CGG** Water depth: 76 m Length: 1.84 m	51-52	960 ± 30 BP	Cal AD 1460 to 1820 (Cal BP 490 to 130)
2		78-79	1140 ± 40 BP	Cal 660 - 720 AD
3		113-114	2130 ± 30 BP	Cal AD 355 to 700 (Cal BP 1595 to 1250)
4	**POPEI 2-1CGP** Water depth: 100 m Length: 1.78 m	60-61	660 ± 30 BP	Cal AD 1705 to Post 1950 (Cal BP 245 to Post 0)
5		89-90	1240 ± 30 BP	Cal AD 1270 to 1505 (Cal BP 680 to 445)
6		132-133	2130 ± 30 BP	Cal AD 355 to 700 (Cal BP 1595 to 1250)
7		158-159	2670 ± 30 BP	Cal BP 335 to AD 130 (Cal BP 2285 to 1820)
8	**MW14-105** Water depth: 79,62 m Length: 2.50 m	79-80	1140 ± 30 BP	Cal AD 1320 to 1645 (Cal BP 630 to 305)
9		125-126	2450 ± 30 BP	-
10		155-156	3280 ± 30 BP	Cal 1630 - 1500 BC
11		165-166	3480 ± 30 BP	Cal 1880 - 1690 BC
12		186-188	4200 ± 30 BP	-
13		204-206	5350 ± 40 BP	Cal 5750 - 5560 BC
14		235-236	8280 ± 30 BP	Cal 7460 - 7190 BC
15	**MW14-107** Water depth: 58.27 Length: 1.25 m	28-29	1380 ± 40 BP	Cal 900 - 960 AD
16		68-69	3380 ± 30 BP	Cal 1740 - 1620 BC
17		90-91	5260 ± 30 BP	-
18		110-111	5600 ± 30 BP	Cal BC 3945 to 3590 (Cal BP 5895 to 5540)

4.1.1.3. Previous interpretation of the offshore seismic reflection profiles from the ASTARTE campaign

The ASTARTE campaign report (Drago et al., 2017) mentions that the depositional architecture consists of a succession of progradational wedges interpreted as forced regressive wedges (FRW) (Figure 23). This unit is truncated by an erosional surface, interpreted as a transgressive surface (TS) at the base of Trasgressive Sediment Deposits (TSD). The interpretation of the lines additionally identifies two lobate bodies overlying the TS. These bodies show diverse internal acoustic facies, varying from stratified to oblique, with some sectors showing chaotic facies (cf in Figure 23) at the base of an erosional scarp. The bodies are interpreted as transgressive deposits (seismic unit TD, in Figure 24) according to their geometry and facies. According to the same report, these transgressive deposits are covered by highstand aggradational or progradational deposits (seismic unit HSD in Figure 23).

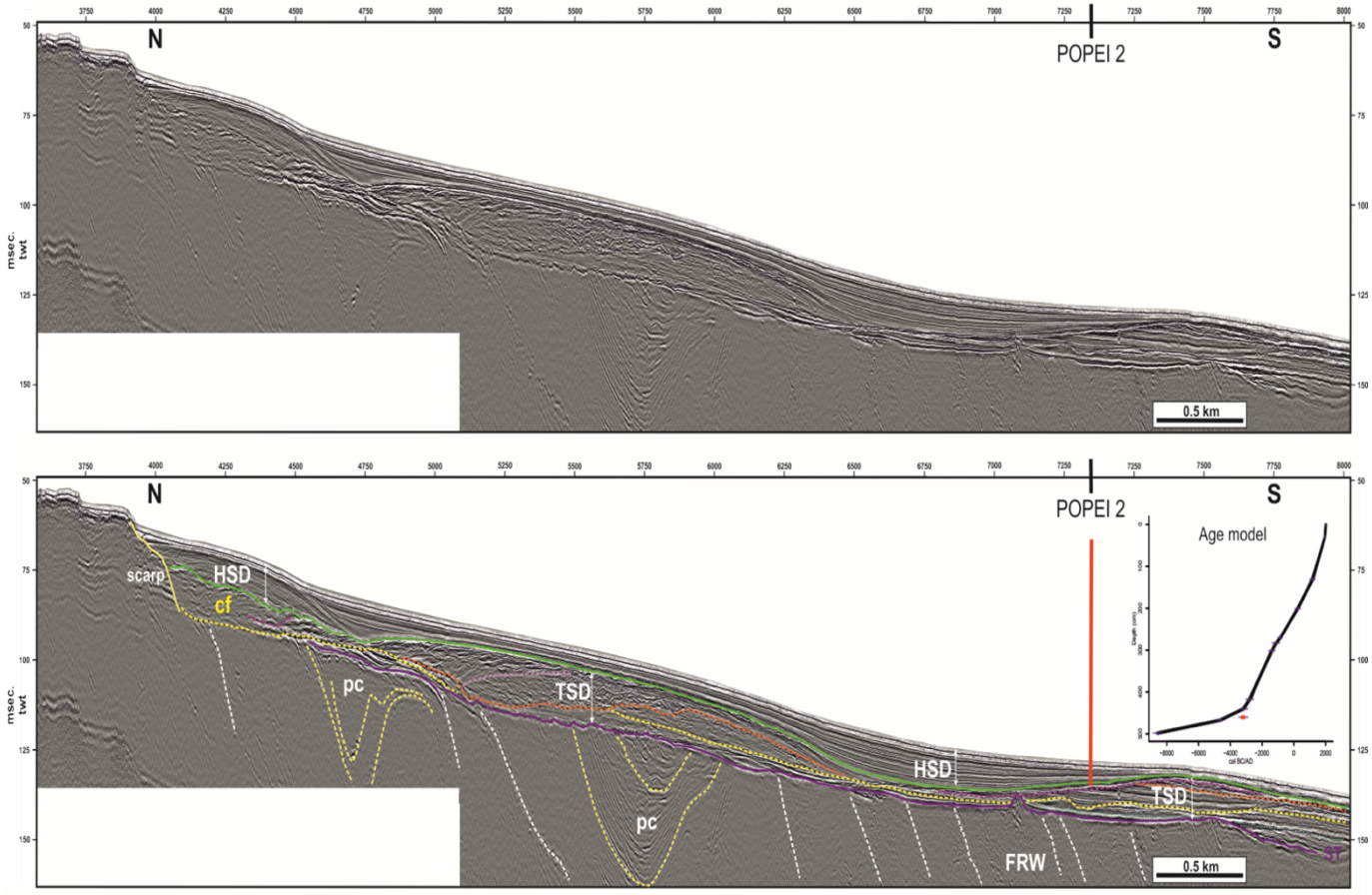

Figure 23 - Seismic reflection line ASTARTE 11 (top) with location of POPEI 2 vibrocore and interpretation (bottom). cf: chaotic facies. FRW: forced regressive wedges. HSD: highstand sedimentary deposit. pc: paleochannels. TSD: transgressive sedimentary deposit. The transgression surface corresponds to the violet reflector. According to the campaign report, the green horizon corresponds to an age slightly older than 8,562 y BP. Stratigraphic calibration of the line was made using the age model by Mil-Homens et al. (2016). The interpreted image and the graphic, containing the age model, in the right corner of the figure, are taken from Drago et al., 2017. See location in Figure 19.

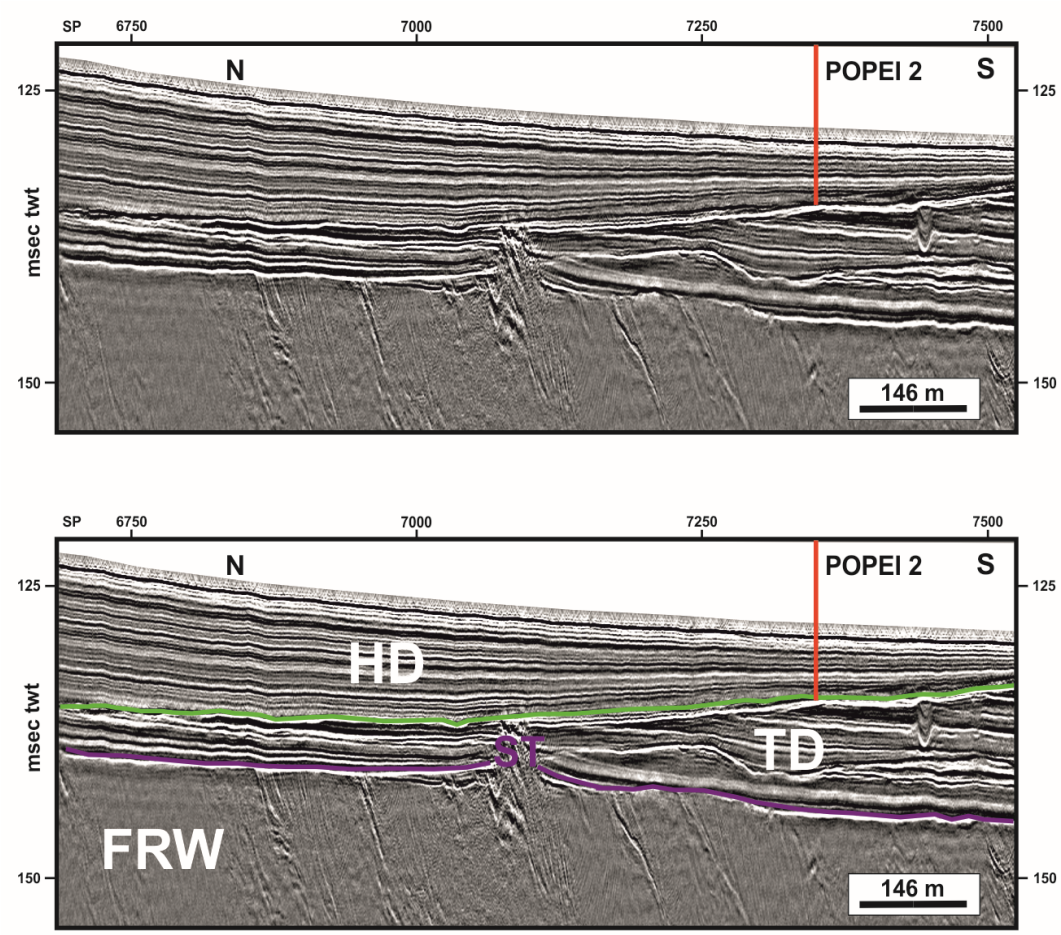

Figure 24 - Zoom in of seismic reflection line ASTARTE 11 showing the stratigraphic calibration with POPEI 2 vibrocore. According to the campaign report the ^{14}C calibrated age (Mil-Homens et al., 2016) of the oldest sediments near the top (green marker) of the transgressive deposit (TD) is 8,562 y BP. FRW: forced regressive wedges. HD: highstand deposits. TD: transgressive deposits. The interpreted images are taken from Drago et al., 2017. See location in Figure 19.

The campaign report concluded that the results indicate that this shelf is a suitable recorder of high-energy, eventually tsunamigenic events as shown as the chaotic sedimentary facies within TSD sequences at the front of erosive scarps.

5. Methods and Data

5.1. Seismic data

During this work, thirty ASTARTE profiles were analysed and interpreted in the seismic lab - Marine Geology and Geophysics Laboratory (SEISLAB) - from IPMA (*Instituto Português do Mar e da Atmosfera*), with the *DecisionSpace* software (Landmark), designed to support, among other things, seismic interpretation.

The length of each profile is showed in Table 4 and the total length of ASTARTE seismic lines analysed is 353,33 km.

Table 4 – ASTARTE profiles designation and length (see Figure 19 for seismic line location).

Seismic Profiles	Length (m)
ASTARTE_02	10 026
ASTARTE_02 transit	4 361
ASTARTE 03A Part1	30 221
ASTARTE 03A Part2	
ASTARTE 03A Part3	
ASTARTE_04	3 286
ASTARTE_04A	21 800
ASTARTE 05	26 851
ASTARTE_06A	29 072
ASTARTE_06B	9 871
ASTARTE 07	12 285
ASTARTE 07A	12 079
ASTARTE_08	9 785
ASTARTE_08A	9 450
ASTARTE_09 part1	20 398
ASTARTE_09 part2	
ASTARTE_10	22 322
ASTARTE 10A	4 105
ASTARTE_10 transit	3 808
ASTARTE_11	17 463
ASTARTE_13 part1	17 613
ASTARTE_13 part2	
ASTARTE_15	2 088
ASTARTE_15B	11 960
ASTARTE_17	14 233
ASTARTE_19	14 296
ASTARTE_21	12 398
ASTARTE_23	14 669
ASTARTE_25A	9 359
ASTARTE_27	95 33
	Total: 353 332 m

5.1.1. Seismic interpretation

Considering the data we have access to, consisting of seismic lines and cores, the analyses were made through seismic stratigraphy and its subsequent integration and age data.

To analyse the seismic stratigraphy, we first look at the foundations on which it is based. Roque (2007) mentions the foundations of seismic stratigraphy based on the following three assumptions: (1) sedimentation is a cyclical process; (2) primary seismic reflections are produced where there is an abrupt contrast in acoustic impedance, parallel to stratification surfaces and discordances; and (3) the reflections have chronostratigraphic significance. It is assumed that the geometric relationships between reflections reflect geological relationships between layers and discontinuities. According to Roque (2007), the analysis of seismic facies can be made by consecutive stages. The following analysis stages are highlighted:

1) **Type of reflection termination**: onlap, downlap, toplap, truncation and conformable.
2) **Character of the reflections**: amplitude, continuity, and frequency.
3) **Configuration of the internal reflections of the seismic units**: transparent, semi-transparent, chaotic, parallel, sub-parallel, convergent, divergent and progradational.

For the interpretation of the available data, firstly, the main seismic discontinuities present in each seismic profile of the ASTARTE campaign were recognised through the analysis of the above-mentioned stages. By recognising the main discontinuities, i.e., those that separate large sedimentary packages, it was possible to identify the main seismic units and analyse their seismic facies, to recognise the occurrence of stratigraphic changes. With this recognition we can infer different lithologies and depositional environments. After the seismic stratigraphic analysis, the stratigraphic calibration of the reflections and seismic units was also carried out using cores, namely the data from Table 3.

In order to understand the overall geological processes that governed the formation and evolution of the depositional system imaged on the seismic profiles all the core data was integrated in the analysis.

5.2. Core data

The information provided by the cores was described above. The cores used in this work where the ones with a location coincident with some of the ASTARTE seismic lines (ASTARTE _09 part2, ASTARTE 19, ASTARTE 17, and ASTARTE 11). Their location can be seen in Figure 20. From the previous data mentioned about the cores, the information that was used for this work was their location, water depth, core length, lithology, and the AMS C^{14} dating.

Firstly, the data that was used from the cores was uploaded to the seismic database. This was done using the "Pseudo Well" tool provided by the software, where the information about the coordinates and total depth of the cores was placed. In order to place this information, some mathematical conversions were made. The software uses a TWT (Two-Way Time) scale. This refers to the time it takes a signal to travel down to a subsurface layer and back-up to the surface and is measured in milliseconds (ms).

To transfer the available data about the depth of the cores to the system there was conversions that needed to be made. The depths of each core were converted to time. To convert the cores depth (m) to Time TWT (ms), we need to account for the velocity of the seismic wave in the water (1507 m/s) and in the sediments (1700 m/s), because sound velocity in water and sediment layers is different, and we must account for the different velocities when the seismic wave passes through different environments. The number for the velocity of the sediment for these conversions was chosen because it is used with some frequency for this type of sediment, but this value can be higher or lower and depending on this velocity the line that will symbolise the depth of the core in the programme will become shorter or longer. It is important to note that the same formulas are used for both water and sediment calculations, the only factor that changes is the velocity. After we find the Time TWT (ms), we need to check in the software at what depth below sea floor (bsf) (ms) are each of the cores. Once we have that number, we

can calculate the TWT depth (ms). The mathematical equations used to convert the data are showed below and the results are shown in Table 5.

$$1.\quad Sound\ velocity\ TWT\ (\mathrm{ms/m}) = \frac{\frac{Sound\ velocity\ (\mathrm{m/s})}{1000}}{2}$$

$$2.\quad Time\ TWT\ (ms) = \frac{Depth\ (m)}{Sound\ velocity\ TWT\ (m/ms)}$$

$$3.\quad Depth\ (m) = Time\ TWT\ (ms) \times Sound\ velocity\ TWT\ (m/ms)$$

Having the cores placed in the database, the system will provide their exact location and depth, allowing us to locate the cores on each seismic line, and to check the relative position of dated sediments and seismic reflections.

Table 5: Calculations made to convert the AMS C^{14} depths data for input into the seismic database.

Event Number	Core	Depth (cm)	Depth (m)	Sediment velocity (m/s)	Sediment velocity TWT (m/s)	Sediment velocity TWT (ms/m)	Time TWT (ms)	Depth bsf (ms)	Depth TWT (ms)
1	POPEI 1-1CGG	52	0,52	1700	850	0,85	0,6118	97,19	97,80
2	POPEI 1-1CGG	79	0,79	1700	850	0,85	0,9294	97,19	98,12
3	POPEI 1-1CGG	114	1,14	1700	850	0,85	1,3412	97,19	98,53
4	POPEI 2-1 CGP	61	0,61	1700	850	0,85	0,7176	129,48	130,20
5	POPEI 2-1 CGP	90	0,9	1700	850	0,85	1,0588	129,48	130,54
6	POPEI 2-1 CGP	133	1,33	1700	850	0,85	1,5647	129,48	131,04
7	POPEI 2-1 CGP	159	1,59	1700	850	0,85	1,8706	129,48	131,35
8	MW14-105	80	0,8	1700	850	0,85	0,9412	102,99	103,93
9	MW14-105	126	1,26	1700	850	0,85	1,4824	102,99	104,47
10	MW14-105	156	1,56	1700	850	0,85	1,8353	102,99	104,83
11	MW14-105	166	1,66	1700	850	0,85	1,9529	102,99	104,94
12	MW14-105	188	1,88	1700	850	0,85	2,2118	102,99	105,20
13	MW14-105	206	2,06	1700	850	0,85	2,4235	102,99	105,41
14	MW14-105	236	2,36	1700	850	0,85	2,7765	102,99	105,77
15	MW14-107	29	0,29	1700	850	0,85	0,3412	74,07	74,41
16	MW14-107	69	0,69	1700	850	0,85	0,8118	74,07	74,88
17	MW14-107	91	0,91	1700	850	0,85	1,0706	74,07	75,14
18	MW14-107	111	1,11	1700	850	0,85	1,3059	74,07	75,38

5.3. Maps

In order to better understand the dynamics that occur in the study area, interpolated surface maps and thickness maps were made. The interpolated surface maps were made using the already interpreted seismic profile data and with the creation of a polygon in the program around the areas that are interpreted, i.e. where we have reflectors. For each horizon (D1 through D4) a map was created using the "Grid and Contour" tool. This tool interpolates the map only in the area where the polygon is and with the data provided by the interpretation previously made. The surfaces were interpolated using the software's interpretation algorithm. The final interpolated surface maps also provide the isobaths, which are lines that show the depth of an underwater surface in milliseconds. The thickness maps were made by creating a new horizon. This horizon was made using the geology calculator, provided by the program; the thickness of a unit is calculated by subtracting the two horizons that delimit the unit, i.e., the base minus the top. Once the new horizon is made, a polygon was created around the areas that are interpreted. The last step is to use the "Grid and Contour" tool to create the thickness map, just like for the interpolated surface map. The final thickness map also has isopachs, which show the distribution of the thickness of a geological layer in milliseconds.

6. Results

6.1. Stratigraphic analysis

The seismic profile ASTARTE 23 was used to exemplify the units and discontinuities as it integrates them all. It extends for about 15 km from nearshore, approximately at 6 m water depth to 140 m water depth, i.e., beyond the present day shelf slope break. An internal scarp is present at approximately 20 m below sea level, less than 1km from the coastline. Both slope breaks (i.e., the shelf breach and the scarp) are associated with the accumulation of prograding sedimentary units that overlie these erosive features, the significance of which will be discussed in this report. The existence of various erosive and constructive discontinuities together with systematic seismic reflections terminations allowed the definition of 4 seismic unit bounding discontinuities (D) and 5 main seismic units (U). The discontinuities are shown in Figure 25 through Figure 27. Discontinuity D1 is an erosive surface that cuts through a package of a monocline series of horizons that extend from the continental slope break to the nearshore and constitute the basement (U1) of the more recent sedimentary packages that are object of this study. The discontinuity D1 truncates the reflections that are immediately below it and it is visible throughout the seismic profiles. It has good lateral continuity, and it ends truncated against D2 towards the north. D2 is a second erosive surface that intersects D1 and cuts through U1 as well. The unit U2 shows a complex stratigraphy, with several sub-units. The reflections vary in amplitude between high and low. In terms of geomorphology, the unit differs as we move to the S. Along this N-S route, it increases in thickness, moving from a more compact sequence of internal reflectors (N) to a thicker one at the end of the profiles (S), at depths of around 100 m. The S area of U2 is located at the shelf break and consists of amalgamated prograding reflections while the northern body shows heterogenous morphologies of southerly prograding sub-units and chaotic sub-units with various internal erosive discontinuities. The reflectors terminate with a toplap truncation by D2. The discontinuity D2 is an even surface, visible throughout the seismic profiles. The unit U3 lies on top of D2, and its thickness shows important variations, with a greater volume of sediment to the N and losing its expression as we move towards S. U3 consists of sigmoidal reflections with downlap terminations towards the south, and it is truncated by D3 to the north.

The discontinuity D3 is not visible in all the seismic profiles and when it is visible is only in a small portion of the profiles. The amplitude of the reflections is low and it has good to medium lateral continuity. The unit U4 lies on top of D3 or on top of D2 in some profiles where we have bigger depths of around 80 m. U4 shows some variation in terms of sediment thickness, reaching its maximum thickness to the N of the seismic profiles. U4 displays two different seismic facies, as follows. To the

north, it consists of a laterally confined deposit with internal discontinuous reflections and wavy patterns possibly associated with channeling. To the south, it consists of a sigmoidal seismic unit downlapping to the south with toplaps to the north. These two domains are separated by a high of U3 of southwards progradational sigmoidal reflections. The top of U4 is delimited by D4. The discontinuity D4 is not visible in all profiles. In the areas where D3 and D4 are very shallow, they appear to be in continuity, which makes it difficult to discern between the two. The unit U5 represents the most recent package of sediments. In the N of the seismic profiles, i.e., near shore, the internal reflections are heterogeneous with chaotic and discontinuous reflections, while southward the reflections become sigmoidal downlapping to the south and onlapping to the north. U5 is top lapped by the seafloor. A summary of the seismic characteristics of the seismic units and discontinuities is showed in Table 6.

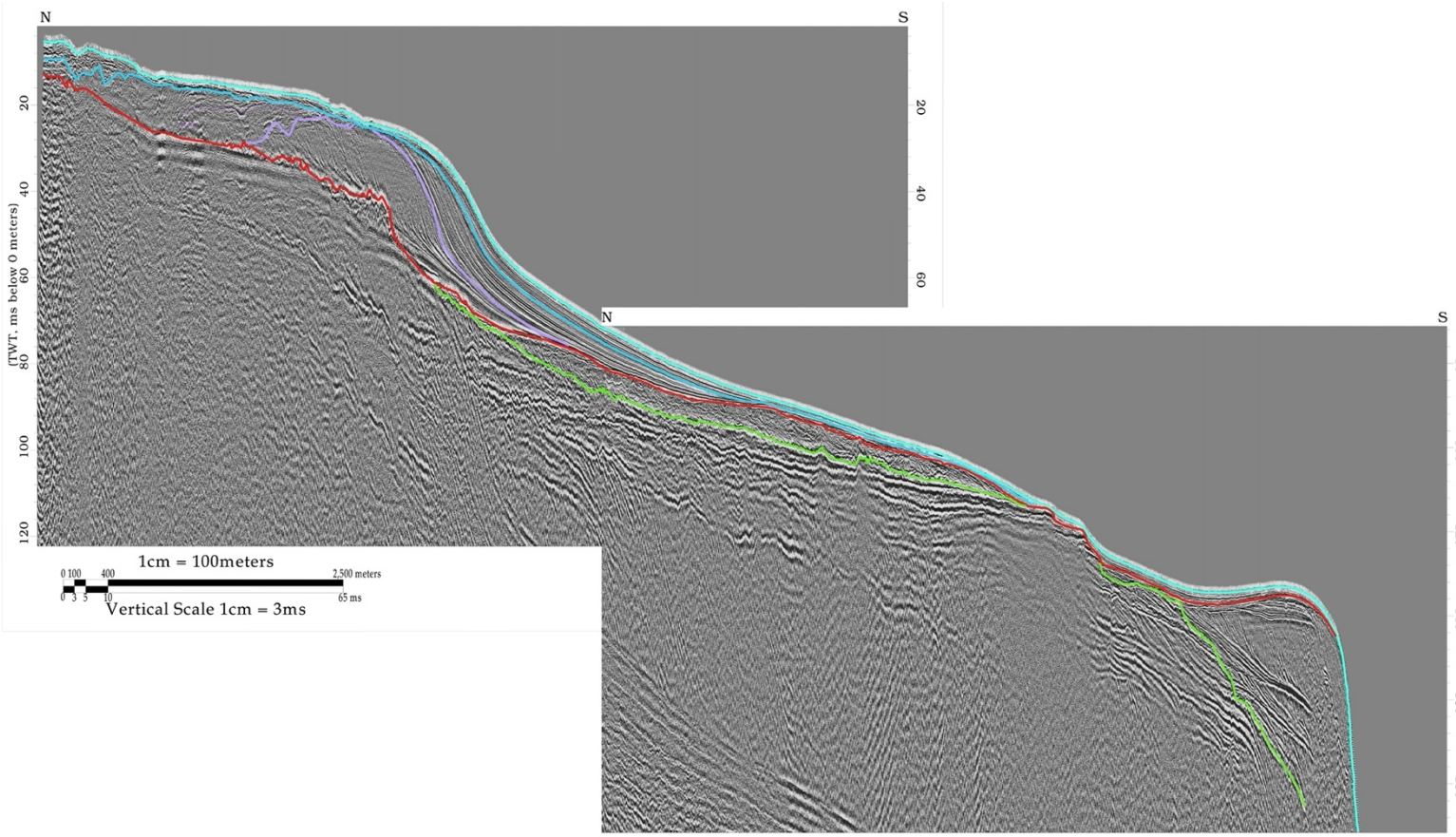

Figure 25: Seismic profile ASTARTE23, with interpreted discontinuities. Top: profile of the onshore region; Bottom: profile of the offshore region. Green reflection = D1; Red reflection = D2; Lilac reflection = D3; Dark blue reflection = D4; Light blue reflection = sea floor. Its location can be seen in Figure 20.

A stratigraphic model of the area of interest is shown using seismic profile ASTARTE 23 (Figure 25 through Figure 27), where all discontinuities and units to be described are visible.

The model in Figure 26 shows some specific packages within the stratigraphic sequence that help with the interpretation of the depositional stages. These stages resemble depositional cycles or system tracts, representing specific phases of the oscillations of the sea level and each as a particular depositional environment and sedimentary process. According to Lobo et al., 2004, the general post LGM sediments are organized in transgressive (TST) and highstand (HST) system tracts. There has been one identified

system tract in the northern part of the stratigraphic model (Figure 27). HST – assumed to have been deposited when the sea level was relatively high and stable or slowly falling. During this period, sediment supply typically exceeds accommodation space leading to progradation. The shoreline moves landward as marine conditions encroach over previously exposed areas.

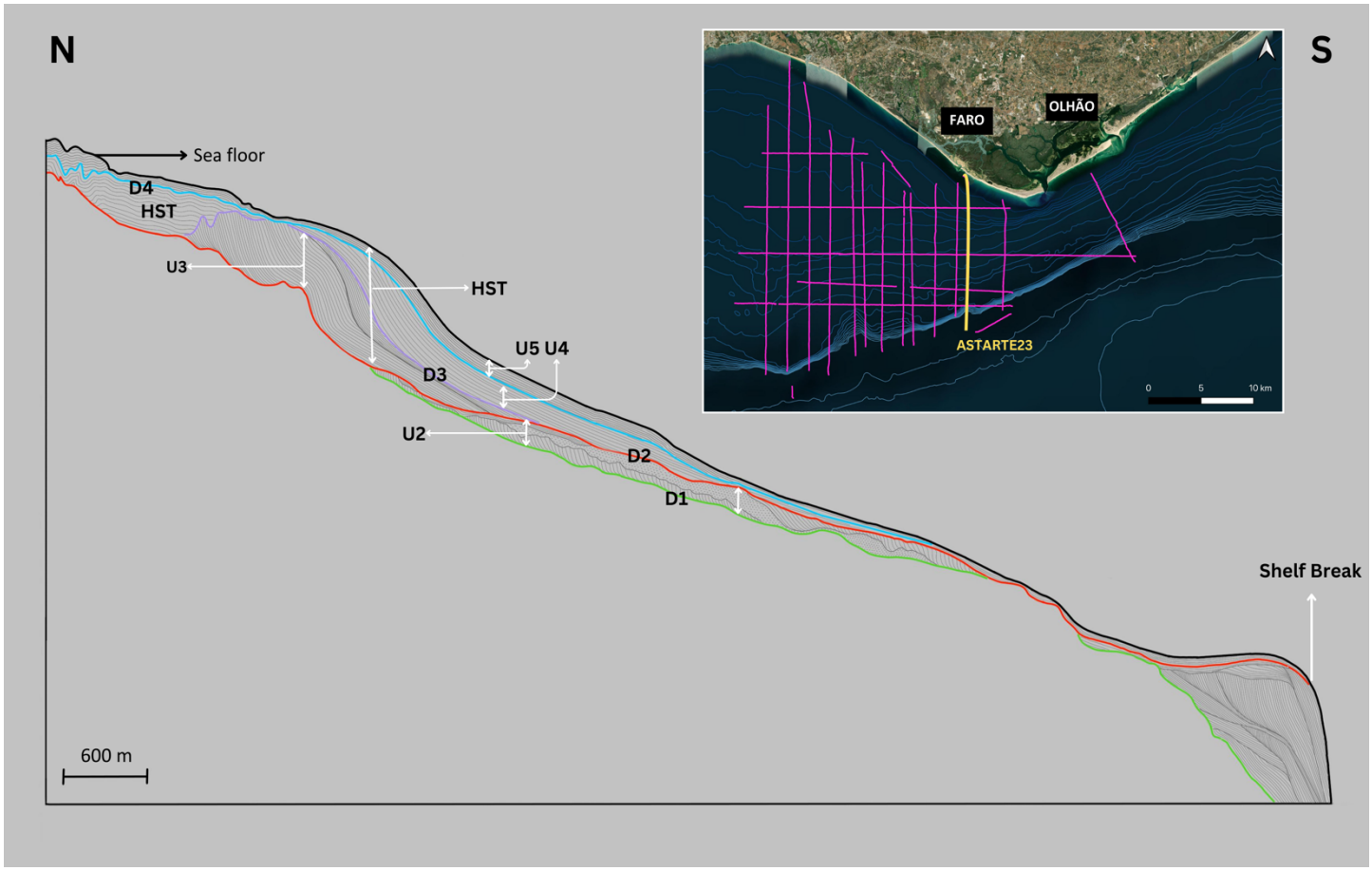

Figure 26: Stratigraphic model made from the seismic line ASTARTE 23, where it shows all the units interpreted from U5 to U1, the discontinuities from D1 to D4, and specific stages within the stratigraphic sequence: HST = Highstand System Tract.

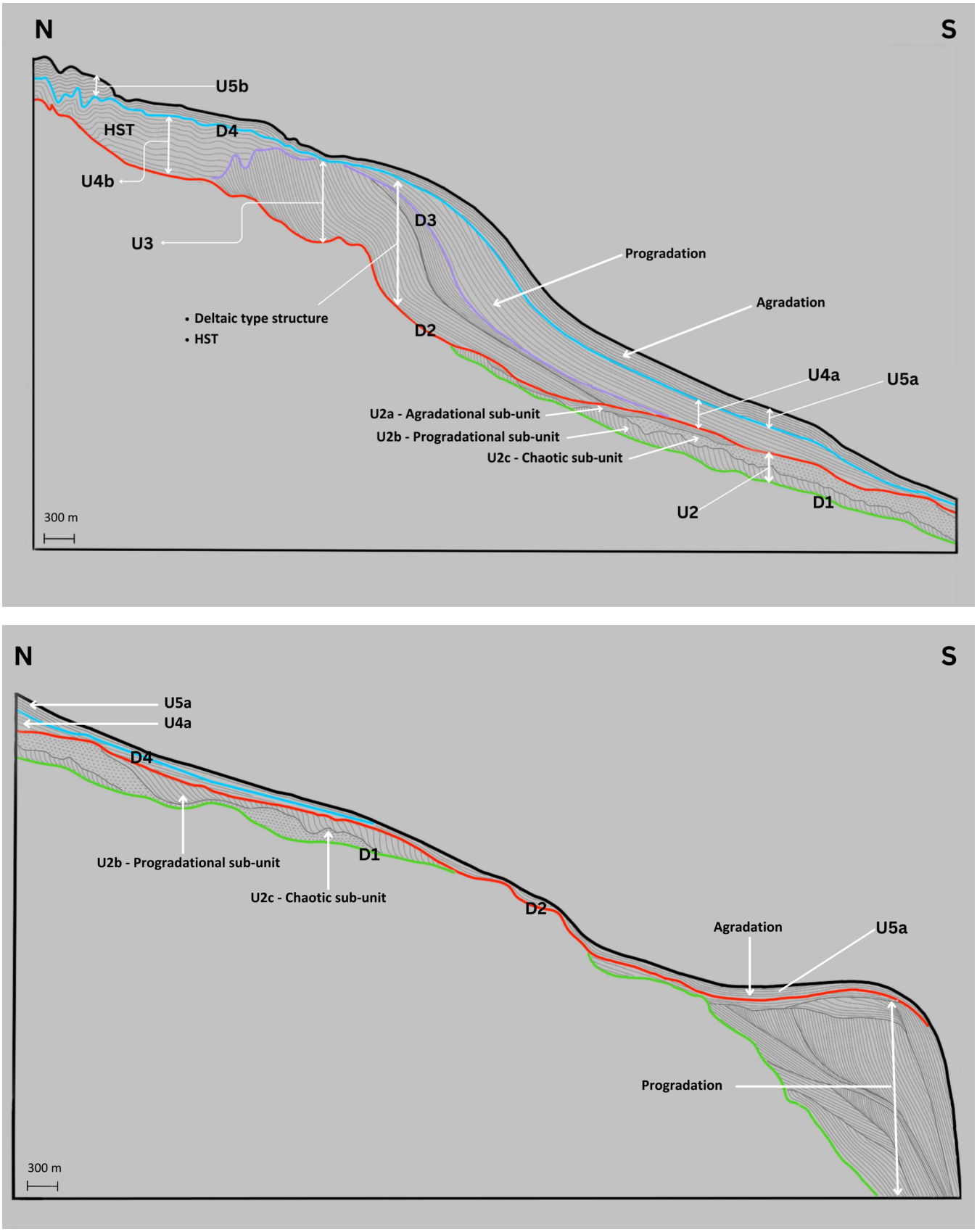

Figure 27: Zoom of the stratigraphic model made from the seismic line ASTARTE 23. The first zoom is of the onshore (north) side of the model, where it shows the four interpreted discontinuities, D1 to D4, and the interpretation of the units facies, as well as sub-units from U2. The bottom zoom is of the offshore (south) side of the model where it shows three of the four discontinuities (D1, D2 and D4), and the interpretation of the units facies, as well as some sub-units from U2.

Table 6: Summary of the characteristics of the seismic units (U) and discontinuities (D) interpreted in the ASTARTE seismic reflection lines.

<table>
<tr><th>Seismic Unit (U)/ Discontinuity (D)</th><th colspan="3">Seismic Character</th><th>Interpretation</th></tr>
<tr><td>U1</td><td colspan="3">Unit with lateral continuity. Reflectors vary in amplitude between low and high, with semi-transparent areas.</td><td>Bottom unit in the system. It is a heterogenous unit and has several sub-units and internal discontinuities.</td></tr>
<tr><td>D1</td><td colspan="3">Reflection with lateral continuity; it can be identified in all the profiles analyzed. The amplitude of the reflections is moderate to high. It is truncated by D2.</td><td>Erosive nature, cutting through south dipping formation of possible Early Quaternary to Pliocene age.</td></tr>
<tr><td rowspan="2">U2</td><td>U2a</td><td>U2b</td><td>U2c</td><td rowspan="2">Composite body. Due to the marked difference in the geometry of the unit and because it is an amalgamated unit, it can be assumed that it may correspond to sediments that were deposited at different eustatic levels, where energy differences occurred. We are faced with a lateral facies variation.</td></tr>
<tr><td>Sub-unit with low amplitude. It has an agradational facies. Towards the coast the unit pinches out truncated by D2.</td><td>Sub-unit with lateral continuity. The reflectors vary between medium to high amplitude. It has a progradational facies. Towards the coast the unit pinches out truncated by D2.</td><td>Sub-unit with lateral continuity. The reflectors vary between low to high amplitude. It has chaotic facies. Towards the south, the unit presents internal erosive discontinuities and seismic facies, namely clinoforms.</td></tr>
<tr><td>D2</td><td colspan="3">Reflection with lateral continuity; it can be identified in all the profiles analyzed. The amplitude of the reflections is high.</td><td>It is characterized by its erosive nature. We can describe this discontinuity as a wave ravinement surface. This structure is associated with changes in sea level, with a change in deposition patterns.</td></tr>
<tr><td>U3</td><td colspan="3">Unit with reflectors with an amplitude that varies between medium and low, with some profiles where the amplitude of the reflections is occasionally high. Lateral continuity. Prograding sigmoidal facies, progressing to more aggrading facies as we move to the S, where the reflections are more horizontal.</td><td>The whole unit is a deltaic-type accretion wedge, probably deposited in a low-energy environment due to its facies.
The thicker packages in this unit are probably the result of the structure that generated the accommodation space in which the unit is deposited, thus creating an accretion wedge</td></tr>
<tr><td>D3</td><td colspan="3">Reflection with good to medium lateral continuity; it can be identified in most profiles, albeit in smaller sections. The amplitude of the reflections is low. The discontinuity ends in downlap against D2</td><td>It is characterized by having an erosive character in the zone near the coast, progressing to paraconformal in the more distal zone.</td></tr>
<tr><td rowspan="2">U4</td><td>U4a</td><td colspan="2">U4b</td><td rowspan="2">We can assume that the sediments in this unit showing prograding facies were deposited in a low-energy environment. Near the coast the deposition patterns change, they are chaotic, perhaps due to the influence of the more agitated energy, associated with coastal zones.</td></tr>
<tr><td>The sub-unit reflections vary between medium and high amplitude, with the reflections more commonly having a lower amplitude. The sub-unit starts with a progradational facies, but as we move towards S it develops a aggrading facies. It generally ends in downlaps onto D2 towards.</td><td colspan="2">The sub-unit reflections vary between low to high amplitude. The internal packages of this unit are mostly semi-transparent. The sub-unit internal reflections are heterogeneous with channels and chaotic facies. It generally ends in toplap against D4.</td></tr>
<tr><td>D4</td><td colspan="3">Reflection with medium to good lateral continuity; it can be identified in most profiles.</td><td>It is characterized by an erosive character in the proximal zone,</td></tr>
</table>

			progressing to conformal in the more distal zone.
U5	U5a	U5b	The top-most unit in the system, possibly contemporaneous with the last sea level rise. It is possible that this unit could be related to the barrier islands.
	Unit with reflectors that vary in amplitude between high and low. It has aggrading facies.	Unit with reflectors that vary in amplitude between moderate and high. Heterogeneous unit	

6.2. Cores

Once the previous acquired data about the cores was uploaded into the software, the information that it gave us was analyzed. It was found that in all the four cores analyzed they don't pierce any of the interpreted discontinuities (Figure 28 through Figure 31), allowing the discussion about the age of the system from present to D4 time.

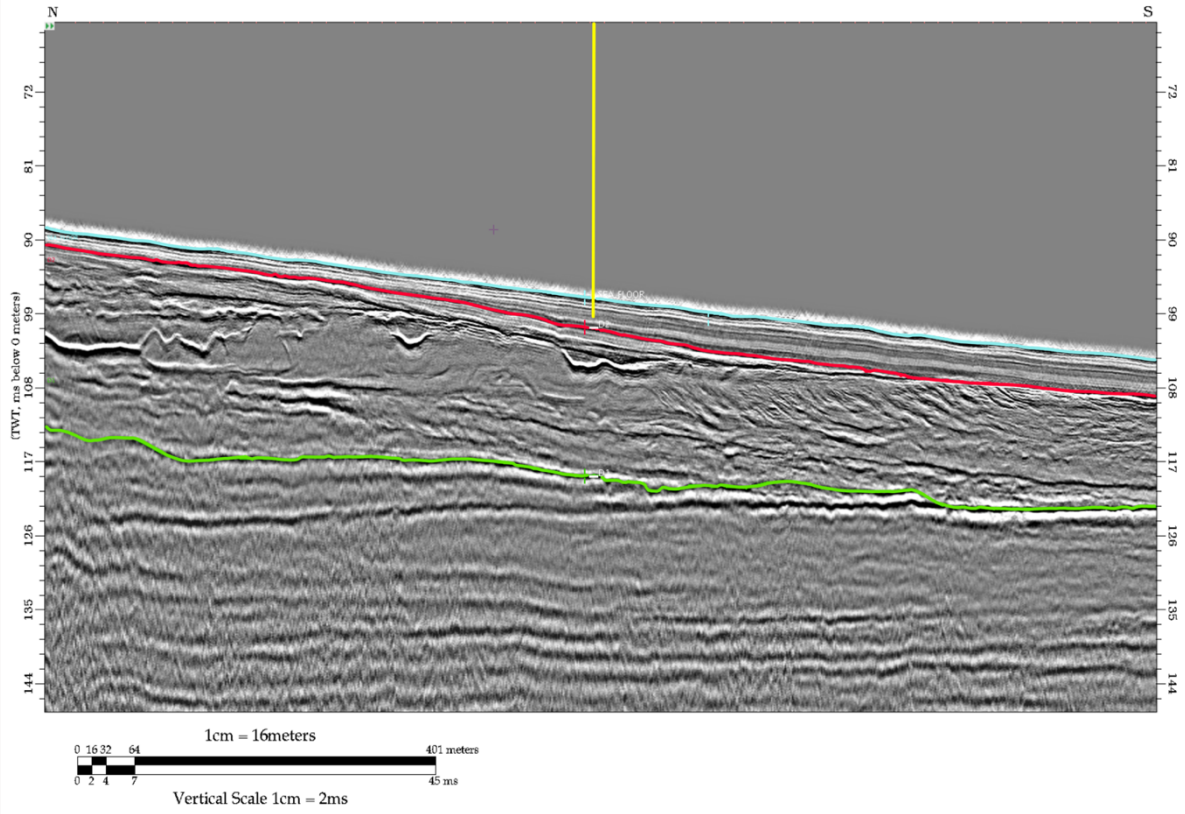

Figure 28: Seismic profile ASTARTE17 where the yellow line represents the POPEI1 core. Green reflection = D1; Red reflection = D2; Light blue reflection = sea floor. Its location can be seen in Figure 20.

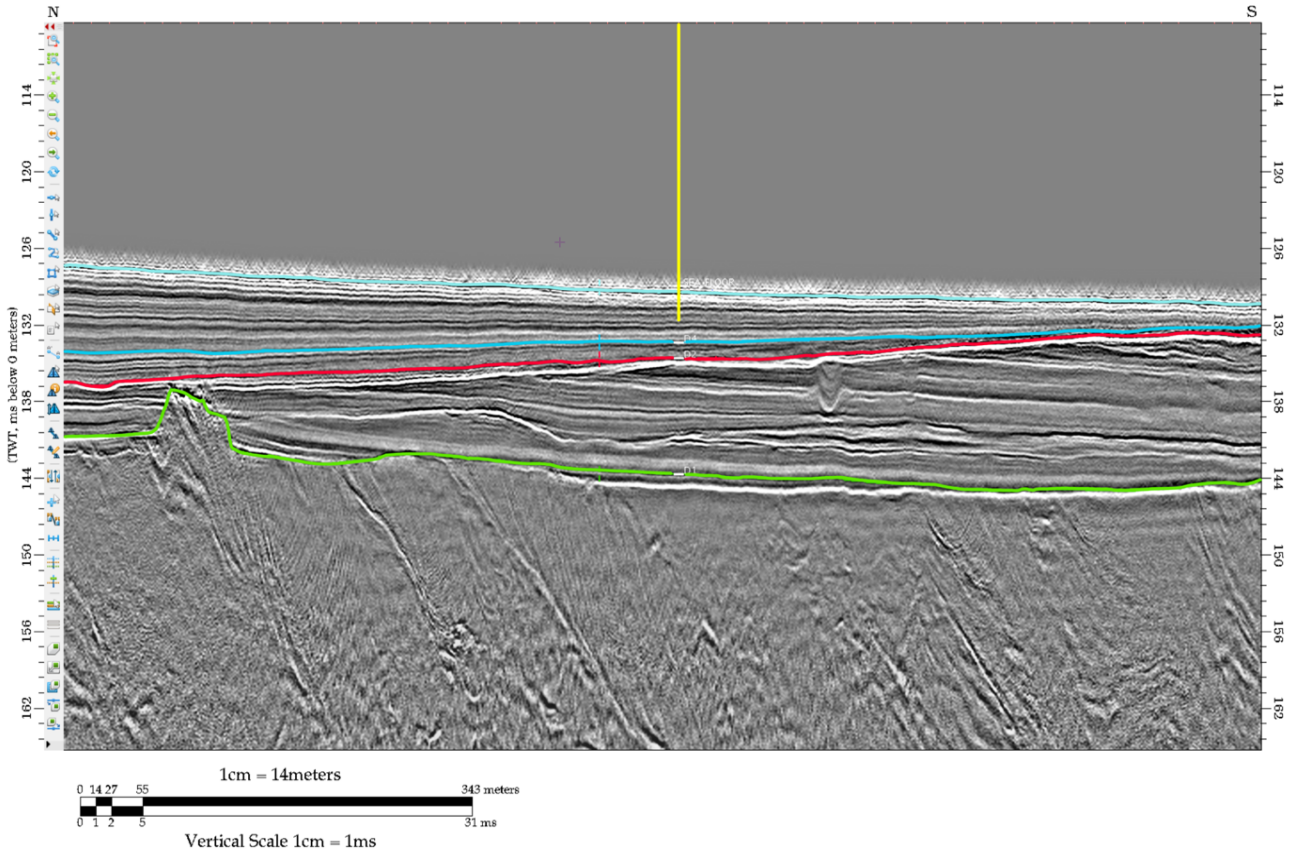

Figure 29: Seismic profile ASTARTE11 where the yellow line represents the POPEI2 core. Green reflection = D1; Red reflection = D2; Dark blue reflection = D4; Light blue reflection = sea floor. Its location can be seen in Figure 20.

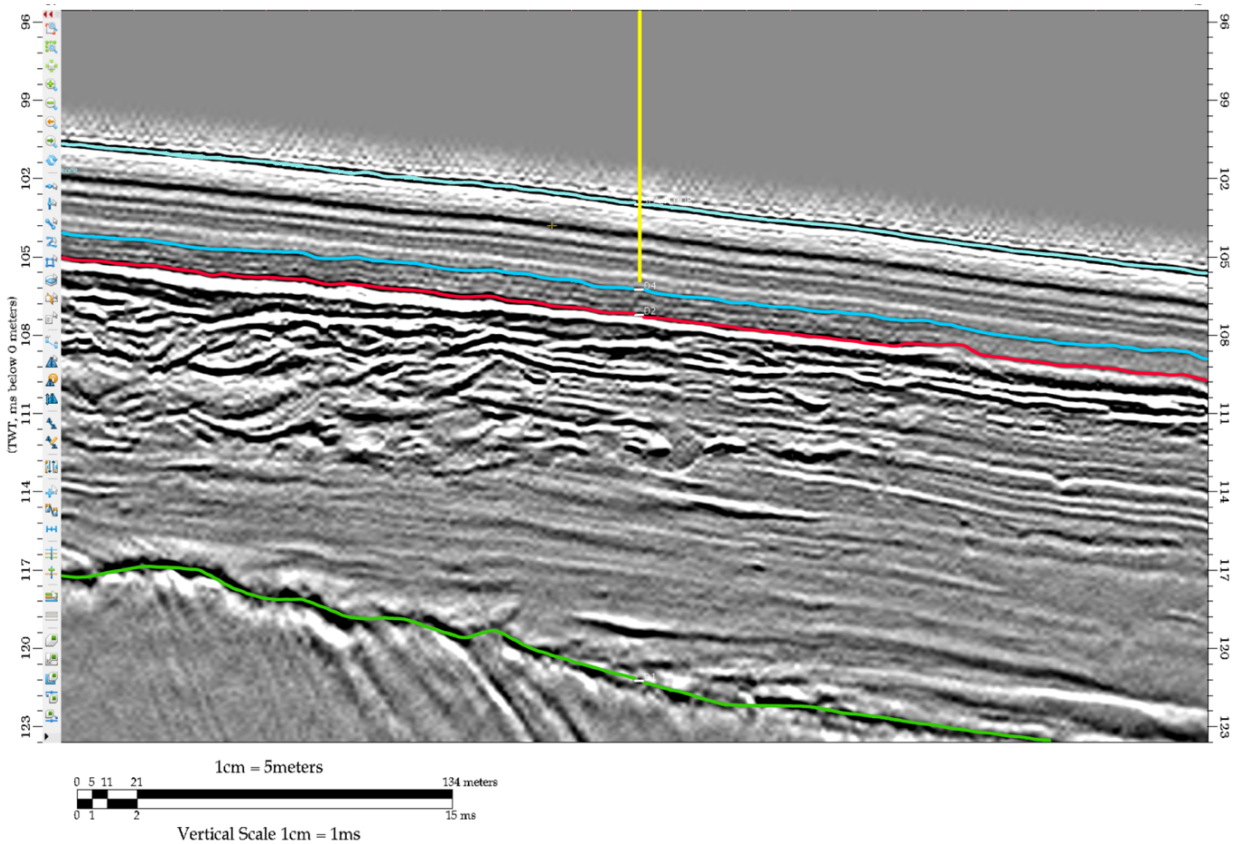

Figure 30: Seismic profile ASTARTE9part2 where the yellow line represents the MW14-105 core. Green reflection = D1; Red reflection = D2; Dark blue reflection = D4; Light blue reflection = sea floor. Its location can be seen in Figure 20.

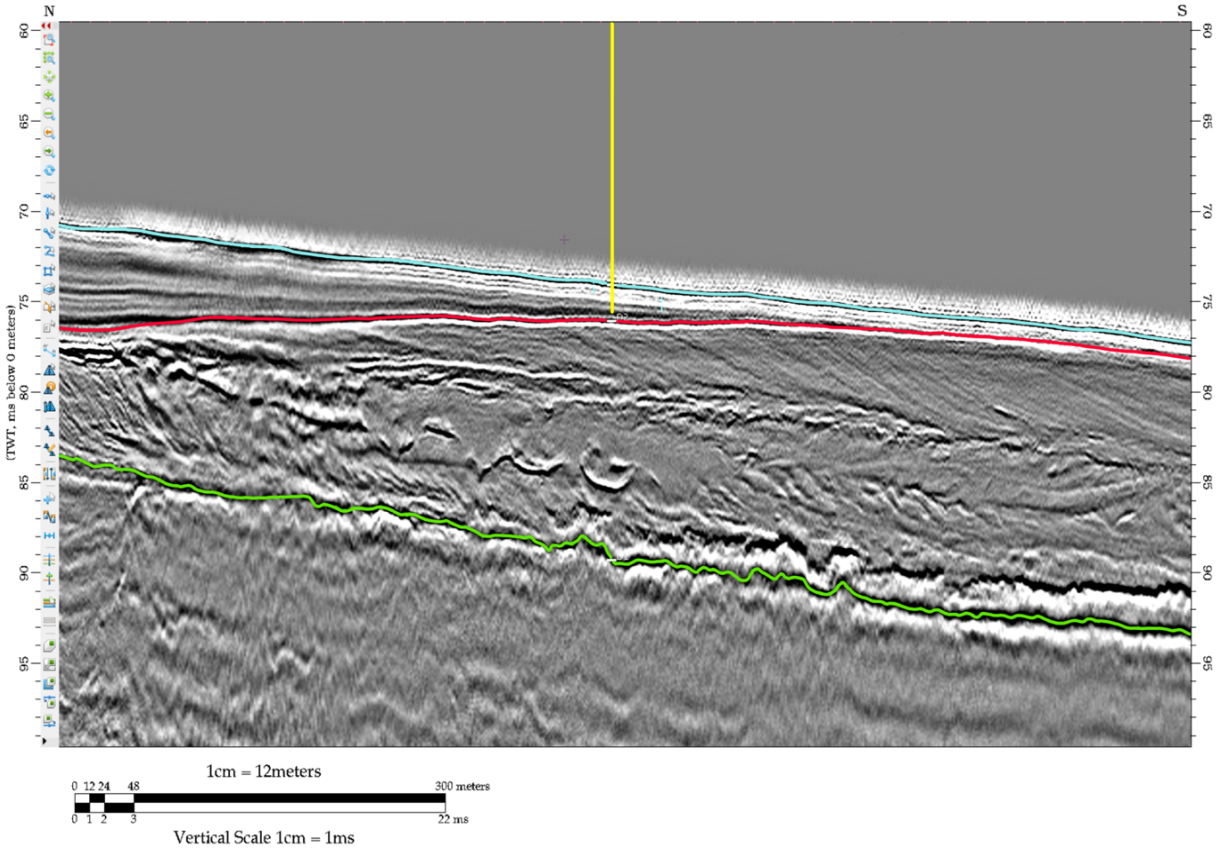

Figure 31: Seismic profile ASTARTE19 where the yellow line represents the MW14-107 core. Green reflection = D1; Red reflection = D2; Dark blue reflection = D4; Light blue reflection = sea floor. Its location can be seen in Figure 20.

Using the data from the depths that were associated with the ages of the sediments, previously converted to the software, a horizon was created for each of the depths belonging to each of the four cores, so that we could see the extent of the reflection. The aim was to see if the reflections cut through any discontinuities and thus check the age of the units underneath unit U5, since the measurements taken in the laboratory were all of sediments belonging to unit U5.

After all the horizons were created, it was clear that none of the measurements go beyond the U5 unit. Knowing that the oldest date registered in the cores is on the MW14-105 (Figure 32) at 235-236 cm bsf depth, yielding an age of 8280±30 BP (Conventional Age), it means that the age of U5 is around that age, so the sediments in that unit were all deposited during Holocene times and that the units that are set bellow it are older than the age mentioned.

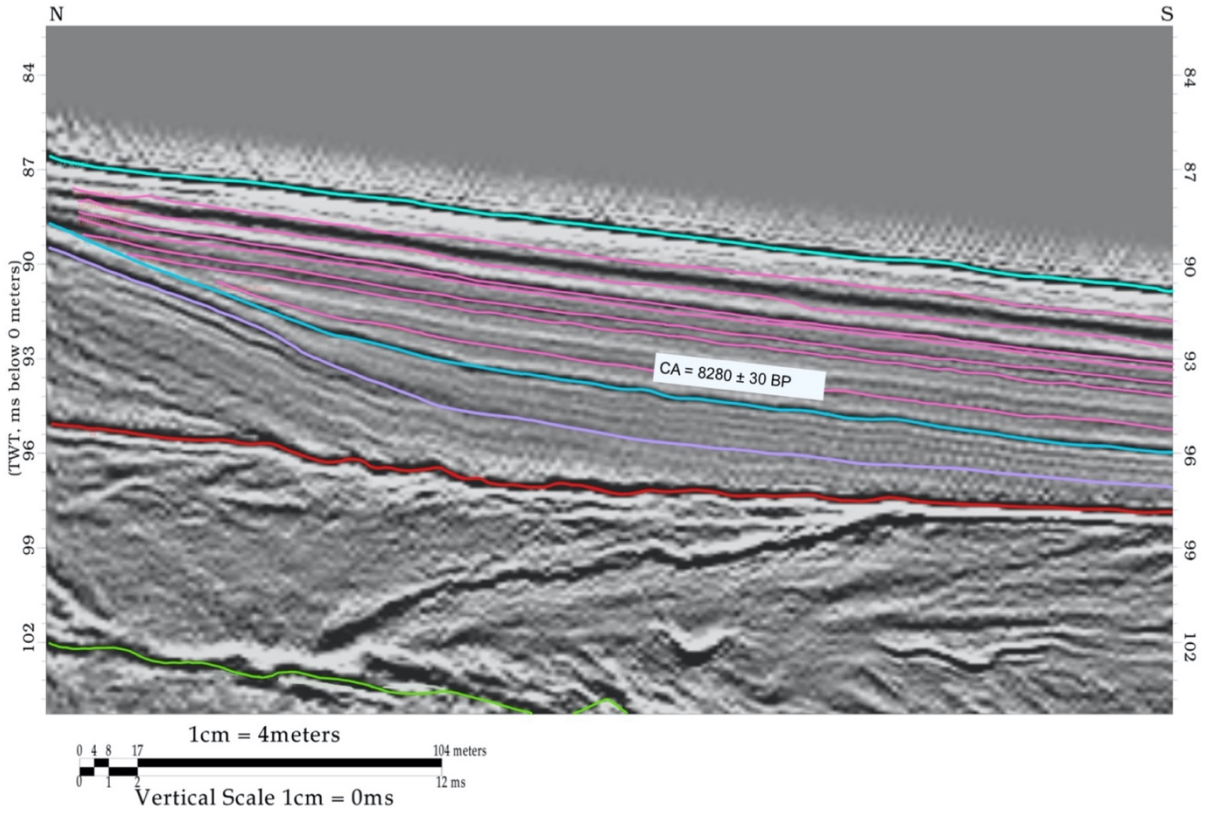

Figure 32: Seismic profile ASTARTE 9 part2 showing the horizons created (pink reflections) for the MW14-105 core measurements, with reference to the oldest date registered. Green reflection = D1; Red reflection = D2; Lilac reflection = D3; Dark blue reflection = D4; Light blue reflection = sea floor. Location of the profile and the core can be seen in Figure 20.

6.3. Maps of seismic units

To better understand the dynamics of the interpreted data maps of interpolated TWT depth and thickness were made, isobath and isopach maps, respectively. Future work is still needed in order to convert bathymetry values and TWT values into the same datum, convert time depth maps into depth maps (in metres) after selecting the best seismic velocity model and solve interpolation calculations that generated localized negative values in the isopach maps.

6.3.1. Interpolated surface maps

Four interpolated surface maps were created corresponding to the four main horizons interpreted, D1 through D4 (Figure 33 through Figure 35).

From the observation of all the maps, it is seen that the general tendency of the D1 to D4 bathymetry is similar to the present day bathymetry (Figure 19). However, some exceptions are worthwhile noting, as follows:

i) Discontinuity D1 shows one, ~6 km, long N-S trending conspicuous trough with no resemblance on the later discontinuities, 13 to 210 ms (TWT), and another less conspicuous but also striking N-S of ~10 km of length both near the edge of the slope break;

ii) Discontinuity D2 shows a wriggly pattern of 60 ms (TWT) isobaths, unlike all other isobaths that have smooth curvilinear shapes;

iii) Discontinuity D3 and D4 covers a much smaller area when compared to the other discontinuities and it has a W to E finger –like the outline around the 30 ms (TWT) isobath.

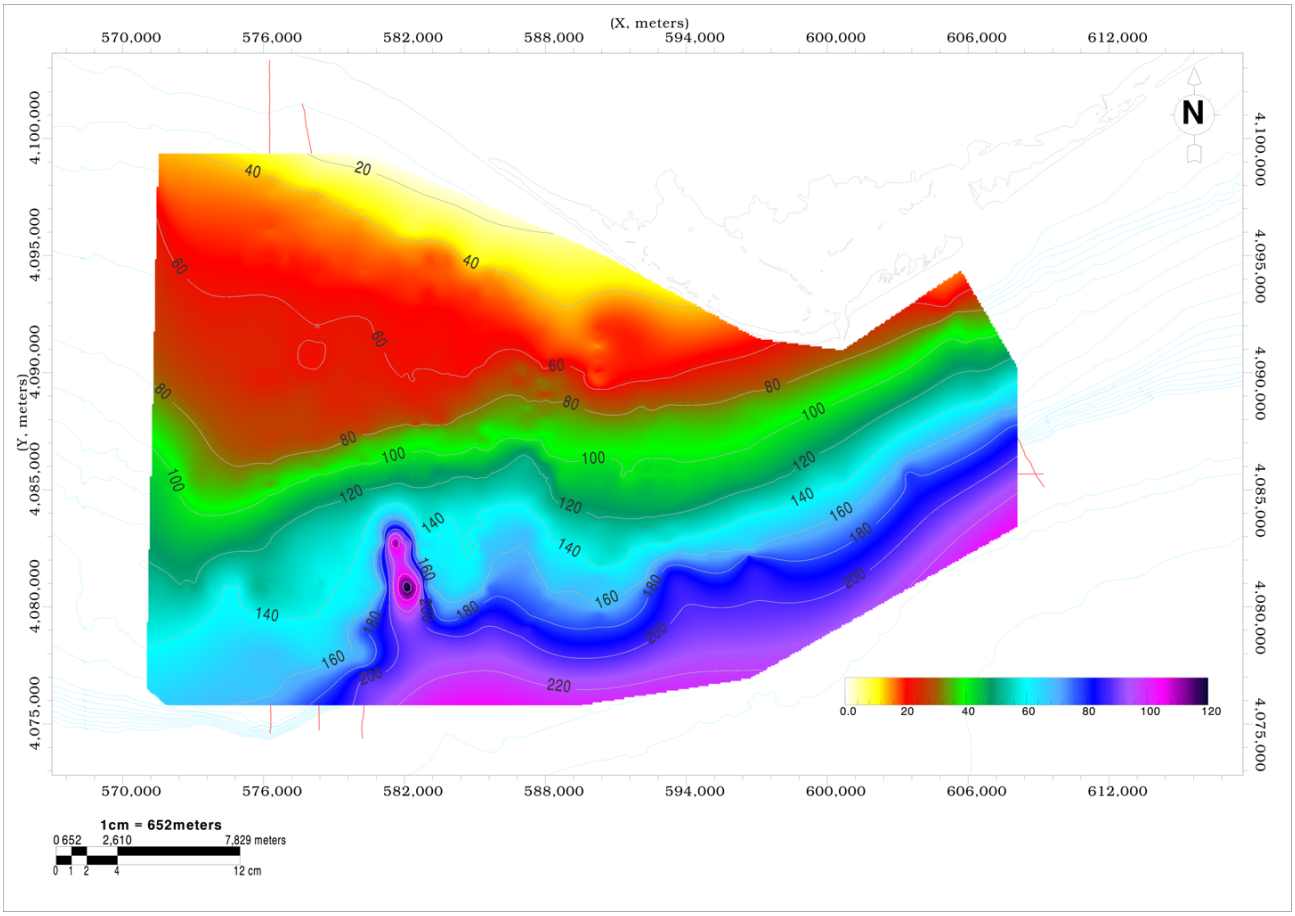

Figure 33: Interpolated surface map of the D1 horizon with colour scale intervals and isobath lines in ms.. Note the two North to South trending anomalies near the shelf break at longitudes ~582000 and 587000. Interpolated

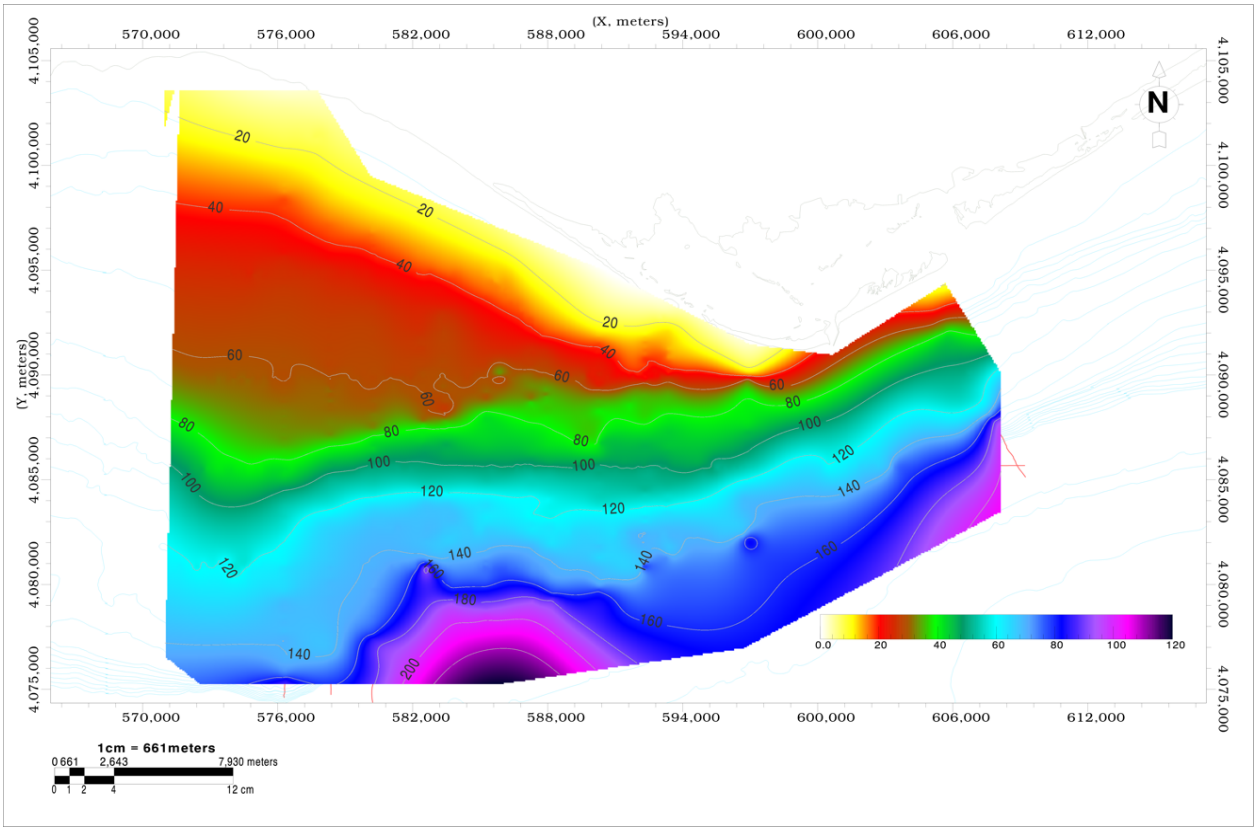

Figure 34: Interpolated surface map of the D2 horizon with colour scale intervals and isobath lines in ms. Note the wriggly patter of the 80 ms (TWT) isobath.

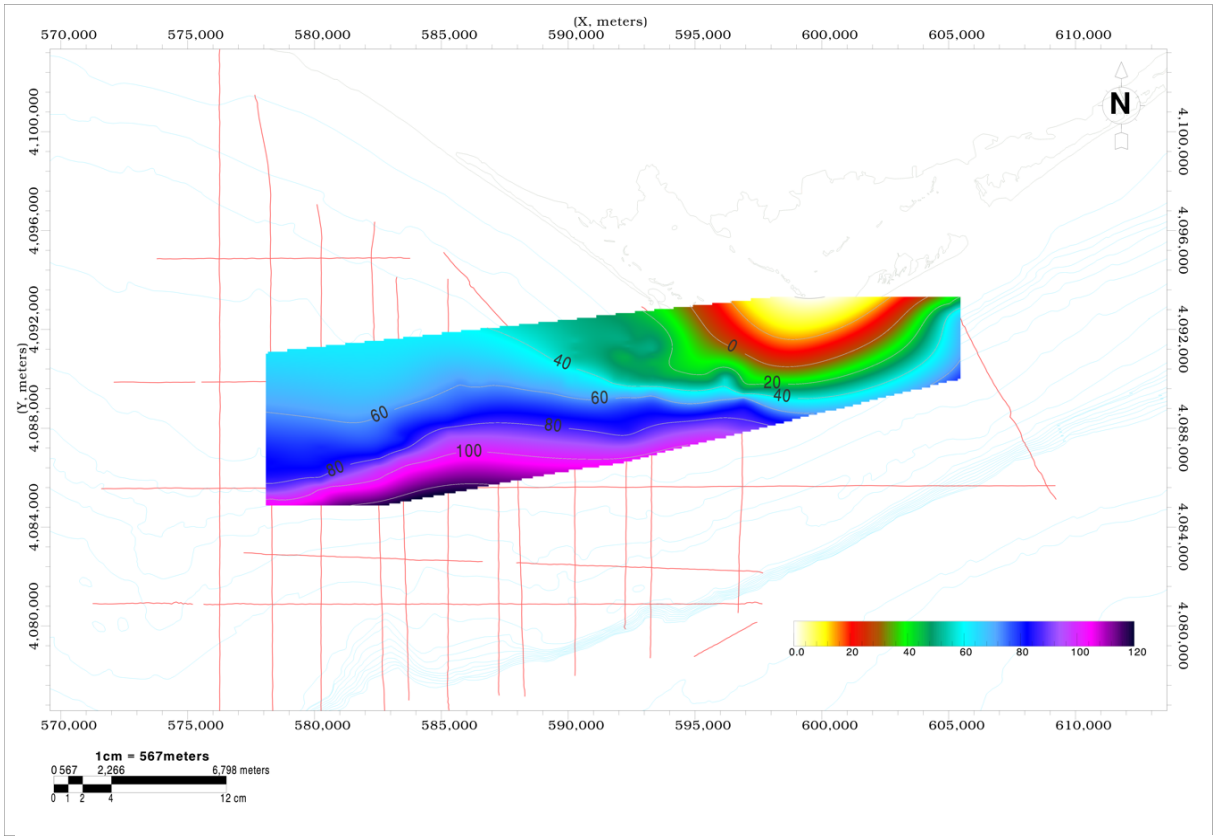

Figure 36: Interpolated surface map of the D3 horizon with colour scale intervals and isobath lines in ms. Note the West to East trending much narrow coverage of D3 with respect to the other Discontinuities and the finger-like outline of 30 ms (TWT) isobath.

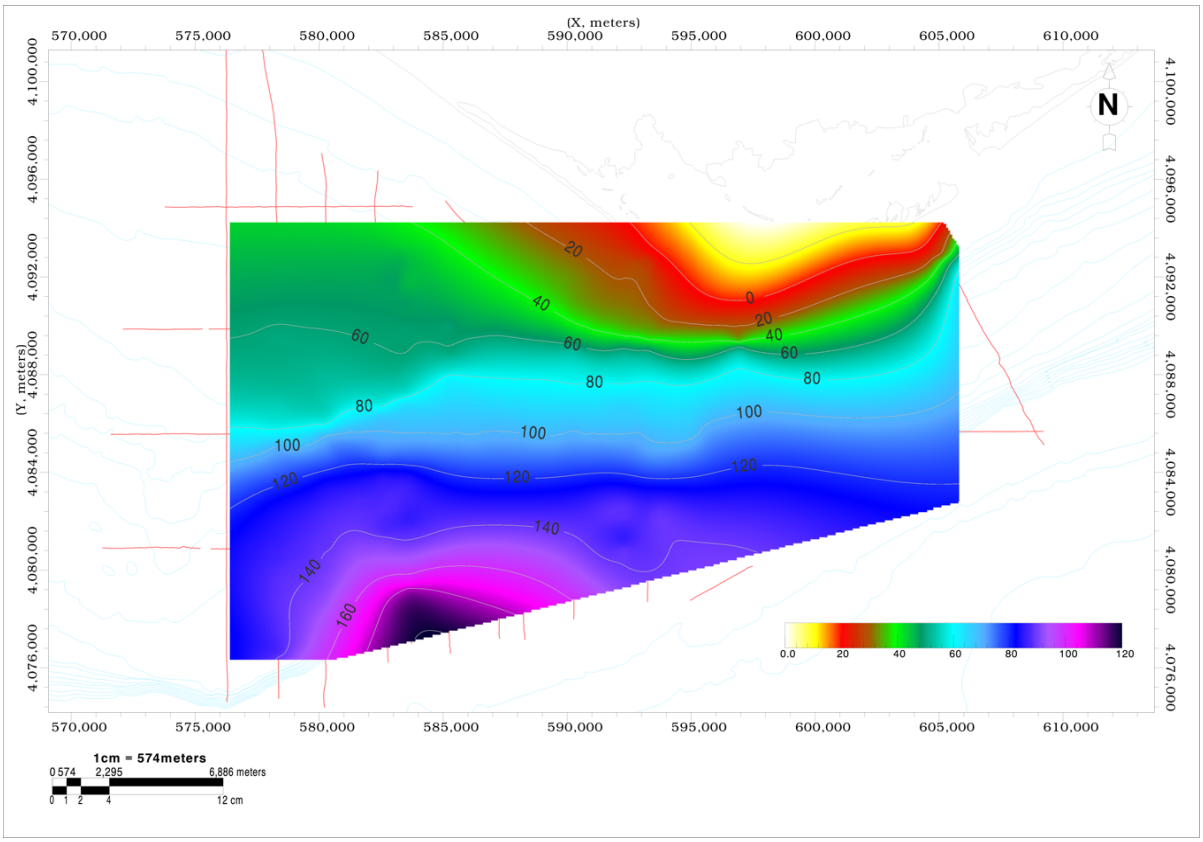

Figure 35: Interpolated surface map of the D4 horizon with colour scale intervals and isobath lines in ms.

6.3.2. Unit's thickness maps

Four thickness maps were created for the units U2 through U5 (Figure 37, Figure 39, Figure 40 and Figure 41). Negative values in isopachs are localized and result from automatic interpolation, a problem to solve in future work. Every map has a color bar, showed in the bottom right corner, and it is in milliseconds/10 (ms). In this bar, the lighter colours represent less thick, thinner, units, and the darker colours represent thicker units. The isopachs contours are in milliseconds (ms).

The isopach map of unit U2 (Figure 37), shows a fairly regular thickness distribution except beyond the slope break and the two N-S trending depocenters. The first correspond to amalgamated progradant wedges located at the slope break and the second to the infill of localized subsiding structures as shown in Figure 38. It is noteworthy that the top part of U2 in the subsiding structures consists of sigmoidal prograding facies dipping from both sides into the depression, while the lower part is made of parallel reflections. These thickness anomalies possibly acted as channels where the sediments were accommodated inside it.

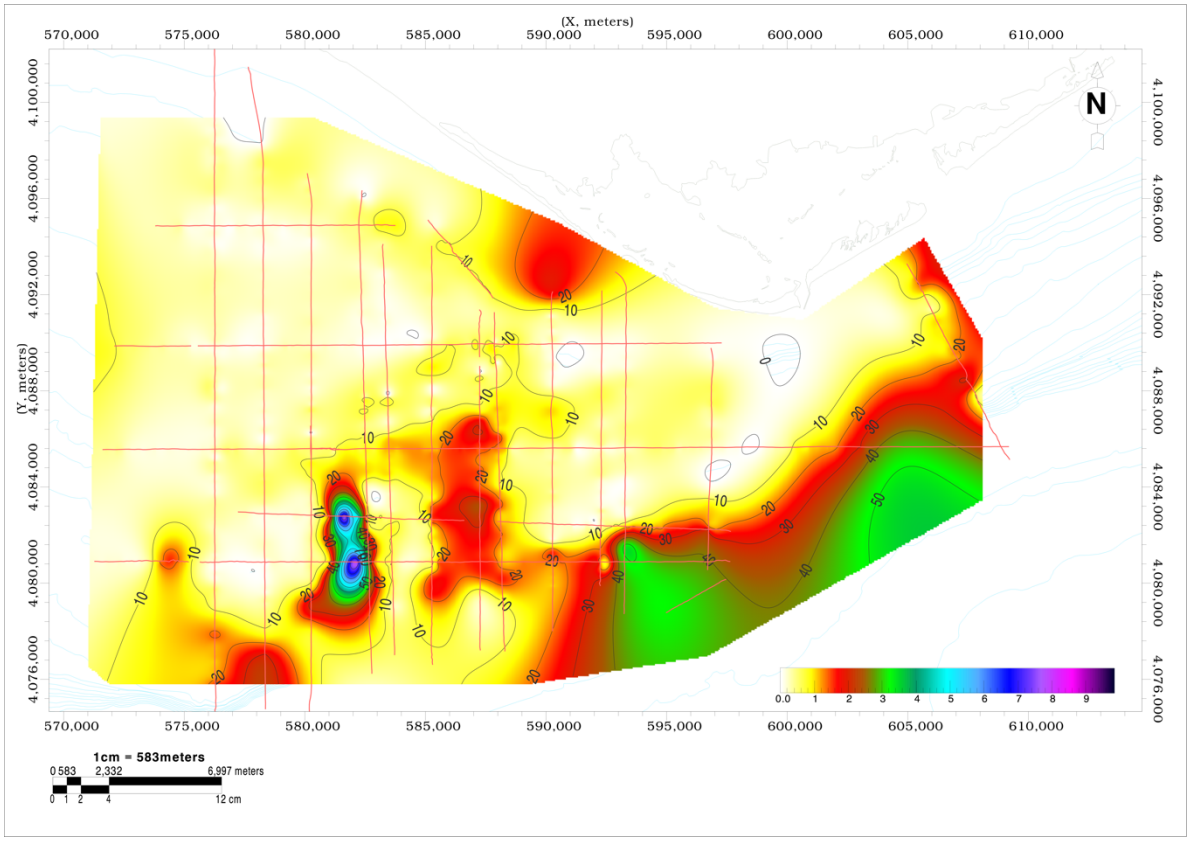

Figure 37: Thickness map of unit U2 with isopach lines in ms and color bar in ms/10. Note the regular thickness distribution with exception to the N-S trending anomalies and they are to the SE. The first correspond to infill structures (either subsiding structure of paleo-channels) and the second to wedge structures deposited at the limit of the slope break.

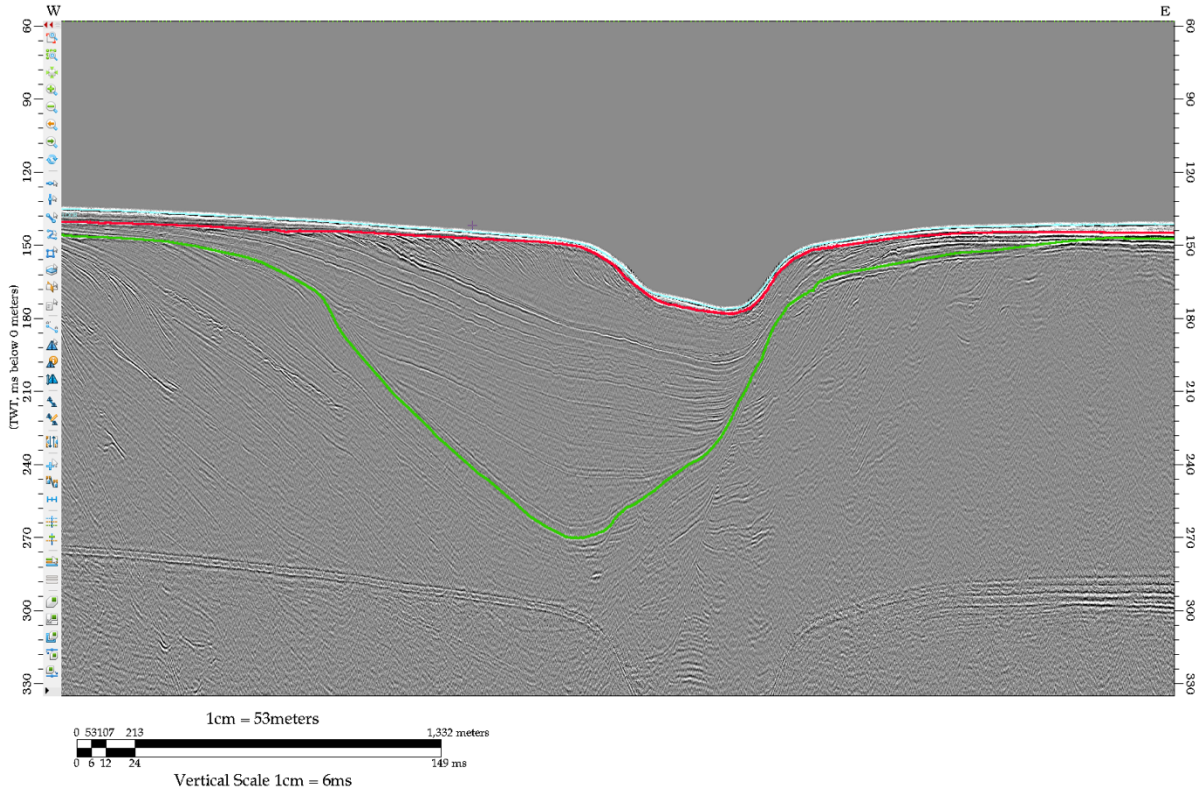

Figure 38: Seismic profile of ASTARTE 10 showing of the anomaly thickness observed in the unit U2 thickness map (Figure 35). Green reflection = D1; Red reflection = D2; Light blue reflection = sea floor. The location of the seismic profile can be seen in Figure 20.

The isopach map of unit U3 (Figure 39), is strikingly different of the U2 as it displays strong heterogeneity in the distribution of U3 thickness. The finger-like thick bodies with a West to East strike tendency are real and do not correspond to fill in of accommodation space as can be confirmed from the inspection of D2 isobath map in Figure 33.

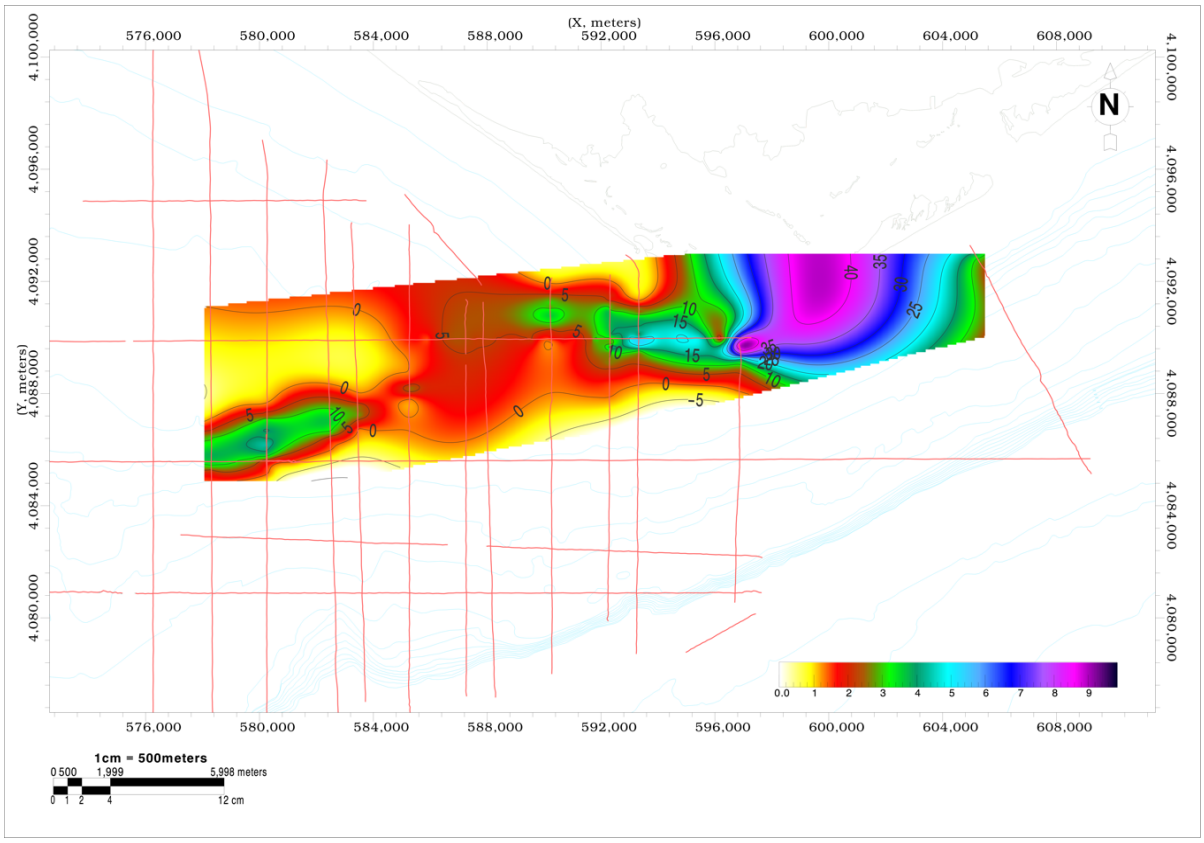

Figure 39: Thickness map of unit U3 with isopach lines in ms. Note that, i) the semi-circular depocenter is an artefact of interpolation and ii) the approximately West to East striking finger-like depocenters are sediment build ups, suggestive of a spit-like sand barrier.

The isopach map of unit U4 (Figure 40), shows that this unit, like the unit U3 map, is only well represented along a West to East part of the study area. It is worthwhile noting that the northern and southern depocenters are separated by a West to East high that corresponds to the thickest part of U3. These U4 depocenters have distinctly different seismic facies, progradational to the south and aggradational to the north, which is compatible with an open offshore face to the south and marine restricted domain to the north with respect to the U3 high.

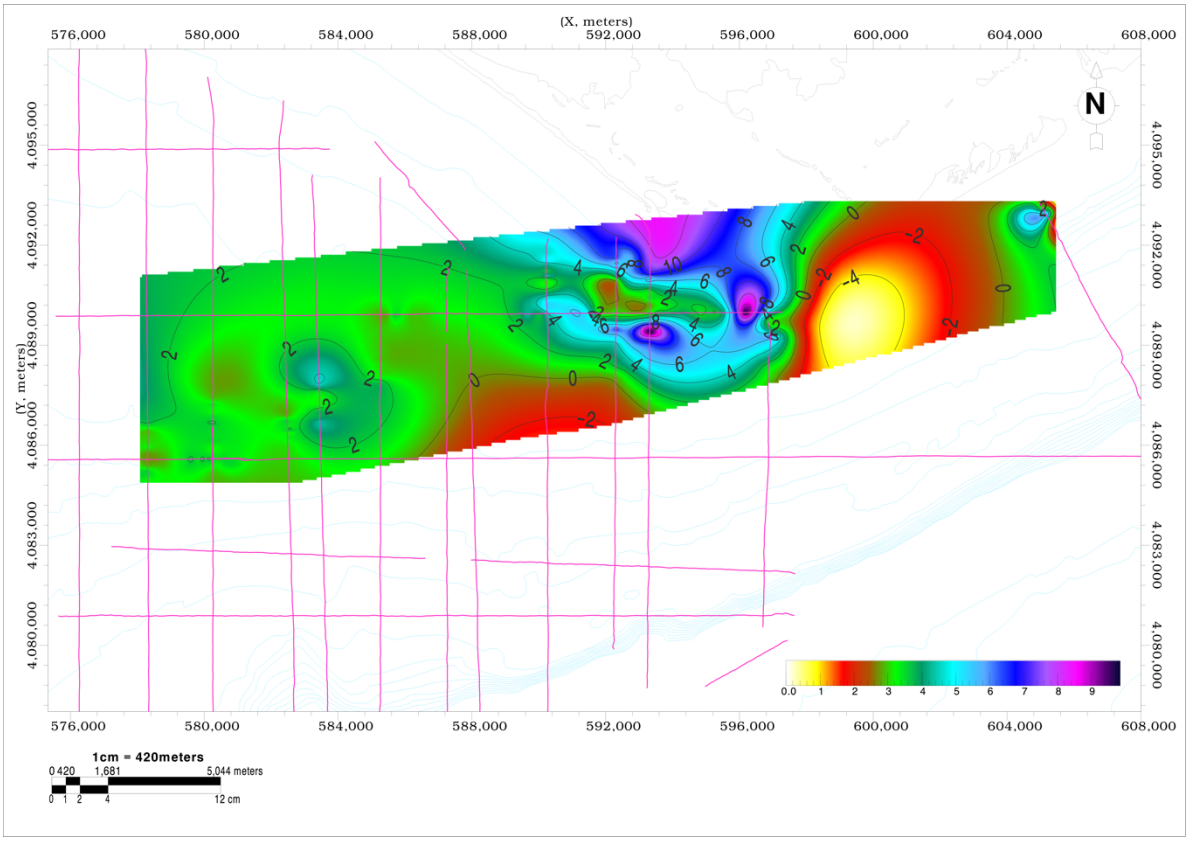

Figure 40: Thickness map of unit U4 with isopach lines in ms. Note that the West to East trending linear zone of thin thickness of U4 corresponds to the U3 structural high that separated a U4 northern and southern domains. The northern one corresponds to aggrading seismic facies and the southern one facing the offshore is made of sigmoidal wedge dipping to the south.

In the isopach map of unit U5 (Figure 41), is observed that this unit is thicker to the south of the U3 and U4 depocenters. The U5 two depocenters. The depocenters are set more or less in the direction of those of unit U3.

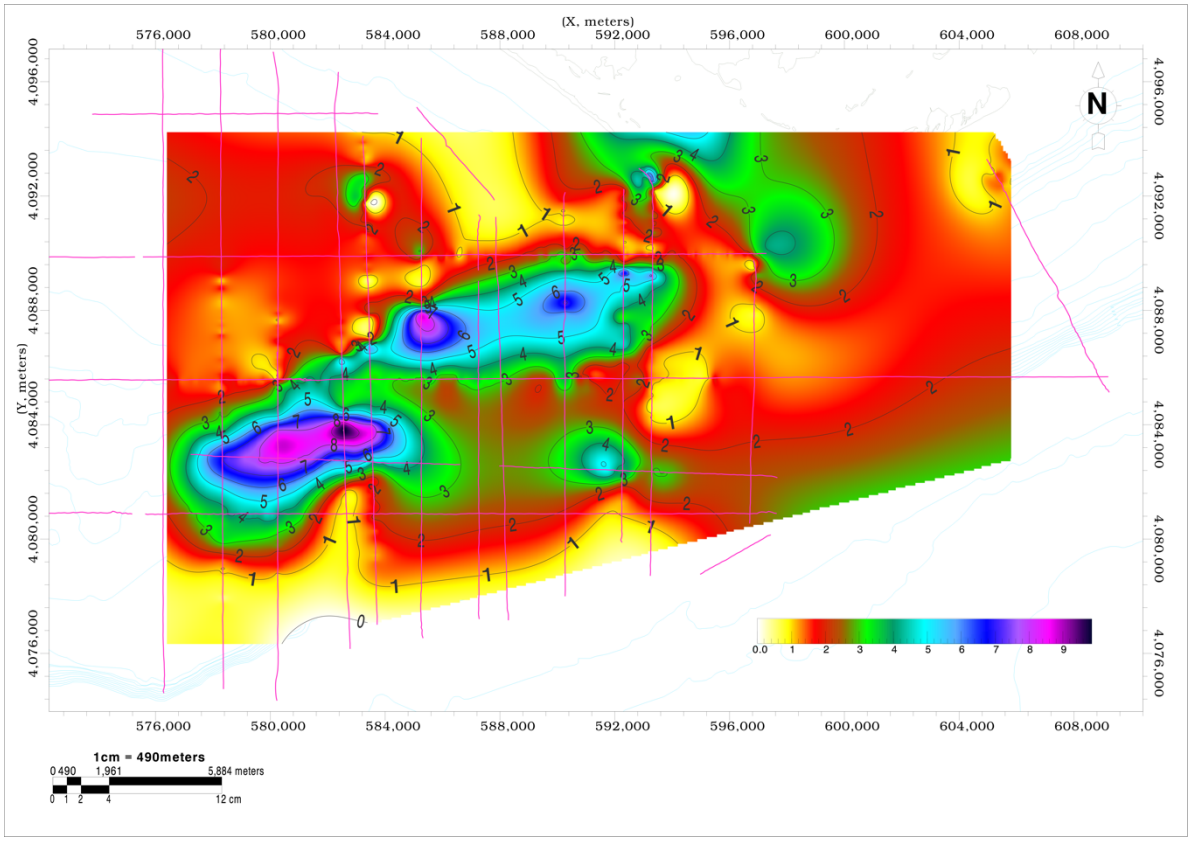

Figure 41: Thickness map of unit U5 with isopach lines in ms. The two depocenters are approximately parallel to those of U3.

7. Discussion

7.1. Stratigraphic model

The analysis of the very high resolution seismic profiles allowed the identification of 4 seismic unit bounding discontinuities (D) and 5 main seismic units (U), as we can see in the stratigraphic model present in Figure 26. The discontinuities D1 and D2 are possibly marine ravinement/erosional surfaces, with the formation of paleoscarps, according to the classification of Zecchin et al. (2019). D1 is possibly an older ravinement surface and D2, probably the last marine ravinement surface, although it could not be confirmed. The prograding wedges (U2b) at the slope break cut by the discontinuity D2 are interpreted as typical low stand slope edge bodies, which favors this interpretation, i.e., part of a Lowstand System Tract (LST). A LST represents the period during which sea level is at its lowest in a cycle of sea-level change, often during the end of a regression (when sea level falls) or the beginning of a transgression (when sea level starts to rise again). The paleo-scarps in the mid continental shelf are also evidence of sea level stand still possibly during a previous sea-level transgression. Also in agreement with this is the internal heterogeneous facies constitution of unit U2, an amalgamation of southwards dipping bodies intersected by channels, chaotic and transparent bodies. U2 is interpreted as a condensed amalgamation of sedimentary bodies deposited during a transgressive-regressive cycles.

Not quite withstanding with this interpretation is the presence of U3 and U4 downlapping horizons. However, as there is little sediment deposited on the shelf, as this is a sediment-starved shelf, any nearshore sediment source could have been the origin of these progradational features.

The discontinuities D3 and D4 are both paraconformal surfaces, bounding units U3, U4 and U5 that prograde shoreward. U4 and U5 are made up of two sub-facies, a sigmoidal one located to the south of the sediment high U3 (these sigmoidal bodies are aggradant northwards) and a channel –like one to the north of U3.

The unit U3 is very characteristic for having a large progradational deposit, and hypothetically we can characterise it as a linear sandy feature advancing from E to W because it trends sub-parallel to the general shoreline (Figure 39) and shows both northwards and southwards progradational sigmoidal foresets (Figure 42). In this case it is hypothesized that U3 could have been a sort of sand spit formed during sea-level rise on top of a sub-horizontal platform on top of a paleo-scarp (figure 25). U3 was deposited in the existing accommodation space, created by the break of slope (i.e., scarp). The prograding unit forms, what we called, a delta type structure, because of the similarities showed in the morphology of the structure with deltas.

The unit U4 is divided in two sub-units: U4a – set on the offshore side, being prograding at the beginning of the sub-unit and as we move towards S it becomes aggrading, probably deposited during the rise in sea level; and U4b – set on the onshore side, Is a heterogeneous sub-unit, with channels and parallel and/or chaotic reflections.

The unit U5 is divided by two sub-units: U5a – set on the offshore side, being prograding at the beginning of the sub-unit and as we move towards S it becomes aggrading, probably deposited with the rise in sea level; and U5b - set on the onshore side is a heterogeneous sub-unit, with channels and chaotic reflections.

The unit U4 and U5 are very similar in stratigraphic terms, and it was only necessary to separate them due to fact that unit U4 is being eroded by U3, onshore, so it was seen that there was a discontinuity in this area, which ended up being D4, ultimately separating U4 and U5.

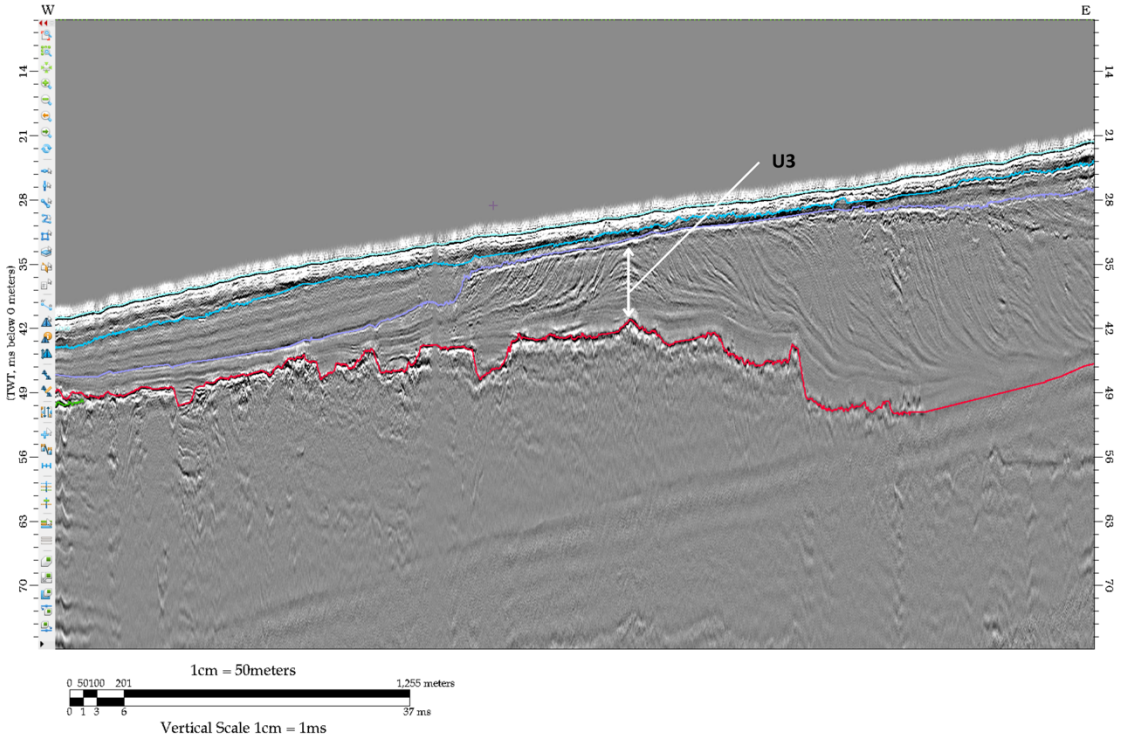

Figure 42: Seismic profile of ASTARTE 04A, showing the different directions of the reflectors in unit U3. See Figure 20 for the line location.

7.2. Geochronology

After integrating all the data presented above, we are able to make a geological timeframe of the system, using the information displayed throughout the work. The oldest date age recorded in the AMS C^{14} analyzed was 8280±30 BP (Conventional Age) in the MW14-105 core (Figure 20). Since it was shown that the measurements of the dating don't pierce any of the interpreted discontinuities and that those ages belong to the unit U5, we can say that all of the units bellow U5 are older than the age mentioned. It is not unreasonable to say that U4 may be very close in age to the oldest age shown, since, as already mentioned, the U5 and U4 units are very similar.

The unit U3 was probably deposited during the rise in sea level. So, if we look at the curve of sea level variations (Figure 15) we can see that the sea level began to rise, due to the deglaciation, at ~16.5-7 ky (Lambeck et al., 2014), we can hypostasize a time location that can be used as a starting point is: ? < U3 < 16.5 ky.

The unit U2 is very complex to determinate a period of time. Since at the shelf break the unit possibly represents a LST and maybe it was not the only one but the addition of several as shown by the number of sub-units. At the middle of the platform the unit can represent a rise or fall in sea-level.

The unit U1 is the oldest one, possibly belonging to older and different times, possibly comprehending Plio-Pleistocene times.

7.3. Depositional model

Starting with unit U1, since it is the oldest unit, so it was the first to be deposited, it represents an ancient depositional environment, though its characteristics are less well defined due to the units complexity and age. Above the U1 unit sets the unit U2. At the shelf break, U2 contains prograding sub-units interpreted as part of a/or various (condensed) LST. This suggests that U2 was deposited during a period of low sea-level. As the sea level rose, U2 might also include deposits from the transgression that

followed. Above unit U2 sets the unit U3. This unit suggests the formation of a sand spit migrating from E to W, and it fills the accommodation space created by the break of slope. U3 was likely deposited during a still stand or slow rise in sea-level. Unit U3 might be the same Holocene deposit already observed in Lobo et al., (2005). They recognised the unit as a significant deposit in terms of thickness and stratigraphic significance and identified it as an Infralittoral Prograding Wedge (IPW) and interpreted to be part of the Holocene HST. Apart from the area that was mapped in this work, that extends to Barreta Island (ASTARTE 27), Lobo et al., (2005), also identified another depocenter off the coast of Tavira, which means that the unit extends beyond the area delimited by the analysed profiles. In Hernández-Molina et al., (2000), the IPW is also mentioned and described as a sedimentary body that developed during the last HST of the last fourth-order cycle which took place during the last 6.500 ky BP. Looking at the U3 bodies, it is possible that they are not linked to the current beach dynamics, as there is some age disconnection. As we were able to confirm, the oldest dating that we know in this work is set on unit U5, and the IPW, if it is the same unit, in this interpretation is set in unit U3, and that dating is older than 6.500 ky BP. So, probably these structures present in the unit may have been linked to non-current beach dynamics when the sea level was lower. The top of the U3 unit is at approximately 20 ms and converted to meters that is 15 m (remembering that these numbers may have to be adjusted because the seismic datum may not correspond to the real datum), then 10 ky ago this structure wouldn't have been flooded, according to the global sea-level variations curve. This means that there was a very rapid rise in sea-level, which helps us to justify the fact that some of the structures we see in unit U3 have been preserved, as they were flooded very quickly and were therefore not completely eroded. The unit U4 set above the unit U3, and it is divided into two units. This unit is very similar to U5, as it was previously mentioned, only separated by the discontinuity D4. Unit U5 is set above unit U4. U5 is the youngest unit of the system, and, for that reason, it is believed that it is related to the formation of the islands.

This is a tentative of an interpretation of what might have happen, since we still have doubts on many aspects of what might have happen, like if unit U3 is a spit formed during the past sea-level rise, when did that happened, and why did it grew E-W, when nowadays the sediment goes on a W-E direction, and what age is unit U4. To answer these and other questions still at bay, more data, especially dating data, is needed to actually frame the whole evolution of the system, as accurately as possible.

8. Conclusion

This work presents an analysis using seismic profiles to investigate the evolution of the RFBIS, based on previously collected data. Understanding the evolution of these systems over geological time is crucial for grasping how they respond to environmental and climate changes. While general characteristics of barrier islands are discussed, the Ria Formosa system presents atypical features.

The analysis provides insights into the geological timeline and the complex interactions of sea-level changes, sediment supply, and erosion that shaped the Ria Formosa barrier system.

Since the study area is extremely complex, we cannot determinate yet all the steps for the reconstruction of the RFBIS as it is currently, but some aspects are clearer than others with the analysis that was made throughout the work:

- The dual facies character of unit U4 and U5 is separated by the sediment/structural high formed by U3 and its internal facies allows postulating the following:
  - **1st.** Unit U3 formed during sea level rise as a linear sand body from East to West. It's sort of sand spit on top of a platform break at the top of a paleo-scarp;
  - **2nd.** The dual character of unit U4 and U5 is the first evidence of sedimentary deposits of lagoonal facies (to the north) and open marine facies to the south;

3rd. The unit U3 through unit U5 shows that transgressive deposits are a precursor of the present day lagoon-barrier islands system, installed at the very end of the last eustatic sea level rise, i.e., at the inundation phase stage;

4th. Units U3, U4 and U5 were deposited during the Last Sea Level Rise;

5th. Unit U2 is an earlier deposit possibly condensing past transgressive-regressive cycles and unit U1 comprehends Mid to Early Pleistocene and Pliocene deposits and a continuation of what is the basement of the RFBIS.

The work provides insights into the timing of these events, linking them to global sea-level fluctuations, sediment supply and underlying geology offering a framework for further geological and paleoenvironmental interpretation of the region, but the stratigraphy of the shelf cannot be used directly to infer the formation of the islands before more dating is obtained.

References

-Achab, M., Ferreira, Ó., Alveirinho Dias, J.M., 2014. Evaluation of sedimentological and morphological changes induced by the rehabilitation of sandy beaches from the Ria Formosa Barrier Island System (South Portugal). Thalassas 30, 21−31.

-Almeida LP, Ferreira O, Pacheco A (2011a) Thresholds for morphological changes on an exposed sandy beach as a function of wave height. Earth Surf Process Landf 36:523−532

- Andrade, C., 1990. *O ambiente de barreira da Ria Formosa (Algarve, Portugal)*. Dep. Geol. University of Lisbon, Lisbon.

- Andrade, C., Freitas, M. C., Moreno, J., & Craveiro, S. C. (2004). Stratigraphical evidence of Late Holocene barrier breaching and extreme storms in lagoonal sediments of Ria Formosa, Algarve, Portugal. *Marine Geology, 210*(1–4), 339–362. https://doi.org/10.1016/j.margeo.2004.05.016

- Ceia, F. R., Patrício, J., Marques, J. C., & Dias, J. A. (2010). Coastal vulnerability in barrier islands: The high risk areas of the Ria Formosa (Portugal) system. Ocean & Coastal Management, *53*(8), 478–486. https://doi.org/10.1016/j.ocecoaman.2010.06.004

--Chiocci, F. L., & Orlando, L. (1996). Lowstand terraces on Tyrrhenian Sea steep continental slopes. *Marine Geology*, *134*(1–2), 127–143. https://doi.org/10.1016/0025-3227(96)00023-0

- Costas, S., Gallego-Fernández, J. B., Bon De Sousa, L., & Kombiadou, K. (2022). Ecogeomorphic response of a coastal dune in southern Portugal regulated by extrinsic factors. *CATENA*, *221*, 106796. https://doi.org/10.1016/j.catena.2022.106796

- Costas, S., de Sousa, L.B., Kombiadou, K., Ferreira, Ó., Plomaritis, T.A., 2020. Exploring foredune growth capacity in a coarse sandy beach. Geomorphology 371, 107 435. https://doi.org/10.1016/j.geomorph.2020.107435

- Costa M, Silva R, Vitorino J (2001) *Contribuição para o estudo do clima de agitação marítima na costa portuguesa*. Proceedings of 2as *Jornadas Portuguesas de Engenharia Costeira e Portuária,* International Navigation Association PIANC, Sines, Portugal (in Portuguese)

- Dias, João. (1985). *Registos da migração da linha de costa nos últimos 18.000 anos na plataforma continental portuguesa setentrional.* Actas da I Reun. Quat. Ibér (Lisboa), pp. 281-295.

- Dias, João., Rodrigues, A. & Magalhães, Fernando. (1997). *Evolução da linha de costa, em Portugal, desde o último máximo glaciário até à actualidade: Síntese dos conhecimentos. Estudos Do Quaternário.* 1. 53-66. 10.30893/eq.v0i1.8.

- Dias, João. (1988). *Aspectos Geológicos do Litoral Algarvio*. Geonovas (ISSN: 0870-7375), Lisboa, Portugal. 10. 113-128.

- Dias, J. M. A., Boski, T., Rodrigues, A., & Magalhães, F. (2000). Coast line evolution in Portugal since the Last Glacial Maximum until present Ð a synthesis. *Marine Geology*.

- Dias, J.A., Ferreira, Ó., Matias, A., Vila-Concejo, A., Sá-Pires, C., 2003. Evaluation of soft pro- tection techniques in Barrier Islands by monitoring Programs: case studies from Ria Formosa (Algarve-Portugal). J. Coast. Res. https://doi.org/10.2307/40928755

- Davis, R. A. (2003). Coastal Geology. Encyclopedia of Physical Science and Technology (Third Edition*)*, 123-153. https://doi.org/10.1016/B0-12-227410-5/00113-7

- ESAGUY, A.S., 1987. *Ria de Faro, Barra de Tavira. Evolução*. *Direcção Geral de Portos Internal Report*, 13 p. (in Portuguese).

- Ferreira, Ó., Matias, A., & Pacheco, A. (2016). The East Coast of Algarve: A Barrier Island Dominated Coast. *Thalassas:* An International Journal of Marine Sciences, *32*(2), 75–85. https://doi.org/10.1007/s41208-016-0010-1

- Garcia, T., Ferreira, Ó., Matias, A., & Dias, J. A. (2010). Overwash vulnerability assessment based on long-term washover evolution. *Natural Hazards*, *54*(2), 225–244. https://doi.org/10.1007/s11069-009-9463-3

- Garnier, E., Ciavola, P., Spencer, T., Ferreira, O., Armaroli, C., & McIvor, A. (2018). Historical analysis of storm events: Case studies in France, England, Portugal and Italy. *Coastal Engineering*, *134*, 10–23. https://doi.org/10.1016/j.coastaleng.2017.06.014
- Gerald E., Reinson. Transgressive Barrier Island and Estuarine Systems. Facies Models Response to Sea Level Change, Walker RG and James NP (eds) (1992). 2nd Edition. St. John's: Geological Association of Canada.
- Hayes. M.O. (1979). Barrier island morphology as a function of tidal and wave regime. In: Leatherman, S.P. rEd.i, Barrier Islands: From the Gulf of St. Lawrence to the Gulf of Mexico. New York: Academic, pp. 1-28.
- Herrero, X., Costas, S., Kombiadou, K., 2020. Coastal ridge constructive processes at a multi-decadal scale in Barreta Island (southern Portugal). Earth Surf. Process. Landforms 45, 411–423. https://doi.org/10.1002/esp.4742.
- Hernández-Molina, F. J., Fernández-Salas, L. M., Lobo, F., Somoza, L., Díaz-del-Río, V., & Alveirinho Dias, J. M. (2000). The infralittoral prograding wedge: A new large-scale progradational sedimentary body in shallow marine environments. *Geo-Marine Letters*, *20*(2), 109–117. https://doi.org/10.1007/s003670000040
- Jacob, J., & Cravo, A. (2019). Recent evolution of the tidal prisms at the inlets of the western sector of the Ria Formosa, south coast of Portugal. *Regional Studies in Marine Science*, *31*, 100767. https://doi.org/10.1016/j.rsma.2019.100767
- Kombiadou, K., Matias, A., Ferreira, Ó., Carrasco, A. R., Costas, S., & Plomaritis, T. (2019). Impacts of human interventions on the evolution of the Ria Formosa barrier island system (S. Portugal). *Geomorphology*, *343*, 129–144. https://doi.org/10.1016/j.geomorph.2019.07.006
- Kombiadou, K., Matias, A., Costas, S., Rita Carrasco, A., Plomaritis, T. A., & Ferreira, Ó. (2020). Barrier island resilience assessment: Applying the ecological principles to geomorphological data. *CATENA*, *194*, 104755. https://doi.org/10.1016/j.catena.2020.104755
- Kombiadou, K., Carrasco, A. R., Costas, S., Ramires, M., & Matias, A. (2024). The birth of backbarrier marshes in Culatra Island (Ria Formosa, South Portugal). *Estuarine, Coastal and Shelf Science*, *296*, 108589. https://doi.org/10.1016/j.ecss.2023.108589
- Lambeck, K., Rouby, H., Purcell, A., Sun, Y., & Sambridge, M. (2014). Sea level and global ice volumes from the Last Glacial Maximum to the Holocene. *Proceedings of the National Academy of Sciences*, *111*(43), 15296–15303. https://doi.org/10.1073/pnas.1411762111
- Leatherman, S.P. (1979) (Editor) – Barrier Islands, from the Gulf of St. Laurence to the Gulf of Mexico. Academic Press, 325p.
- Leorri, E., Cearreta, A., & Milne, G. (2012). Field observations and modelling of Holocene sea-level changes in the southern Bay of Biscay: Implication for understanding current rates of relative sea-level change and vertical land motion along the Atlantic coast of SW Europe. *Quaternary Science Reviews*, *42*, 59–73. https://doi.org/10.1016/j.quascirev.2012.03.014
- Lobo, F. J., Sánchez, R., González, R., Dias, J. M. A., Hernández-Molina, F. J., Fernández-Salas, L. M., Díaz Del Río, V., & Mendes, I. (2004). Contrasting styles of the Holocene highstand sedimentation and sediment dispersal systems in the northern shelf of the Gulf of Cadiz. *Continental Shelf Research*, *24*(4–5), 461–482. https://doi.org/10.1016/j.csr.2003.12.003
- Lobo, F. J., Fernández-Salas, L. M., Hernández-Molina, F. J., González, R., Dias, J. M. A., Del Río, V. D., & Somoza, L. (2005). Holocene highstand deposits in the Gulf of Cadiz, SW Iberian Peninsula: A high-resolution record of hierarchical environmental changes. *Marine Geology*, *219*(2–3), 109–131. https://doi.org/10.1016/j.margeo.2005.06.005
- Lopes, F. C., & Cunha, P. P. (2010). The Algarve continental shelf and adjacent provinces: A geomorphological analysis.

- Luque, L, Lario, J., law, C, Goy, j.L, Dabrio, Cj., Borja, E, 2002. Sedimentary record of historical tsunamis in the Bay of Cadiz (Spain). Journal of Quaternary Science 17,623-631.
- Mariotti, G., & Hein, C. J. (2022). Lag in response of coastal barrier-island retreat to sea-level rise. Nature *Geoscience*, *15*(8), 633–638. https://doi.org/10.1038/s41561-022-00980-9
- Martins L, Madeira J, Youbi N, Munhá J, Mata J, Kerrich R (2008) Rift-related magmatism of the Central Atlantic magmatic prov- ince in Algarve, southern Portugal. Lithos 101:102–124
- Mil-Homens Mário, Vale C., Naughton F, Brito P., Drago T., Anesa B., Raimundo J., Schmidt S. and Caetano M. (2016) - Footprint of roman and modern mining activities in a sediment core from the southwestern Iberian Atlantic shelf. Science of The Total Environment, Volume 571, 15 November 2016, Pages 1211–1221.
- Moita, I., 1986. *Noticia Explicativa da Carta dos Sedimentos Superficiais da Plataforma*. Folha SED 8, Instituto Hidro- gráfico, 18pp.
- Moura D, Veiga Pires L, Albardeiro T, Boski T, Rodrigues AL, Tareco H (2007) Holocene sea level fluctuations and coastal evolution in the central Algarve (southern Portugal). Mar Geol 237:127–142
- Noiva, J. (2008). Report of the ERSTA-SANDEX campaign carried out off Quarteira and Vilamoura coast.
- Noiva, J., Terrinha, P., Magalhães, V., Brito, P. (2014). Final cruise report from the ASTARTE campaign (Assessment, Strategy And Risk Reduction for Tsunamis in Europe, ENV.2013.6.4-3: Coasts at threat in Europe: tsunamis and climate-related risks).
- Oertel, G. F. (1985). The barrier island system. *Marine Geology*, *63*(1–4), 1–18. https://doi.org/10.1016/0025-3227(85)90077-5
- Pacheco, A., Ferreira, Ó., & Williams, J. J. (2011). Long-term morphological impacts of the opening of a new inlet on a multiple inlet system. *Earth Surface Processes and Landforms*, *36*(13), 1726–1735. https://doi.org/10.1002/esp.2193
- Pais J, Legoinha P, Elderfield H, Sousa L, Estevens M (2000) The Neogene of Algarve (Portugal). Ciências da Terra 14:277–288
- Pilkey Jr, O.H. & Neal, William & Monteiro, J.H. & Dias, Joao. (1989). Algarve Barrier Islands: a Noncoastal-plain System in Portugal. *Journal of Coastal Research. 5. 239-261.*
- Ramos, A., Fernández, O., Terrinha, P., & Muñoz, J. A. (2015). Extension and inversion structures in the Tethys–Atlantic linkage zone, Algarve Basin, Portugal. International Journal of Earth Sciences, *105*(5), 1663–1679. https://doi.org/10.1007/s00531-015-1280-1
- Righetti, A. (2021). The geology and environmental processes that govern the origin of the continental shelf of Iberia.
- Roque, C., (2007). *Tectonostratigrafia do Cenozóico das margens continentais Sul e Sudoeste Portuguesas: Um modelo de correlação sismostratigráfica.* (Doctoral Dissertation) Universidade de Lisboa.
- Roque, C., Hernández-Molina, F. J., Lobo, F., Somoza, L., Díaz-del-Río, V., Vázquez, J. T., & Dias, J. (2010). Geomorphology of the Eastern Algarve proximal continental margin (South Portugal, SW Iberia Peninsula): Sedimentary dynamics and its relationship with the last asymmetrical eustatic cycle.
- Ruiz, E, Rodriguez Ramirez, A, Caceres, L, Rodriguez Vidal, j., Carretero, M.I., Abad, M., Olias, M., Pow, M., 2005. Evidence of high-energy events in the geological records: mid-Holocene evolution of the southwestern Donana national park (SW Spain). *Paleogeography, Paleoc1imatology, Paleoecology* 229, 212-229.
- Santos, F., Lopes, A., Moniz, G., Ramos, L., Taborda, R., 2014. *Gestão da Zona Costeira - O Desafio da Mudança.*
- Schwartz R (1975) Nature and genesis of some storm washover deposits. Technical Memorandum 61, Coastal Engineering Research Center, 69 pp

- Sousa, C., Boski, T., Gomes, A., Pereira, L., Lampreia, J., & Oliveira, S. (2014). *Reconstrução holocénica do sistema lagunar da Ria Formosa (Sul de Portugal) com base num modelo digital de paleosuperfície pré-Holocénica.*
-Sousa, C., Boski, T., & Pereira, L. (2018). Holocene evolution of a barrier island system, Ria Formosa, South Portugal. *The Holocene*, *29*(1), 64–76. https://doi.org/10.1177/0959683618804639
- Stutz, M. L., & Pilkey, O. H. (2000). A Review of Global Barrier Island Distribution. 15–22.
- Stutz, Matthew. (2011). Open-Ocean Barrier Islands: Global Influence of Climatic, Oceanograpic, and Depositional Settings. Journal of Coastal Reserarch. 27.207-222. 10.2307/29783233.
-Swift, D.J.P., 1976. Continental shelf sedimentation. In: Stanley, D.J., and Swift, D.J.P., (Eds.), in *Marine Sediment Transport and Environmental Management*. New York: Wiley, pp. 311-350.
- Swift, D.J.P., 1975. Barrier island genesis: Evidence from the Central Atlantic Shelf, Eastern U.S.A./ *Sedimentary Geology,* 14, 1-43.
- Terrinha, P., Rocha, R., Rey, J., Cachão, M., Moura, D., Roque, C., Martins, L., Valadares, V., Cabral, J., Azevedo, M. R., Barbero, L., Clavijo, E., Dias, R. P., Gafeira, J., Matias, H., Matias, L., Madeira, J., Rebelo, L., Ribeiro, C., … Youbi, N. (2006). *A Bacia do Algarve: Estratigrafia, Paleogeografia e Tectónica.*
- Terrinha, P., Carrara, G., Noiva, J., Duarte, H., Brito, P., Pinheiro, L., Sousa,K., Ribeiro, T., Bensalah, O., Roque, C., Valadares, V. (2011). Report of the TOPOMED-FREEZE seismic reflection survey.
- Terrinha P, Ribeiro C, Kullberg JC, Rocha R, Ribeiro A (2002) Compression episodes during rifting and faunal isolation in the Algarve Basin, southwest Iberia. J Geol 110:101–113
- Vila-Concejo, A., Matias, A., Ferreira, Ó., Duarte, C., & Dias, J. M. A. (2002). Recent Evolution of the Natural Inlets of a Barrier Island System in Southern Portugal. Journal of Coastal Research, *36*, 741–752. https://doi.org/10.2112/1551-5036-36.sp1.741
- Vinhas, A., Rodrigues, A. (2022). *Geomorfologia da plataforma continental do Algarve no sector compreendido entre o cabo de São Vicente e Albufeira.*
- Zecchin, M., Catuneanu, O., & Caffau, M. (2019). Wave-ravinement surfaces: Classification and key characteristics. *Earth-Science Reviews*, *188*, 210–239. https://doi.org/10.1016/j.earscirev.2018.11.011